Simulation of Regional Ground-Water Flow in the Upper Deschutes Basin, Oregon

U.S. DEPARTMENT OF THE INTERIOR
U.S. GEOLOGICAL SURVEY
Water-Resources Investigations
Report 03-4195

Prepared in cooperation with
OREGON WATER RESOURCES DEPARTMENT;
CITIES OF BEND, REDMOND, AND SISTERS;
DESCHUTES AND JEFFERSON COUNTIES;
THE CONFEDERATED TRIBES OF THE
WARM SPRINGS RESERVATION OF OREGON;
and U.S. ENVIRONMENTAL PROTECTION AGENCY

Cover photographs:

Top: Steelhead Falls on the Deschutes River near Crooked River Ranch, Oregon.

Middle: Crooked River Canyon at Crooked River Ranch, Oregon.

Bottom: North and Middle Sister with a wheel-line irrigation system in the foreground, near Sisters, Oregon. (Photographs by Rodney R. Caldwell, U.S. Geological Survey.)

U.S. Department of the Interior
U.S. Geological Survey

Simulation of Regional Ground-Water Flow in the Upper Deschutes Basin, Oregon

By MARSHALL W. GANNETT and KENNETH E. LITE JR.

Water-Resources Investigations Report 03-4195

Prepared in cooperation with Oregon Water Resources Department;
Cities of Bend, Redmond, and Sisters; Deschutes and Jefferson Counties;
The Confederated Tribes of the Warm Springs Reservation of Oregon;
and U.S. Environmental Protection Agency

Portland, Oregon
2004

U. S. DEPARTMENT OF THE INTERIOR
GALE A. NORTON, Secretary

U.S. GEOLOGICAL SURVEY
CHARLES G. GROAT, Director

For additional information:

District Chief
U.S. Geological Survey
10615 S.E. Cherry Blossom Dr.
Portland, OR 97216-3103
E-mail: info-or@usgs.gov
Internet: http:// or.water.usgs.gov

Copies of this report may be purchased from:

U.S. Geological Survey
Branch of Information Services
Box 25286
Denver Federal Center
Denver, CO 80225-0286
Telephone: 1-888-ASK-USGS

Suggested citation: Gannett, M.W., and Lite, K.E., Jr., 2004, Simulation of regional ground-water flow in the upper Deschutes Basin, Oregon: U.S. Geological Survey Water-Resources Investigations Report 03–4195, 84 p.

CONTENTS

FIGURES

TABLES

CONVERSION FACTORS AND VERTICAL DATUM

Multiply	By	To obtain
inch (in)	25.40	millimeter (mm)
inches per year (in/yr)	25.40	millimeters per year (mm/yr)
foot (ft)	0.3048	meter (m)
feet per second (ft/s)	0.3048	meters per second (m/s)
feet per day (ft/d)	3.528×10^{-6}	meters per second (m/s)
feet per year (ft/yr)	0.3048	meters per year (m/yr)
square feet (ft^2)	0.0929	square meters (m^2)
acre-feet per year (acre-ft/yr)	1,233.482	cubic meters per year (m^3/yr)
mile (mi)	1.609	kilometer (km)
square mile (mi^2)	2.590	square kilometer (km^2)
cubic foot per second (ft^3/s)	0.02832	cubic meter per second (m^3/s)
gallon per minute (gal/min)	6.308×10^{-5}	cubic meters per second (m^3/s)

Elevation: In this report, elevation is referenced to the National Geodetic Vertical Datum of 1929 (NGVD29).

Specific conductance is given in microsiemens per centimeter (μS/cm) at 25°C.

Temperature in degrees Fahrenheit (°F) may be converted to degrees Celsius (°C) as follows:

$$°C = (°F - 32) / 1.8$$

Temperature in degrees Celsius (°C) may be converted to degrees Fahrenheit (°F) as follows:

$$°F = (1.8 \times °C) + 32$$

MAPPING SOURCES:

Base map modified from U.S. Geological Survey 1:500,000 State base map, 1982, with digital data from U.S. Bureau of the Census, TIGER/Line (R), 1990, and U.S. Geological Survey Digital Line Graphs published at 1:100,000. Projection: Universal Transverse Mercator projection, Zone 10, 1927 North American Datum.

LOCATION SYSTEM

The system used for locating wells, springs, and surface-water sites in this report is based on the rectangular system for subdivision of public land. The State of Oregon is divided into townships of 36 square miles numbered according to their location relative to the east-west Willamette baseline and a north-south Willamette meridian. The position of a township is given by its north-south "Township" position relative to the baseline and its east-west "Range" position relative to the meridian. Each township is divided into 36 one-square-mile (640-acre) sections numbered from 1 to 36. For example, a well designated as 18S/11E-29AAC is located in Township 18 south, Range 11 east, section 29. The letters following the section number correspond to the location within the section; the first letter (A) identifies the quarter section (160 acres); the second letter (A) identifies the quarter-quarter section (40 acres); and the third letter (C) identifies the quarter-quarter-quarter section (10 acres). Therefore, well 29AAC is located in the SW quarter of the NE quarter of the NE quarter of section 29. When more than one designated well occurs in the quarter-quarter-quarter section, a serial number is appended.

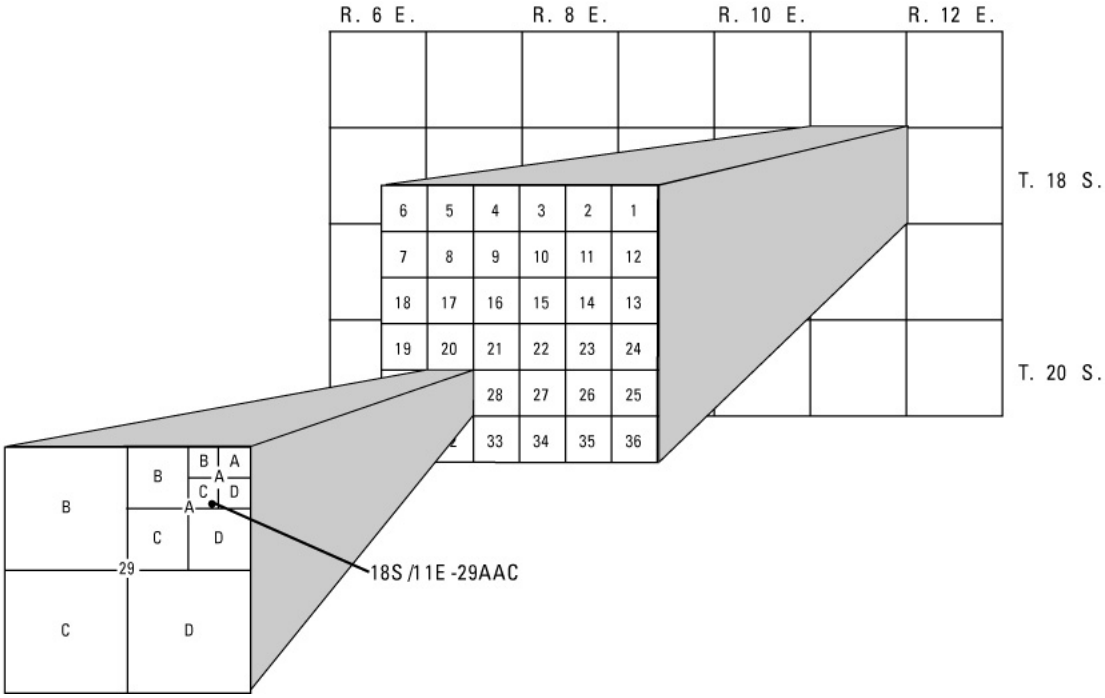

Well- and spring-location system.

Each well is assigned a unique 8-digit identification number known as the log-id number. The first two digits of the log-id number indicate the county code from the Federal Information Processing Standards (FIPS) code file for the county in which the well exists. The FIPS codes for the counties in the study area are as follows: 13, Crook County; 17, Deschutes County; 31, Jefferson County; and 35, Klamath County. The last 6 digits of the number correspond to the State of Oregon well-log number (a unique number assigned by the Oregon Water Resources Department to the report filed by the well driller).

Simulation of Regional Ground-Water Flow in the Upper Deschutes Basin, Oregon

By Marshall W. Gannett *and* Kenneth E. Lite Jr.

Abstract

This report describes a numerical model that simulates regional ground-water flow in the upper Deschutes Basin of central Oregon. Ground water and surface water are intimately connected in the upper Deschutes Basin and most of the flow of the Deschutes River is supplied by ground water. Because of this connection, ground-water pumping and reduction of artificial recharge by lining leaking irrigation canals can reduce the amount of ground water discharging to streams and, consequently, streamflow. The model described in this report is intended to help water-management agencies and the public evaluate how the regional ground-water system and streamflow will respond to ground-water pumping, canal lining, drought, and other stresses.

Ground-water flow is simulated in the model by the finite-difference method using MODFLOW and MODFLOWP. The finite-difference grid consists of 8 layers, 127 rows, and 87 columns. All major streams and most principal tributaries in the upper Deschutes Basin are included. Ground-water recharge from precipitation was estimated using a daily water-balance approach. Artificial recharge from leaking irrigation canals and on-farm losses was estimated from diversion and delivery records, seepage studies, and crop data. Ground-water pumpage for irrigation and public water supplies, and evapotranspiration are also included in the model.

The model was calibrated to mean annual (1993–95) steady-state conditions using parameter-estimation techniques employing nonlinear regression. Fourteen hydraulic-conductivity parameters and two vertical conductance parameters were determined using nonlinear regression. Final parameter values are all within expected ranges. The general shape and slope of the simulated water-table surface and overall hydraulic-head distribution match the geometry determined from field measurements. The fitted standard deviation for hydraulic head is about 76 feet. The general magnitude and distribution of ground-water discharge to streams is also well simulated throughout the model. Ground-water discharge to streams in the area of the confluence of the Deschutes, Crooked, and Metolius Rivers is closely matched.

The model was also calibrated to transient conditions from 1978 to 1997 using traditional trial-and-error methods. Climatic cycles during this period provided an excellent regional hydrologic signal for calibration. Climate-driven water-level fluctuations are simulated with reasonable accuracy over most of the model area. The timing and magnitude of simulated water-level fluctuations caused by annual pulses of recharge from precipitation match those observed reasonably well, given the limitations of the time discretization in the model. Water-level fluctuations caused by annual canal leakage are simulated very well over most of the area where such fluctuations occur. The transient model also simulates the volumetric distribution and temporal variations in ground-water discharge reasonably well. The match between simulated and measured volume of and variations in ground-water discharge is, however, somewhat dependent on geographic scale. The rates of and variations in ground-water discharge are matched best at regional scales.

Example simulations were made to demonstrate the utility of the model for evaluating the effects of ground-water pumping or canal lining. Pumping simulations show that pumped water comes largely from aquifer storage when pumping begins, but as the water table stabilizes, the pumping increasingly diminishes the discharge to streams and, hence, streamflow. The time it takes for pumping to affect streamflow varies spatially depending, in general, on the location of pumping relative to the discharge areas. Canal-lining simulations show similar effects.

INTRODUCTION

Background and Study Objectives

The upper Deschutes Basin is presently one of the fastest growing population centers in Oregon. The number of people in Deschutes County, the most populous county in the basin, quadrupled between 1970 and 2001. Approximately 160,000 people lived in the upper Deschutes Basin as of 2001. Growth in the region is expected to continue, and residents and government agencies are concerned about water supplies for the growing population and the consequences of increased development for existing water users. Surface-water resources in the area have been closed to additional appropriation for many years. Therefore, virtually all new development in the region must rely on ground water as a source of water. Prior to this study, very little quantitative information was available on the ground-water hydrology of the basin. This lack of information made ground-water resource-management decisions difficult and was generally a cause for concern.

To fill this information void, the U.S. Geological Survey (USGS) conducted a cooperative study with the Oregon Water Resources Department (OWRD); the Cities of Bend, Redmond, and Sisters; Deschutes and Jefferson Counties; The Confederated Tribes of the Warm Springs Reservation of Oregon; and the U.S. Environmental Protection Agency. The objectives of this study were to provide a quantitative assessment of the regional ground-water system and provide the understanding and analytical tools for State and local government agencies, hydrologists, and local residents to make informed resource-management decisions. This report is one in a series that presents the results of the upper Deschutes Basin ground-water study. The conceptual understanding of regional ground-water flow on which the numerical model presented herein is based was described by Gannett and others (2001). The geologic framework of the regional ground-water flow system was described by Lite and Gannett (2002). Much of the hydrologic data on which the conceptual understanding and simulation work is based can be found in Caldwell and Truini (1997).

Purpose and Scope

This report describes the mathematical simulation of regional ground-water flow in the upper Deschutes Basin in central Oregon. The report includes a description of the ground-water hydrology of the upper Deschutes Basin and how the hydrologic system was represented in the numerical model. The hydrologic data used for model calibration and the calibration procedures are also described. A discussion of model reliability and simulation of some hypothetical ground-water management scenarios are also included.

Numerical models presently provide the best method for synthesizing the data and the conceptual understanding for analyzing and predicting the behavior of a complex natural system. Numerical models allow the testing of conceptual models by placing them in a physically based mathematical framework constrained by data. Errors in conceptual models are often made obvious during numerical model development. If a numerical model is properly calibrated, meaning it accurately simulates the observed behavior of the system, then it can be used to predict the behavior of the system under new conditions. The uncertainty of the predictions, however, can be large if the new conditions differ markedly from the range of conditions over which the model was calibrated.

The purpose of the simulation work in the upper Deschutes Basin was to test the reasonableness of the conceptual understanding of regional ground-water flow, provide insights into the behavior of the system, and evaluate the behavior of the ground-water system under possible future conditions. Of particular interest in the upper Deschutes Basin are changes in the location and amount of ground-water discharge to streams caused by increases in the rate of ground-water pumping and reduction of artificial ground-water recharge due to sealing of leaking irrigation canals.

The simulation work described in this report was constrained by the limited geographic distribution of data and the scarcity of time-series data on such quantities as head and ground-water discharge. Most of the area of the upper Deschutes Basin is public land with very few wells to provide subsurface hydrologic information. Therefore, there are large geographic regions throughout which hydraulic head data and subsurface geologic data are scarce. Moreover, in the areas where there are wells, most penetrate only the upper part of the thick saturated section. Because of this, there is very little information on the deep parts of the flow system anywhere in the basin. This scarcity of data coupled with the geologic and hydrologic complexity of the area create inherent uncertainty in simulation results.

Regardless, the simulation work described in this report has helped to refine the conceptual understanding of the regional flow system and provides important insights as to how the system will likely respond to changing conditions.

Study Area Description

The upper Deschutes Basin study area encompasses approximately 4,500 mi^2 (square miles) of the Deschutes River drainage basin in central Oregon (fig. 1). The area is drained by the Deschutes River and its major tributaries: the Little Deschutes River, Tumalo and Squaw Creeks, and the Metolius River from the west, and the Crooked River from the east. Land-surface elevation ranges from less than 1,300 feet near Gateway in the northern part of the study area to more than 10,000 feet in the Cascade Range. The study area includes the major population centers in the basin, where ground-water development is most intense and resource-management questions are most urgent. The major communities include Bend, Redmond, Sisters, Madras, Prineville, and La Pine.

The study area boundaries were chosen to coincide as much as possible with natural hydrologic boundaries across which ground-water flow can be reasonably estimated or assumed to be negligible. The study area is bounded on the north by Jefferson Creek, the Metolius River, the Deschutes River, and Trout Creek; on the east by the generalized contact between the Deschutes Formation and the older, much less permeable John Day Formation; on the south by the drainage divide between the Deschutes Basin and the Fort Rock and Klamath Basins; and on the west by the Cascade Range crest.

There are approximately 164,000 acres (256 mi^2) of irrigated agricultural land in the study area. The largest source of irrigation water is the Deschutes River. Most water is diverted from the Deschutes River near Bend and distributed to areas to the north through several hundred miles of canals. Smaller amounts of irrigation water are diverted from Tumalo and Squaw Creeks, the Crooked River, and Ochoco Creek.

The climate in the Deschutes Basin is controlled primarily by air masses that move eastward from the Pacific Ocean, across western Oregon, and into central Oregon. The climate is moderate, with cool, wet winters and warm, dry summers. Orographic processes result in large amounts of precipitation in the Cascade Range in the western part of the basin, with precipitation locally exceeding 200 in/yr (inches per year), mostly as snow during the winter (Taylor, 1993). Precipitation rates diminish rapidly toward the east to less than 10 in/yr in the central part of the basin (fig. 2). Climate in the Deschutes Basin exhibits year to-year and longer-term variability. This variability generally parallels regional trends in the Pacific Northwest that have been correlated with large-scale ocean-atmosphere climate-variability patterns in the Pacific Basin such as the El Niño/Southern Oscillation (Redmond and Koch, 1991) and the Pacific Decadal Oscillation (Mantua and others, 1997).

Acknowledgements

Numerous people contributed substantially to the modeling efforts in the upper Deschutes Basin described in this report. The authors gratefully acknowledge the following colleagues for their mentorship, insightful discussions, technical assistance, and general sharing of wisdom and ideas: David S. Morgan, Mary C. Hill, Leonard L. Orzol, Daniel T. Snyder, Henry M. Johnson, and Claire Tiedeman.

GROUND-WATER HYDROLOGY

Geologic Framework

The stratigraphic and structural framework of the upper Deschutes Basin influences many aspects of ground-water recharge, flow, and discharge. Episodic volcanic activity in the region over the past several million years has resulted in a variety of volcanic, volcaniclastic, and volcanically derived sedimentary deposits (fig. 3). Volcanic activity and subsequent redeposition and alteration of some deposits have produced strata with a wide range of permeability.

Most ground water in the upper Deschutes Basin originates as recharge from precipitation on Quaternary deposits of the Cascade Range and Newberry Volcano (fig. 3). These deposits are highly permeable, and the fractured character of the lava flows facilitates rapid infiltration of precipitation and snowmelt and movement of ground water to lower elevations. Additional recharge occurs from leakage along sections of unlined irrigation canals near Bend constructed on lava flows from Newberry Volcano. Deposits of the Cascade Range and Newberry Volcano overlay or abut the Deschutes Formation and age-equivalent deposits.

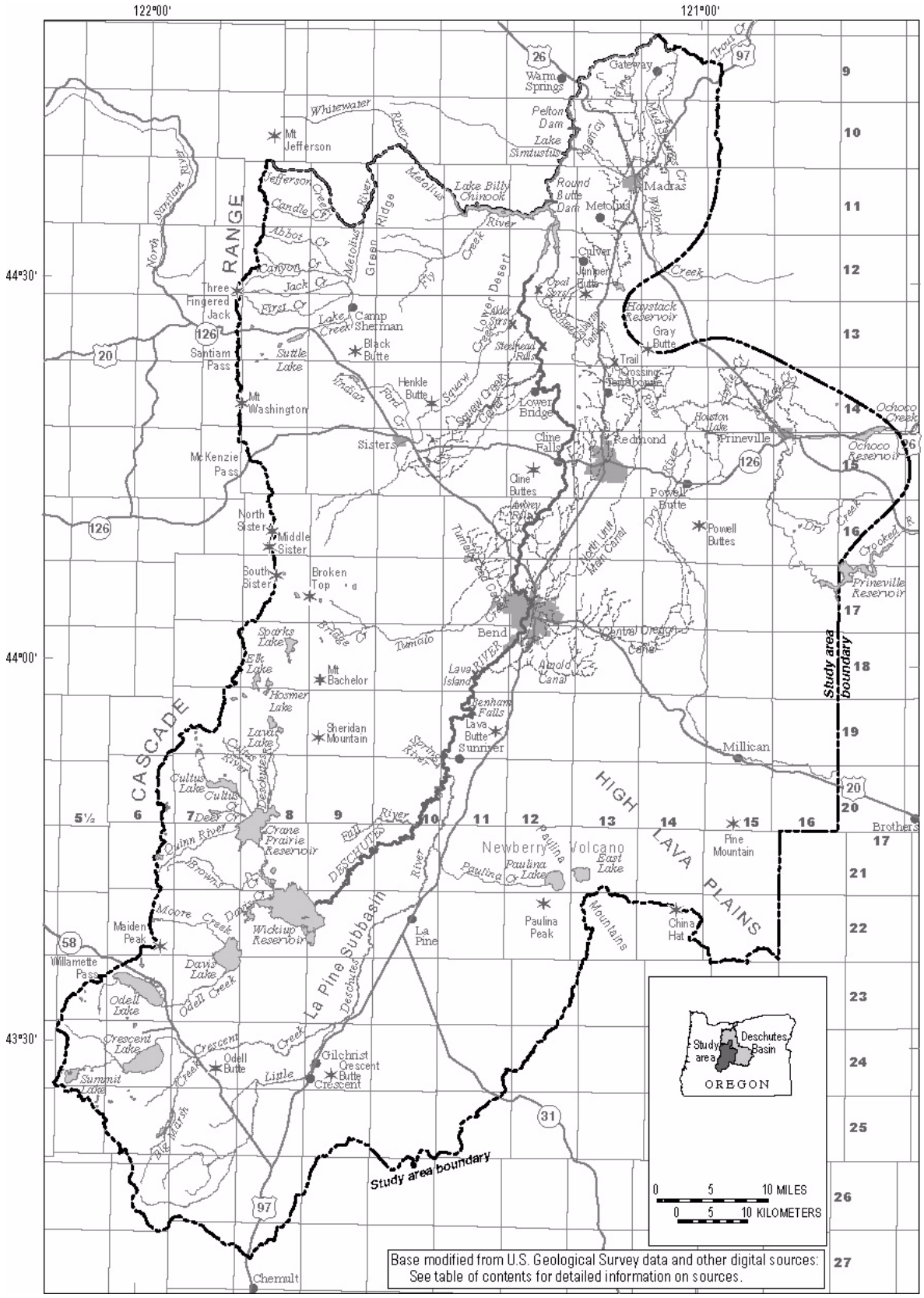

Figure 1. Location of the upper Deschutes Basin, Oregon, and major geographic and cultural features.

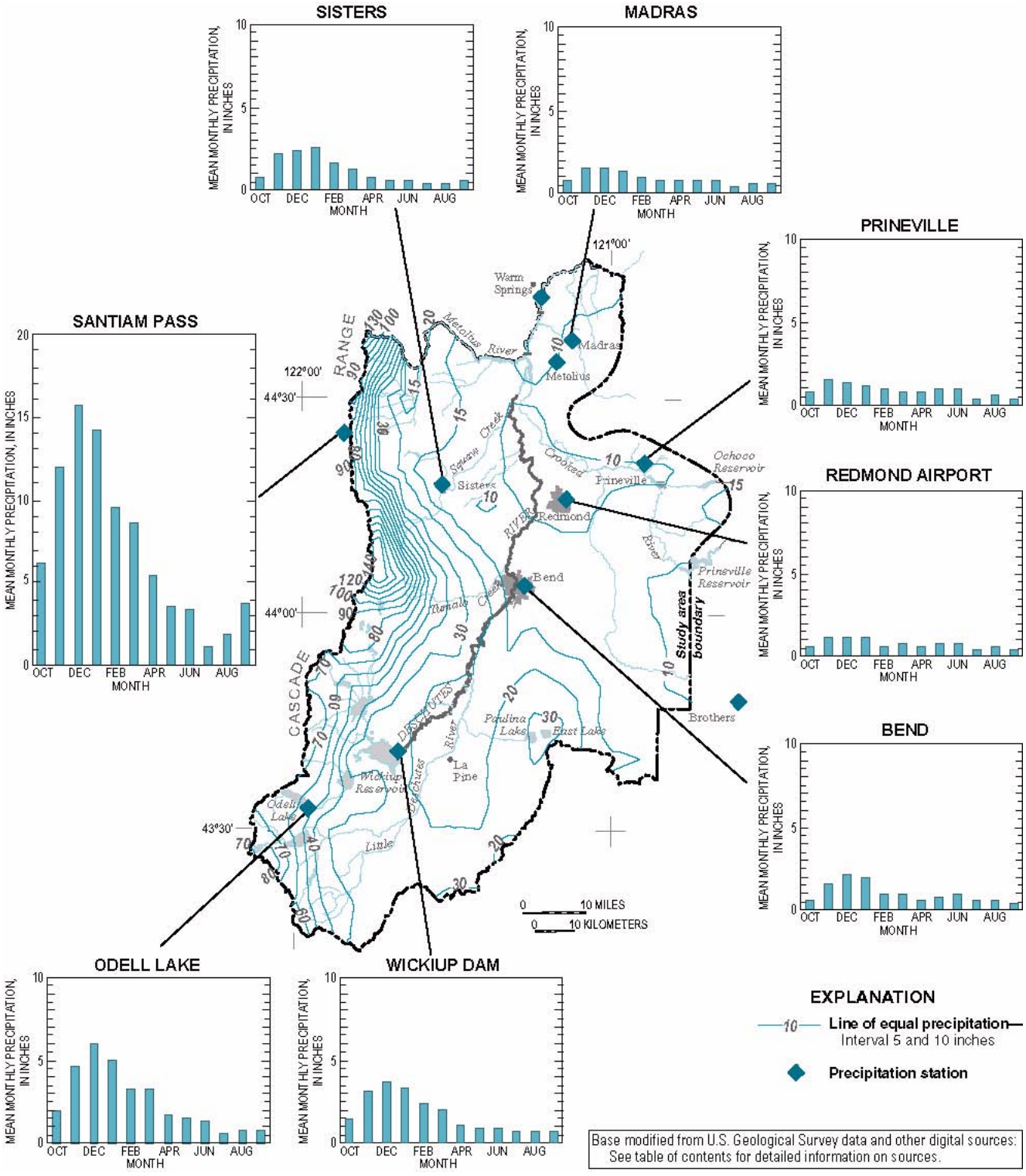

Figure 2. Lines of equal mean annual precipitation in the upper Deschutes Basin and graphs showing mean monthly precipitation at selected precipitation stations.

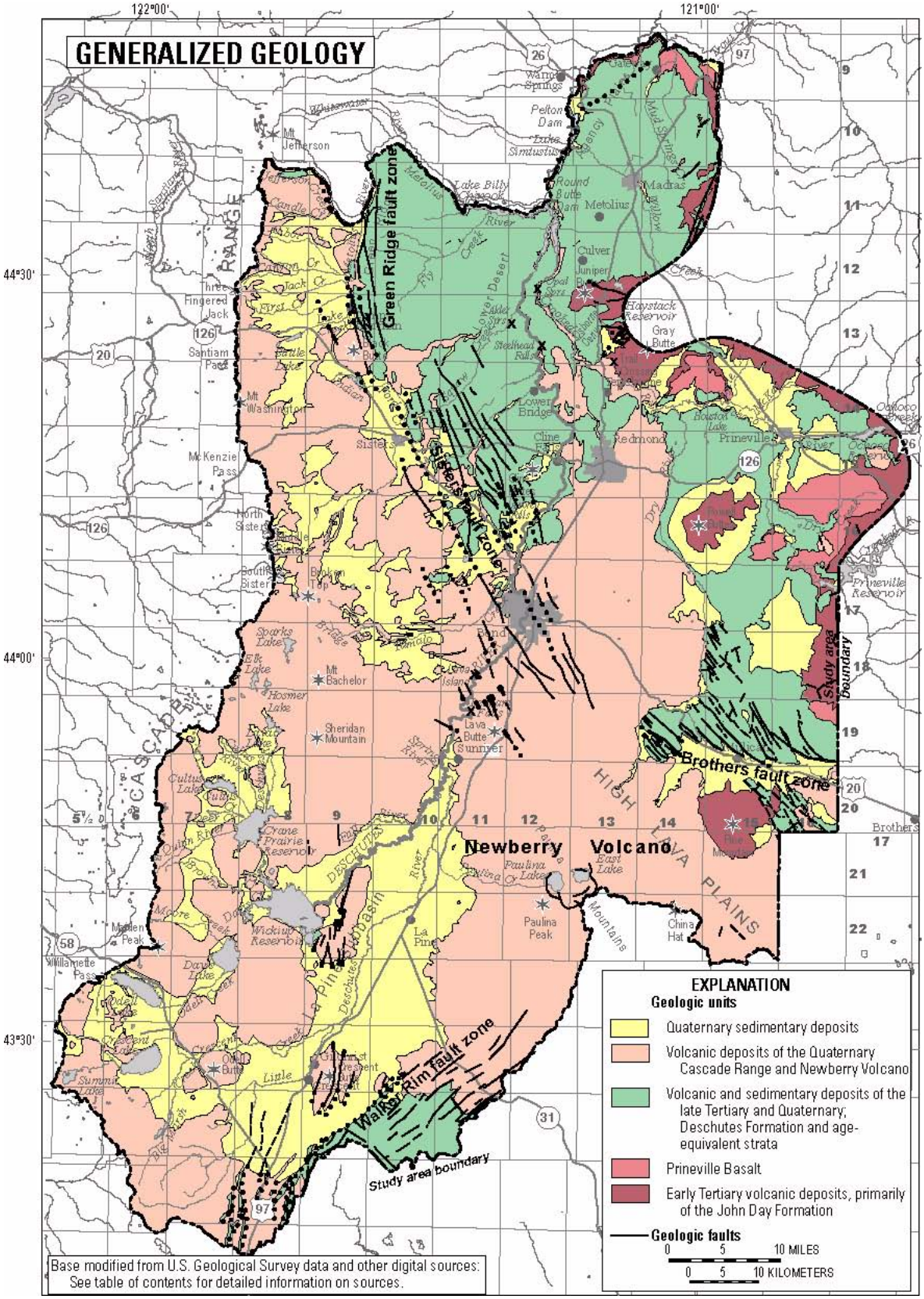

Figure 3. Generalized geology and hydrogeologic units of the upper Deschutes Basin.

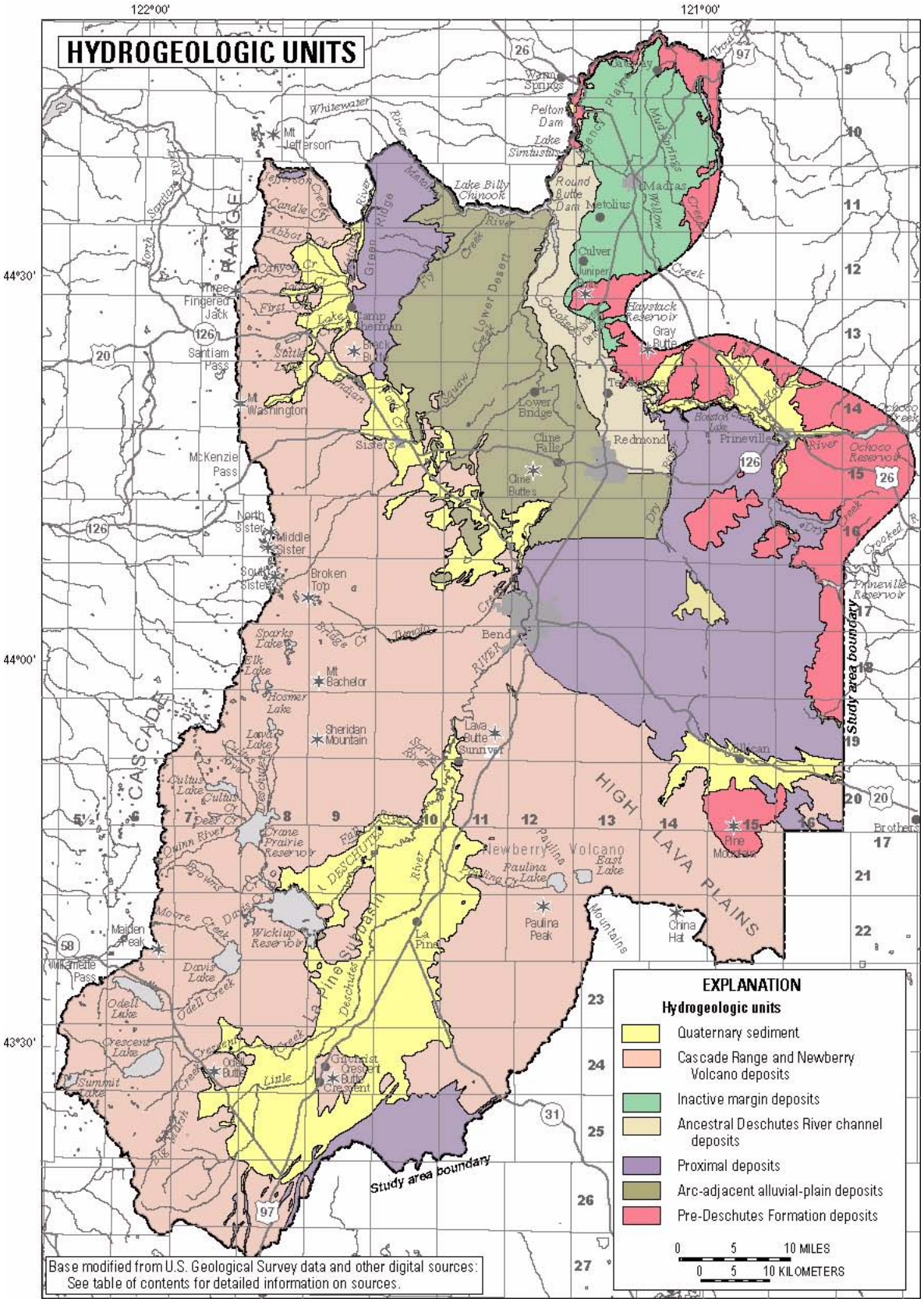

Figure 3. Generalized geology and hydrogeologic units of the upper Deschutes Basin—Continued.

Several saturated Quaternary-age sedimentary deposits occur within the study area (fig. 3). Pleistocene to Holocene sedimentary deposits resulted from several processes, including mass wasting of upland deposits, alluvial deposition by high-energy streams, deposition in low-energy streams and lakes, and glaciation. These sedimentary deposits are locally a few hundred feet thick. The La Pine subbasin occupies a complex graben structure where up to 1,000 feet of sediment has accumulated.

The Deschutes Formation and age-equivalent deposits (fig. 3) are generally highly permeable and are the most widely used ground-water bearing units in the study area. The Deschutes Formation consists of a variety of volcanic and sedimentary deposits ranging in age from late Miocene (~7.5 million years) to Pliocene (~4.0 million years). Smith (1986) described distinct depositional environments and volcanic facies within the Deschutes Formation. The differentiated facies have shown to be useful hydrogeologic subdivisions. These include sedimentary deposits of an arc-adjacent alluvial plain, the ancestral Deschutes River, and an inactive basin margin, as well as proximal volcanic deposits that are chiefly lava flows. Ancestral Deschutes River deposits and some units within an arc-adjacent alluvial plain are among the highest yielding units within the Deschutes Formation, with some wells producing thousands of gallons per minute. Opal Springs basalt, Pelton basalt, and a rhyodacite dome complex near Steelhead Falls are particularly productive subunits within the Deschutes Formation and provide tens to hundreds of cubic feet per second of ground-water discharge to the Deschutes and Crooked Rivers, upstream of Round Butte Dam.

The Prineville Basalt (fig. 3), which locally underlies the Deschutes Formation, is the oldest stratigraphic unit that bears substantial water in the upper Deschutes Basin. The Prineville Basalt is a series of middle Miocene lava flows that have a maximum thickness of nearly 700 feet near Bowman Dam (Smith, 1986). The unit occurs only locally near the eastern and northern boundaries of the upper Deschutes Basin study area. Wells constructed into water-bearing zones within the Prineville Basalt typically yield amounts that are inadequate for irrigation but are suitable for domestic and stock uses.

The oldest rock unit in the upper Deschutes Basin study area, the John Day Formation (fig. 3), is a sequence of upper Eocene to lower Miocene volcanic and sedimentary rocks. Weathering and alteration of the rocks has resulted in very low permeability; consequently, the unit forms the hydrologic basement for the regional ground-water flow system throughout much of the area and the lateral flow boundaries to the east and north.

Hydrothermal alteration and secondary mineralization at depth below the Cascade Range and Newberry Volcano has drastically reduced the permeability of the material at depth in those regions, effectively restricting most ground water to the strata above the altered rocks. The top of the hydrothermally altered region is considered the base of the regional ground-water system beneath the Cascade Range and Newberry Volcano. These boundaries are discussed in more detail in subsequent sections.

Structural features influence ground-water flow within the upper Deschutes Basin mainly by juxtaposing materials with contrasting permeability. Several depositional centers have formed along the base of fault-line scarps or in grabens within the study area, and the infilling sedimentary deposits have permeability that differs from that of the surrounding rocks.

Geologic units in the Deschutes Basin were divided into seven hydrogeologic units by Lite and Gannett (2002) (fig. 3). In some instances, the units correspond to existing stratigraphic divisions. In other instances, hydrogeologic units correspond to different facies within a single stratigraphic unit or formation. The hydrogeologic units include Quaternary sedimentary deposits, volcanic deposits of the Quaternary Cascade Range and Newberry Volcano, four zones corresponding to depositional facies within the late Tertiary and Quaternary Deschutes Formation and age-equivalent strata, and pre-Deschutes-age strata including the Prineville Basalt and John Day Formation.

Ground-Water Flow

The ground-water hydrology of the upper Deschutes Basin is described in detail by Gannett and others (2001), who built on the earlier works of Russell (1905), Stearns (1931), and Sceva (1960, 1968). Regional ground-water flow in the upper Deschutes Basin is primarily controlled by the distribution of recharge, the geology of the area, and the location and elevation of streams. Ground water flows from the principal recharge areas in the Cascade Range and Newberry Volcano toward discharge areas along the margin of the Cascade Range and near the confluence of the Deschutes, Crooked, and Metolius Rivers (fig. 4).

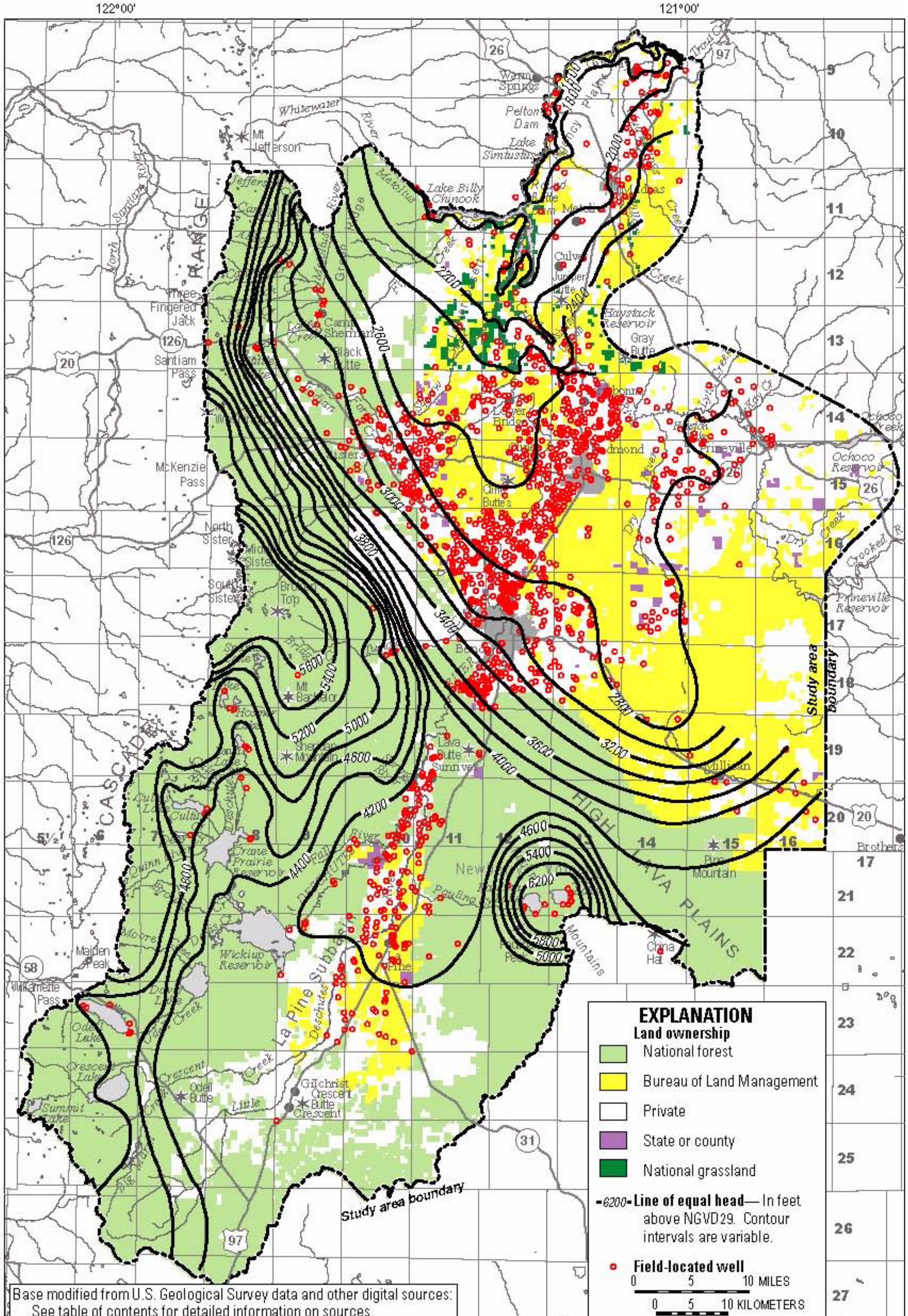

Figure 4. Generalized lines of equal head, locations of field-inventoried wells, and land ownership in the upper Deschutes Basin. (Generalized lines of equal head represent average conditions and are based on static water-level measurements in wells made during different periods and on spring and stream elevations.)

At the regional scale, the distribution of recharge mimics that of precipitation. The annual precipitation rate shows considerable geographic variation throughout the upper Deschutes Basin (fig. 2). The Cascade Range, which constitutes the western boundary of the basin, locally receives in excess of 200 in/yr, mostly as snow. The central part of the study area, in contrast, typically receives less than 10 in/yr. The young Quaternary volcanic deposits and thin soils in the Cascade Range allow rapid infiltration of much of the rain and snowmelt, making the Cascades the locus of ground-water recharge for the basin. The 1993 to 1995 average annual rate of recharge from precipitation basinwide is about 3,500 ft^3/s (cubic feet per second) (Gannett and others, 2001). Precipitation provides relatively little ground-water recharge in the low-elevation areas in the central part of the basin; however, leaking irrigation canals (fig. 1) are locally a significant source of recharge. It is estimated that 46 percent of the water diverted for irrigation is lost through canal leakage (Gannett and others, 2001). The average annual rate of leakage from irrigation canals during 1994 was estimated to be 490 ft^3/s. Part of the ground water recharged in the Cascade Range discharges to spring-fed streams at lower elevations in the range and along margins of adjacent lowlands. The remaining ground water continues in the subsurface toward the central part of the basin, where most of it discharges to the Deschutes, Crooked, and Metolius Rivers in the vicinity of their confluence.

The principal ground-water fed streams along the topographic margin of the Cascade Range include the upper Deschutes River and its tributaries above Wickiup Reservoir, Fall and Spring Rivers farther downstream, and the upper Metolius River and its tributaries. Combined ground-water discharge along the margin of the Cascade Range is estimated to average about 2,600 ft^3/s, which is roughly one-half the total ground-water discharge of the upper Deschutes Basin (Gannett and others, 2001).

Stream gains and losses along the Deschutes and Little Deschutes Rivers in the La Pine subbasin east of the Cascade Range are small, indicating relatively little net exchange between ground water and surface water. North of Sunriver, however, the northward slope of the water table is larger than the slope of the land surface, so depths to ground water generally increase northward toward Bend (fig. 4). In this same reach, however, water is diverted from the Deschutes River into unlined irrigation canals. The combination of leakage from canals, and perhaps from the river itself, supports local shallow, possibly perched, saturated zones that leak water back to the river. Data from several stream gages operated along the Deschutes River between Benham Falls and Bend from 1944 to 1953 (Oregon Water Resources Department, 1965) show that this reach contains both losing and gaining segments. Between Benham Falls and Lava Island, the Deschutes River consistently loses about 84 ft^3/s (Gannett and others, 2001). The reach between Lava Island and the mill pond in Bend gains about 46 ft^3/s. The river then loses about 50 ft^3/s between the mill pond and the gage below Bend. The net loss between Benham Falls and Bend indicated by the 1944 to 1953 data is 88 ft^3/s. This is consistent with the 89 ft^3/s loss indicated by long-term record (1945–95) available from gages at Benham Falls and below Bend.

The Deschutes and Crooked Rivers have incised canyons in the northern part of the study area. The canyons become increasingly deep northward toward Lake Billy Chinook, reaching depths of several hundred feet below the surrounding terrain. About 10 to 15 miles above their confluence, the canyons of the Deschutes and Crooked Rivers are of sufficient depth to intersect the regional water table, and both streams gain flow from ground-water discharge. Streamflow measurements show that the Deschutes River and lower Squaw Creek combined gain about 400 ft^3/s from ground-water discharge in this area prior to entering Lake Billy Chinook, and the lower Crooked River gains about 1,100 ft^3/s before entering the lake. Ground-water discharge to Lake Billy Chinook is roughly 420 ft^3/s. The total ground-water discharge in the confluence area is approximately 2,300 ft^3/s. This ground-water discharge, along with the 1,200 to 1,400 ft^3/s flow of the Metolius River (which is predominantly ground-water discharge during the dry season), makes up virtually all the flow of the Deschutes River at Madras during the summer and early fall.

Geologic factors are the primary cause of the large ground-water discharge in the confluence area. The permeable Neogene deposits, through which nearly all regional ground water flows, become increasingly thin northward as the low-permeability John Day Formation nears the surface. The John Day Formation crops out in the Deschutes River canyon about 10 miles north of Lake Billy Chinook near Pelton Dam, marking the northern extent of the permeable regional aquifer system. Most of the

regional ground water in the upper basin discharges to the Deschutes and Crooked Rivers south of this location. There is no appreciable ground-water discharge directly to the Deschutes River downstream of this point, and the small gains in streamflow that do occur result primarily from tributary inflow.

Ground-water head elevations and ground-water discharge fluctuate in the Deschutes Basin primarily due to decadal climate cycles (Gannett and others, 2001). Ground-water levels in the Cascade Range fluctuate in excess of 20 feet in response to climate cycles. Ground-water discharge varies similarly in response. For example, August mean ground-water discharge to the Deschutes River between Bend and Culver varied over 100 ft^3/s between 1962 and 1997 due to climate cycles. Ground-water discharge to the Metolius River, based on October mean flows, varied over 400 ft^3/s from 1962 to 1997. Combined, climate-driven ground-water discharge fluctuations could account for variations in late-season monthly mean flows of the Deschutes River at Madras on the order of 1,000 ft^3/s (Gannett and others, 2001). Head elevations also fluctuate in response to local stresses such as canal operation and stream-stage variations.

Hydraulic Characteristics

The hydraulic characteristics considered in this section include horizontal and vertical hydraulic conductivity and storage coefficients. Sources of information on the hydraulic characteristics of subsurface materials in the Deschutes Basin include water-well reports (well logs), aquifer tests, and the literature. Information from each of these sources is discussed in the following paragraphs. Both horizontal and vertical hydraulic conductivity are considered. In the following discussion, the term "hydraulic conductivity" with no modifier refers to horizontal hydraulic conductivity. Hydraulic conductivity in the vertical direction is specifically referred to as *vertical hydraulic conductivity*.

Horizontal Hydraulic Conductivity

There is no evidence that horizontal hydraulic conductivity varies with direction at scales of concern in this study. Therefore, horizontal isotropy is assumed. Well logs filed with the State by drillers typically contain specific-capacity tests that can provide information on hydraulic-conductivity values. The methodologies for determining hydraulic-conductivity values from specific-capacity tests contain numerous assumptions that are seldom met, so the values are, at best, rough estimates. Regardless, specific-capacity tests are often used to determine patterns of spatial distribution of hydraulic conductivity for models.

Specific-capacity tests from well logs were of only limited use in the upper Deschutes Basin for two principal reasons. The first problem is that the distribution of wells is uneven both horizontally and vertically, with the majority of wells clustered in the shallowest parts of the flow system in the center part of the study area (fig. 4). The second problem stems from variability in the data. The specific capacity of a single well can vary with the pumping rate due to well inefficiency. Moreover, apparent specific capacities of different wells in the same aquifer can vary due to geologic heterogeneity, different well completion techniques, and pump-test methods. This means that there can be large variations in specific-capacity data from a single geologic unit. These variations are not randomly distributed spatially because controlling factors, such as well types and test methods, are not randomly distributed but may vary systematically with, for example, land-use patterns or working areas of particular drillers. The uneven distribution and large variability in the specific-capacity data precluded their use for creating a detailed map of hydraulic-conductivity distribution. These data were useful, however, in evaluating large-scale patterns in hydraulic conductivity.

Gannett and others (2001) presented an analysis of specific-capacity data from well logs in which only domestic wells were considered in order to minimize the variance that would have been introduced by including large-yield irrigation and municipal wells. Large-scale patterns, on the order of 10 miles, appear to be consistent with geologic factors occurring at equivalent scales. Specific-capacity data show that within the Deschutes Formation, hydraulic conductivities are relatively low along the eastern margin of the basin in areas roughly correlative with the inactive margin facies of Smith (1986) (fig. 3). Data also show that, in general, hydraulic conductivities are lower in the La Pine subbasin aquifers than in the Deschutes Formation to the north.

Aquifer tests are another source of hydraulic-conductivity estimates. Four tests conducted as part of this study, as well as several preexisting tests, were

analyzed to estimate hydraulic conductivity in parts of the basin. In addition, several tests conducted by consultants were also available. The aquifer tests are summarized in Gannett and others (2001). Many of these tests are discussed in the context of geologic units in Lite and Gannett (2002). The analyses of most tests were complicated by very high transmissivity values that resulted in very small drawdowns. Drawdowns in observation wells were commonly too small to resolve, even with pumping rates on the order of 100 to 1,000 gal/min (gallons per minute).

The small number of aquifer tests precludes developing a detailed spatial distribution of hydraulic conductivity. However, the tests provide good estimates of hydraulic characteristics of certain rock types at specific locations, provide insight into the likely conditions in similar geologic settings in the basin, and constrain the overall range of probable values. Tests in volcanic deposits dominated by basaltic lava and scoria of the Deschutes Formation and age-equivalent units yielded hydraulic-conductivity estimates of 14 ft/d (feet per day) to 2,300 ft/d (1.6×10^{-4} to 2.7×10^{-2} ft/s [feet per second]). Hydraulic-conductivity estimates from tests in sedimentary strata ranged from 16 to 150 ft/d (1.9×10^{-4} to 1.7×10^{-3} ft/s). Aquifer testing of the City of Redmond Well Number 3, which produces from both volcanic and fluvial strata, yielded estimates ranging from 1,500 to 2,300 ft/d (1.7×10^{-2} to 2.7×10^{-2} ft/s). Although the small number of tests precluded any detailed assessment of the spatial distribution of hydraulic conductivity, aquifer-test results are consistent with the regional pattern in estimates derived from specific capacity, described previously, and with expectations based on the distribution of geologic facies within the basin.

The published literature is the third source of information on hydraulic characteristics used in this study. Literature values include those presented in general references as typical for particular rock types and those specific to the Deschutes Basin. Values from general references are usually presented as broad ranges, often spanning several orders of magnitude, for particular rock types. The ranges are usually too broad to be of much use, other than indicating the range of possible values. For example, Freeze and Cherry (1979, p. 29) show a range of 5 orders of magnitude for "permeable basalt": 4×10^{-2} to 6×10^{3} ft/d (5×10^{-7} to 7×10^{-2} ft/s). If unfractured basalt is included, the lower limit is 10^{-8} ft/d (10^{-13} ft/s), extending the overall range to 11 orders of magnitude. Hydraulic-conductivity values given for sedimentary deposits ranging from silt to gravel span 9 orders of magnitude, from approximately 2.6×10^{-4} to 2.6×10^{5} ft/d (3×10^{-9} to 3 ft/s).

Outside of this study, there are few published hydraulic-conductivity estimates for the upper Deschutes Basin, and these are average values given to represent regions within the basin. In work covering all of eastern Oregon, Gonthier (1985) estimated hydraulic conductivity for two generalized geologic units in the upper Deschutes Basin (basin-fill and alluvial deposits, and volcanic and sedimentary deposits) using the literature and specific-capacity data. Ranges of estimated hydraulic conductivity given are 25 to 150 ft/d (2.9×10^{-4} to 1.7×10^{-3} ft/s) for the basin-fill and alluvial deposits and 10 to 500 ft/d (1.2×10^{-4} to 5.8×10^{-3} ft/s) for the volcanic and sedimentary deposits. Bolke and Laenen (1989) estimated hydraulic conductivity from specific-capacity data from the Warm Springs Indian Reservation. They estimate that the hydraulic conductivity of alluvium ranges from 100 to 1,000 ft/d (10^{-3} to 10^{-2} ft/s) and give a range of 0.1 to 0.01 ft/d (10^{-7} to 10^{-8} ft/s) for John Day Formation strata. Lite and Gannett (2002) described the regional geology and volcanic-facies distribution in the upper Deschutes Basin and placed the overall large-scale hydraulic-conductivity distribution in a geologic context.

There are very few direct measurements of hydraulic conductivity in the Cascade Range, and most knowledge of the large-scale permeability structure there is inferred from geothermal-gradient measurements and heat-flow studies. In simulating groundwater flow and heat transport in the Cascade Range, Ingebritsen and others (1992) estimated the permeability of rocks younger than 2.3 Ma (mega annum, or million years before present) to be about 10^{-13} ft^2 (10^{-14} m^2), which is equivalent to a hydraulic conductivity of about 0.018 ft/d (2.1×10^{-7} ft/s) assuming a water temperature of 5°C. The permeability of rocks with ages between 4 and 8 Ma was estimated to be 5.4×10^{-15} ft^2 (5.0×10^{-16} m^2) which is equivalent to a hydraulic conductivity of about 9.1×10^{-4} ft/d (1.1×10^{-8} ft/s). Higher near-surface permeability, on the order of 10^{-14} to 10^{-12} m^2 (.018 to 1.8 ft/d), was required in their simulation to match groundwater recharge estimates. Higher near-surface permeabilities are also suggested by well-test data. A specific-capacity test of a well near Mount Bachelor (18S/09E-20BDA) yielded a hydraulic-conductivity estimate of 9 ft/d (1.0×10^{-4} ft/s).

Blackwell and Priest (1996) suggested that the heat-transport pattern in the Cascade Range is predominantly conductive, indicating that the permeability in all but the youngest rocks below a depth of about 330 to 990 feet (100 to 300 meters) is orders of magnitude lower than the estimates of Ingebritsen and others (1992). They also suggested that ground-water flow at velocities sufficient to affect heat flow is restricted to local regions, except in the 0 to 1,600 feet (0 to 500 meters) depth range in the high Cascade Range. The volume of water moving through low-permeability strata at depths greater than 1,600 feet in the Cascade Range is sufficiently small to be considered negligible compared to the overall ground-water budget, and these low-permeability strata are considered in this study to be the base of the regional ground-water flow system. The younger, permeable near-surface strata in the Cascade Range are included in the regional ground-water flow model.

Mathematical modeling of ground-water discharge to spring-fed streams in the Cascade Range by Manga (1996, 1997) yielded permeability values for near-surface rocks less than about 2.0 Ma of about 10^{-10} ft^2 (10^{-11} m^2), which equates to a hydraulic conductivity of about 18 ft/d (2×10^{-4} ft/s) assuming a water temperature of 5°C. This estimate is an order of magnitude larger than the upper value of Ingebritsen and others (1992) for near-surface rocks, where most ground-water flow occurs. The permeability estimates of Manga (1996, 1997) and Ingebritsen and others (1992) are considered to be a reasonable range of values for the younger, near-surface strata in the Cascade Range.

Well- and aquifer-test data are insufficient to allow continuous mapping of the distribution of hydraulic conductivity in the upper Deschutes Basin. Lite and Gannett (2002) delineated seven hydrogeologic units based on stratigraphy, facies distribution, and large-scale rock properties. These seven units provide a context in which to apply the aquifer-test data described above and provide the basis for the hydraulic-conductivity distribution in the model.

Vertical Hydraulic Conductivity

There were no direct measurements or estimates of vertical hydraulic conductivity available for the Deschutes Basin prior to this study. The only vertical hydraulic-conductivity estimates available for volcanic terranes in the Pacific Northwest were derived from modeling studies in the Columbia River Basalt Group and related strata.

Vertical and horizontal hydraulic-conductivity values are commonly related. The ratio of horizontal to vertical hydraulic conductivity, K_{xy} / K_z, is termed the vertical anisotropy. Values of vertical anisotropy vary widely with geologic settings, although vertical hydraulic conductivity is almost always less than horizontal. Anderson and Woessner (1992) state that vertical anisotropy ratios commonly range from 1 to 1,000. Studies in the Columbia River Basalt Group, however, suggest that vertical anisotropy ratios may be considerably larger than 1,000 in some volcanic terranes. Hansen and others (1994) found that vertical anisotropy ratios of 500 to 3,300 gave the best overall results in simulations of regional ground-water flow in the Columbia Plateau in Washington and northern Oregon. Packard and others (1996) found that vertical hydraulic-conductivity values ranging from 4.92×10^{-4} to 1.08×10^{-2} ft/d (5.7×10^{-9} to 1.25×10^{-7} ft/s) gave best simulation results, and that vertical anisotropy ratios ranged from 43 to 2,500. They related vertical anisotropy ratios to structural settings in their model area, and attributed the variations to differing interbed lithologies. Tanaka and others (1974) found that their best vertical head distributions were achieved using a vertical hydraulic-conductivity value for Columbia River basalt of 2×10^{-5} ft/d (2.3×10^{-10} ft/s). Although it is unclear how this figure was applied in their model parameterization, when compared to the range of horizontal transmissivity values they used it suggests that vertical anisotropy ratios may be as high as 10^4 to 10^6. Mac Nish and Barker (1976) suggest that horizontal hydraulic conductivity in the Columbia River basalt may be as large as 432,000 ft/d (5 ft/s) and that vertical hydraulic conductivity may be as small as 4.32×10^{-3} ft/d (5×10^{-8} ft/s), and that vertical anisotropy ratios may approach 10^9. No supporting information or references, however, are provided for these figures. Very large vertical hydraulic-head gradients occur in places in the upper Deschutes Basin, suggesting that large vertical anisotropy ratios occur at least locally.

Storage Coefficients

Measurements of storage coefficients of aquifers in the upper Deschutes Basin are scarce. This is not only because there are few aquifer tests, but the pumping responses in observation wells necessary to calculate storage coefficients are commonly too small to be

useful due to the large transmissivity values of the tested aquifers. Storage coefficients are available from two aquifer tests conducted as part of this study. The City of Madras Well 2, which produces from a confined sand and gravel aquifer, yielded a value of 10^{-4}. The test of the City of Redmond Well 3, which produces from both lava and interbedded sand and gravel, yielded values ranging from 5×10^{-2} to 6×10^{-2}. A third test conducted by a private consultant on the City of Redmond Well 4, which produces from sand and gravel, yielded a storage coefficient of 0.1.

MODEL DESCRIPTION

Ground-water flow in the upper Deschutes Basin was simulated using the U.S. Geological Survey modular three-dimensional finite-difference ground-water flow model (MODFLOW) developed by McDonald and Harbaugh (1988). MODFLOW is a versatile finite-difference modeling program used to construct numerical flow models of specific areas. A MODFLOW model consists primarily of a set of input files that contain information on the physical properties of the modeled system such as the geometry, boundary conditions, internal properties (such as the distribution of hydraulic conductivity and storage coefficients), and sources and sinks such as ground-water recharge, streams, and pumping wells. Once these files are created, the model program is run to solve a set of equations that describe the distribution of head at discrete points within the system and the flow in response to that head distribution.

Both steady-state and transient versions of the upper Deschutes Basin model were constructed. The steady-state model simulates the ground-water flow system as it would exist in equilibrium with a given set of conditions. The transient model simulates the ground-water flow system as it would change in response to varying conditions.

Governing Equations and Model Code

The movement of ground water through porous media is described by the following partial differential equation, which is based on Darcy's law and the conservation of mass (McDonald and Harbaugh, 1988):

$$\frac{\partial}{\partial x}\left(K_{xx}\frac{\partial h}{\partial x}\right) + \frac{\partial}{\partial y}\left(K_{yy}\frac{\partial h}{\partial y}\right) + \frac{\partial}{\partial z}\left(K_{zz}\frac{\partial h}{\partial z}\right) - W = S_s\frac{\partial h}{\partial t} \quad (1)$$

where

K_{xx}, K_{yy}, and K_{zz} are values of hydraulic conductivity in the x, y and z directions along Cartesian coordinate axes, which are assumed to align with principal directions of hydraulic conductivity (LT^{-1}),

h is hydraulic head (L),

W is a volumetric flux per unit volume and represents sinks and/or sources (T^{-1}),

S_s is the specific storage of the porous material (L^{-1}), and

t is time (T).

Equation (1) describes the distribution of hydraulic head and flow throughout a continuous region. Derivations of equation (1) can be found in Freeze and Cherry (1979) and Anderson and Woessner (1992). As mentioned previously, there is no evidence of horizontal anisotropy in the upper Deschutes Basin, therefore K_{xx} and K_{yy} are considered to be equal at any given location and K_{xx} and K_{yy} are replaced in this discussion by the single term K_{xy} to describe horizontal hydraulic conductivity.

Equation (1) is continuous in space and time, and generally cannot be solved analytically for practical applications involving complex systems. In practice, numerical methods are employed in which the continuous system described by equation (1) is replaced by a set of spatially and temporally discrete points in a process known as discretization. Equation (1) is then replaced by a set of simultaneous algebraic equations that describe the distribution of hydraulic head at each point, and flow through the system in response to this head distribution. These simultaneous equations are set up in matrix form and then solved. A variety of techniques are available to solve the set of simultaneous equations. In this application, the preconditioned conjugate-gradient method of Hill (1990) was used. Discussions of the numerical technique used in this study, the finite-difference method, can be found in McDonald and Harbaugh (1988) and in Anderson and Woessner (1992).

Discretization

The numerical method used to approximate equation (1) requires that the modeled domain be divided into discrete volumes, called cells. The three-dimensional array of cells is known as the *model grid*. The center of each cell defines the point for which

hydraulic head is determined. The head is taken to represent the average head within the cell. For transient models, time must also be divided into discrete intervals known as *time steps*. Heads and flows are calculated at the end of each time step.

Spatial Discretization

The regional ground-water flow system of the upper Deschutes Basin was represented as an array of cells arranged in 127 east-west trending rows, 87 north-south trending columns, and 8 layers. The lateral dimensions of the cells range from 2,000 feet to 10,000 feet on a side (fig. 5). The smaller cells coincide with areas where the most hydrologic data are available; generally, the more densely populated parts of the study area, where wells are numerous. The area of smallest cells also corresponds to the main area of ground-water discharge to streams, which is an area of particular interest to resource managers. The larger cells coincide with areas where hydrologic data are scarce; generally, unpopulated areas, where few wells have been drilled. Because the finite-difference model grid must be rectangular, certain cells may represent areas outside the modeled area (which can have any shape). Such cells are considered inactive and the ground-water flow equation is not solved for them.

Eight layers were used in order to represent vertical changes in the geology and allow simulation of vertical head gradients. Each layer has a uniform thickness throughout the model. The upper five layers are 100 feet thick; underlying layers, in order of increasing depth, are 200, 300, and 800 feet thick. The top of the uppermost layer is coincident with the water table. As with the horizontal dimension, the vertical layer thicknesses are smallest where data are most plentiful, and largest where data are sparse. Near the lateral and lower boundaries of the model, where the aquifer system may be thin, the thicknesses of the lowermost layer may be less in places than indicated above. For numerical stability, all layers were simulated as though they were confined, meaning that saturated thickness, and consequently transmissivity, were held constant with respect to head. In reality, it is possible for saturated thickness and transmissivity to vary in the uppermost parts of the flow system as head changes. However, water-level monitoring data indicate that head fluctuations in the basin are small compared to model layer thicknesses, so the error introduced by modeling all layers as confined is considered insignificant.

Temporal Discretization

For transient models, numerical methods require that time also be divided into discrete intervals. The temporal divisions are determined by the timing of the stresses, such as recharge or pumping. Time is divided into *stress periods*, during which the stresses are assumed to remain constant. For example, the irrigation season, during which irrigation pumping occurs, may define a stress period. Stress periods are further subdivided into time steps as described below. The ground-water flow equations in the model are solved for each time step. For this study, ground-water flow in the upper Deschutes Basin was simulated for the 20-year period extending from 1978 to 1997. Each year was divided into two stress periods that were determined by the timing of recharge and irrigation pumping. The delineation of the stress periods is described in a later section. Each of the 40 stress periods was divided into 5 time steps. The 20-year simulation period, therefore, included 200 time steps.

Boundary Conditions

The ground-water flow system in the upper Deschutes Basin is controlled, to a large extent, by the hydrologic and geologic boundaries of the system. Boundary conditions define the geographic extent of the flow system as well as the movement of ground water into and out of the system, such as flow to or from streams.

Three types of boundary conditions were used to define the ground-water flow system in the upper Deschutes Basin: no-flow boundaries, specified-flux boundaries, and head-dependent flux boundaries. Geologic or hydrologic barriers to ground-water flow were simulated using no-flow boundaries. The contact between the permeable ground-water flow system and nearly impermeable bedrock is an example of a no-flow boundary. Known or estimated hydrologic fluxes, such as recharge and well discharge, are represented using specified-flux boundaries. A head-dependent flux boundary is one across which ground water moves at a rate proportional to the hydraulic-head gradient between the boundary and the ground-water system. Streams are usually represented as head-dependent flux boundaries because the movement of ground water to or from a stream is proportional to the difference between the head in the aquifer and the stage of the stream.

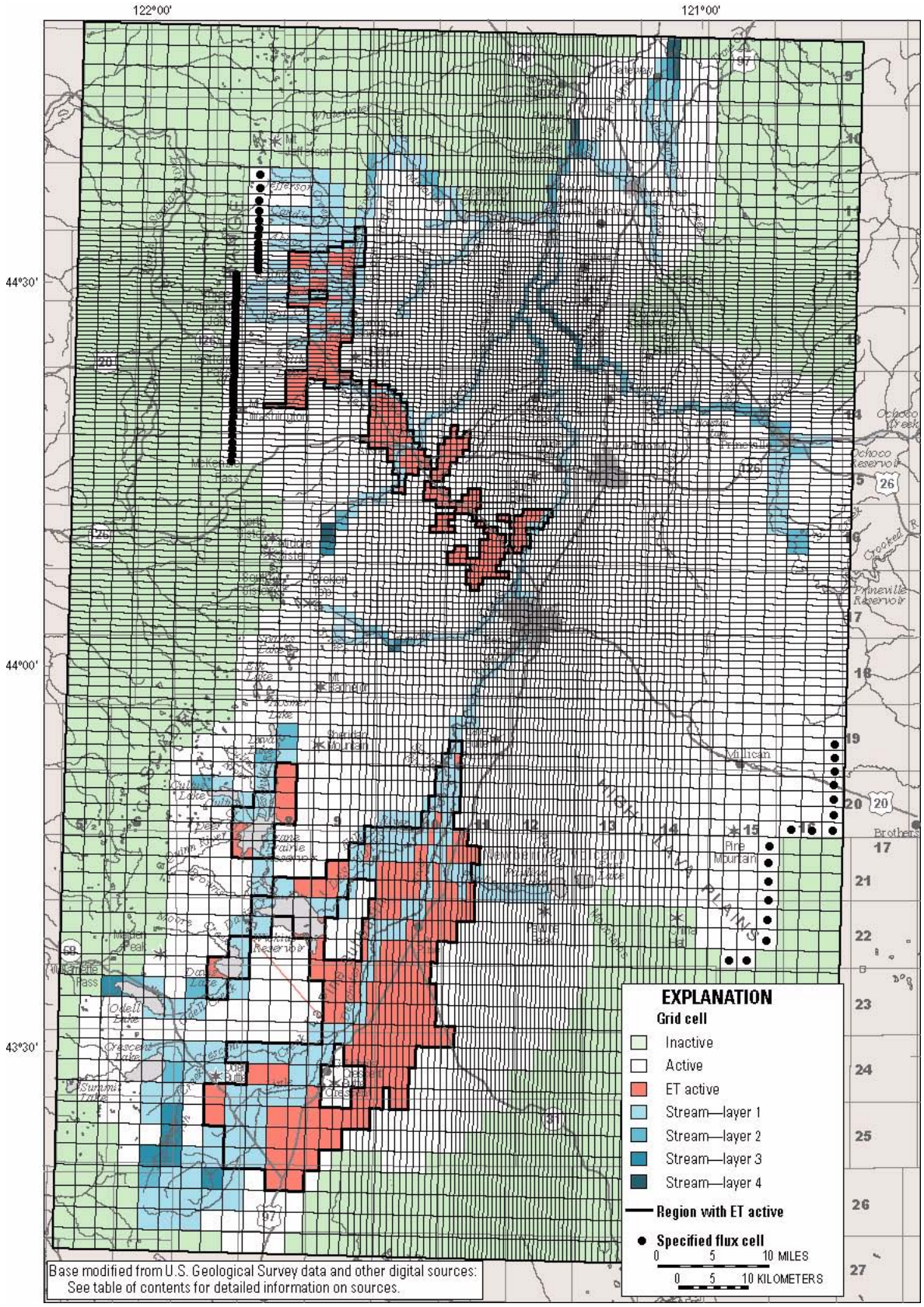

Figure 5. Model grid, boundary conditions, locations of stream cells, and regions where evapotranspiration is active. (ET, evapotranspiration)

For the purposes of this discussion, boundaries in the upper Deschutes Basin regional ground-water flow model are divided into two broad categories. The first group includes boundaries related to the geographic extent of the regional aquifer system, such as contacts with effectively impermeable rock units on the margin of the basin. The second group includes boundaries within the model extent related to hydrologic processes or features, such as stream systems.

Geographic Boundaries

The geographic boundaries of the upper Deschutes Basin regional ground-water model were chosen to correspond as closely as possible with natural hydrologic boundaries across which ground-water flow can be assumed negligible, such as ground-water divides, or can be reasonably estimated. Major topographic divides are often considered no-flow boundaries because topographic divides are typically coincident with ground-water divides. Ground water on either side of a ground-water divide flows away from the divide and not across it, so the divide itself acts as a no-flow boundary. Topographic divides often coincide with ground-water divides because upland areas commonly have larger amounts of precipitation and recharge than surrounding areas, so the water-table surface develops a coincident high-elevation region from which ground-water flow diverges.

Major streams can also act as no-flow boundaries, particularly if they are regional ground-water discharge points. In these circumstances, ground water flows toward and discharges to the stream from both sides but does not flow across the vertical plane extending downward from the stream. Streams may also coincide with no-flow boundaries when they flow parallel to ground-water flow, basically following ground-water flow streamlines. In situations such as this, ground water would not flow either toward or away from the stream. In some circumstances, however, the hydraulic-head distribution at depth beneath streams may be such that there is a component of regional ground-water flow at depth across the stream. Therefore, streams should be considered no-flow boundaries only when there is hydraulic-head information supporting their function as regional sinks, or when their orientation is parallel to ground-water flow.

The lateral boundaries of the upper Deschutes Basin flow model are generally represented as no-flow boundaries, with the exception of two areas where they are represented as specified-flux boundaries (fig. 5). The western boundary of the model coincides with the topographic crest of the Cascade Range. The distribution of precipitation along this western margin generally mimics the topography, with the highest precipitation occurring at the crest of the range. In the northern part of the western margin (the Metolius River subbasin), however, the area of maximum precipitation occurs west of the topographic divide (see Taylor, 1993). This suggests that there may be ground-water flow eastward beneath the crest of the Cascade Range, a phenomenon also indicated by the hydrologic budget of the Metolius River subbasin. Average ground-water discharge to the Metolius River in the study area above the gage near Grandview (station number 14091500, which is just upstream of Lake Billy Chinook) is approximately 1,300 ft^3/s, whereas the mean annual recharge from precipitation in the Metolius River subbasin above this point in the study area is approximately 500 ft^3/s (Gannett and others, 2001). The difference, 800 ft^3/s, must come from subsurface flow from an adjacent basin. Hydraulic-head gradients shown by Gannett and others (2001) indicate that the most plausible sources for this additional water are the upper Santiam and the North Santiam River Basins to the west. To simulate this probable interbasin ground-water flow and balance the hydrologic budget, a constant 800 ft^3/s flux is specified at the western boundary of the model in the Metolius River subbasin.

The northern boundary to the model is defined by the east-west segment of the Metolius River and the generally east-west trending Jefferson Creek. These streams generally parallel regional ground-water flow directions, and ground-water flow into or out of the model area from the adjacent area is considered to be negligible. This part of the model boundary is represented as a no-flow boundary.

North of the confluence of the Metolius and Deschutes Rivers, the western boundary of the model is defined by the Deschutes River. Hydraulic-head measurements and streamflow measurements by Bolke and Laenen (1989) indicate that the Deschutes River is a regional ground-water sink in this area. North of Pelton Dam, the river has cut down to the nearly impermeable John Day Formation. Regional ground-water flow across the Deschutes River north of the Metolius River confluence is unlikely, and it is therefore modeled as a no-flow boundary.

The eastern boundary of the model to south of Prineville Reservoir generally coincides with the contact between the permeable Deschutes Formation and older rocks of the John Day Formation which are, in general, nearly impermeable. The part of the boundary coinciding with the contact with John Day Formation is modeled as a no-flow boundary.

From south of Prineville Reservoir, through Millican and the China Hat area, the eastern model boundary does not coincide with either a topographic divide or a geologic contact. The region east of this area was excluded from the model because of the lack of subsurface hydrologic information, very low recharge, and distance from the areas of primary concern. Head data, however, indicate there is some flow across this boundary into the modeled area from the southeast. Therefore, this area was represented as a specified-flux boundary (fig. 5). The boundary flux was estimated using a variety of methods. The part of the Deschutes Basin east of this boundary is very dry (10 to 15 in/yr average annual precipitation) and has a poorly developed drainage system with no perennial streams. The divide between this part of the Deschutes Basin and the Fort Rock and Christmas Lake Basins to the south is poorly defined and interbasin flow is likely. Miller (1986) states that flow to the Deschutes Basin from the Fort Rock Basin "probably exceeds 10,000 acre-ft/yr" (acre feet per year) which equals about 14 ft^3/s. Estimates based on the Darcy equation using measured head gradients, and estimated hydraulic conductivity and aquifer thickness suggest that the flux into the modeled area could possibly be as high as 100 ft^3/s. Additional estimates were derived using a water-budget approach. The probable area contributing to the boundary flux was defined using hydraulic-head maps from the Deschutes Basin and the Fort Rock Basin from Miller (1986). Flux rates were calculated using a range of recharge values from Newcomb (1953), Miller (1986), and McFarland and Ryals (1991). Using a contributing area of 648 mi^2 and recharge estimates ranging from 0.5 to 3.0 in/yr, the boundary flux could range from 25 to 145 ft^3/s. The boundary flux in this region was ultimately set at a constant 48 ft^3/s (the figure using 1.0 in/yr recharge in the contributing area) because it provided the best fit to the head data during preliminary model calibration.

The southern model boundary coincides entirely with the drainage divides between the Deschutes Basin and the Fort Rock and Klamath Basins. It is represented as a no-flow boundary.

The lower boundary of the model corresponds to the contact of the permeable rocks of the Deschutes Formation, age-equivalent units, and younger strata, with underlying low-permeability rock units. The underlying low-permeability rocks correspond to either the John Day Formation or equivalent rocks, or to younger rocks in which the permeability has been nearly eliminated by hydrothermal alteration or secondary mineralization. The subsurface permeability structure is discussed in detail in Lite and Gannett (2002). This lower boundary of the model is simulated as a no-flow boundary.

Hydrologic-Process Boundaries

The second broad category of boundaries in the model are those related to hydrologic processes including recharge, ground-water flow to and from streams, evapotranspiration from the water table, and pumpage.

Ground-water recharge constitutes a specified-flux boundary condition. Recharge to the ground-water system from infiltration of precipitation, canal leakage, and deep percolation of applied irrigation water (on-farm loss) is simulated as a specified flux to the uppermost layer of the model. The specified flux varies from cell to cell. Recharge also varies with time, and is the largest factor influencing the transient behavior of the regional ground-water flow system. Therefore, the specified recharge flux to each uppermost cell is varied with time during the transient simulation.

The methods used to estimate recharge from all sources are described in detail in Gannett and others (2001). Recharge from precipitation was estimated using the Deep Percolation Model (DPM) of Bauer and Vaccaro (1987), which uses a variety of data to calculate a daily water balance. This technique yields daily estimates of recharge, but practical considerations require that these be aggregated into longer time periods. A graph of average monthly recharge from precipitation for the basin (fig. 6) shows a period of high recharge from November to April, and a period of low recharge from May to October.

Recharge from canal leakage was estimated by Gannett and others (2001) using diversion and delivery records from irrigation districts, canal-seepage measurements from the Oregon Water Resources Department and Bureau of Reclamation, and information on canal geology and geometry. Recharge from on-farm loss was estimated using information on irrigation deliveries, prevalent irrigation techniques, crop-type distribution, and evapotranspiration estimates.

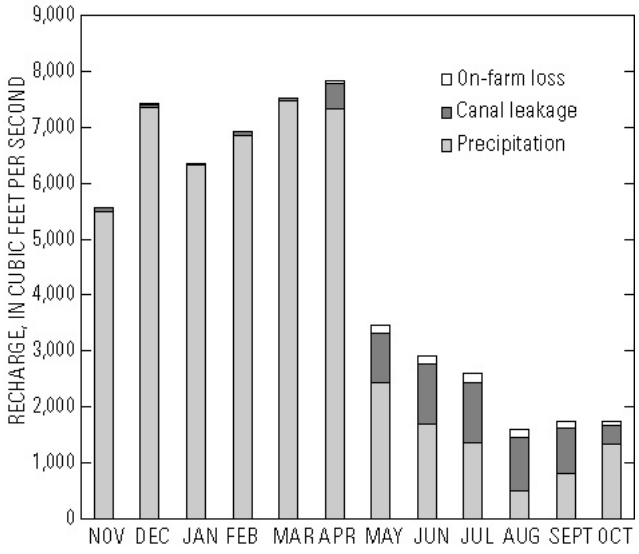

Figure 6. Mean monthly recharge from precipitation, canal leakage, and on-farm loss for 1978 to 1997.

Recharge from canal leakage occurs primarily during the irrigation season from April to October, with the highest rates from May to September (fig. 6). On-farm losses were determined by comparing consumptive use figures for specific crop types with information on water application rates and irrigation method efficiencies (Gannett and others, 2001). The timing of recharge from on-farm loss is similar to that of canal leakage, and is essentially the inverse of the timing of recharge from precipitation.

The temporal distribution of recharge was used to determine appropriate stress periods for the transient simulation. The timing of recharge from precipitation and canal leakage define two distinct periods during each year: a period of high recharge from precipitation and low recharge from canal leakage from November to April, and a period of lower recharge from precipitation and high recharge from canal leakage from May to October. Pumping stresses in the basin also match the semiannual stress periods. Municipal pumping is lowest and irrigation pumping is effectively zero during the November to April period. Municipal pumping increases and irrigation pumping occurs during the May to October period. In this report, we define a *model water year* that runs from November 1 to October 31. Recharge rates from precipitation, canal leakage, and on-farm loss are shown for each semiannual stress period from model water years 1978 to 1997 in figure 7.

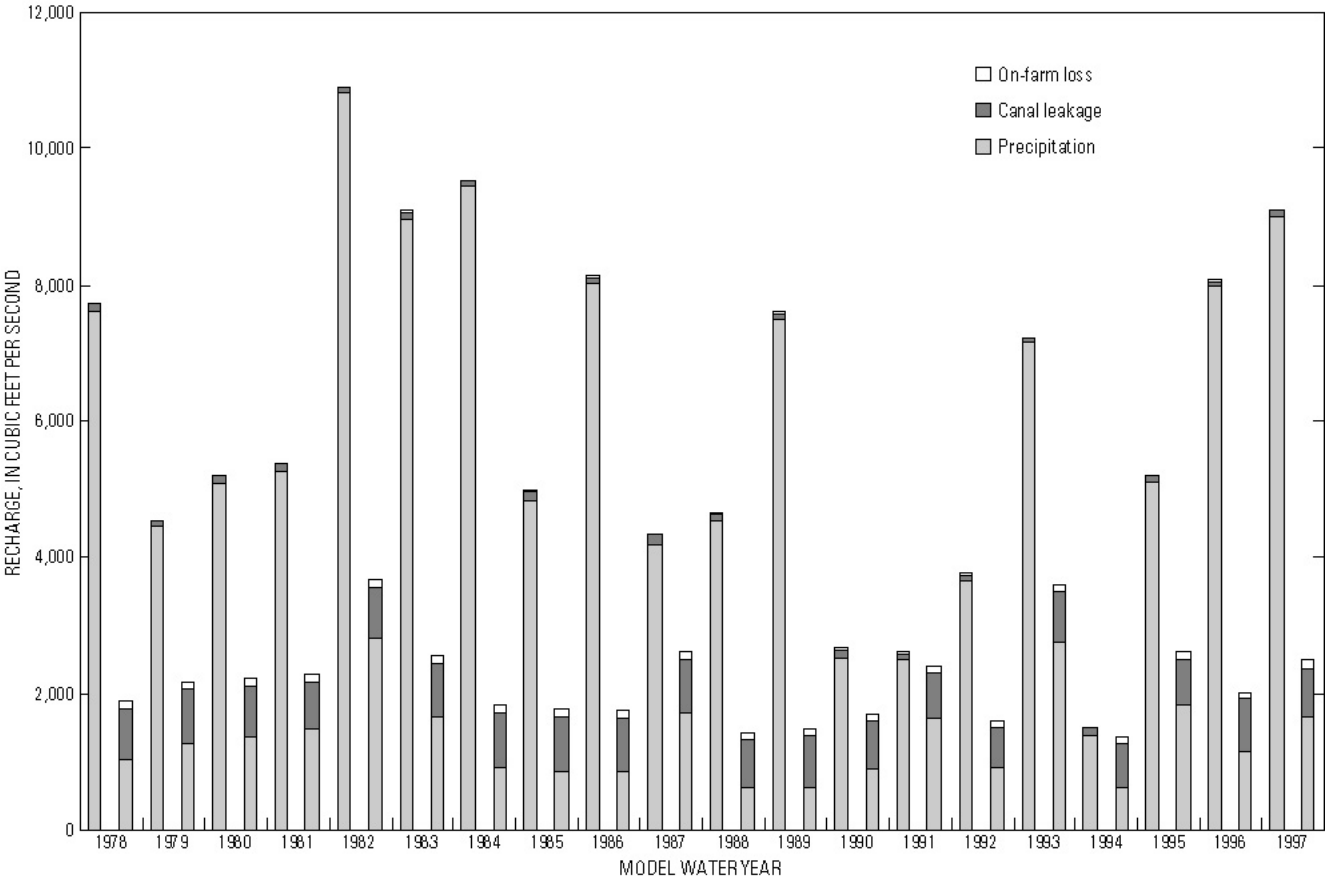

Figure 7. Recharge from precipitation, canal leakage, and on-farm loss for each semiannual stress period from 1978 to 1997.

The movement of ground water to and from streams is another important boundary condition. The flux of water between the ground-water system and streams is, in part, dependent on the hydraulic head in the ground-water system and is simulated as a head-dependent flux boundary. Cells in the model that correspond to the locations of major streams (fig. 5) are mathematically represented in a manner that allows ground water to move between the aquifer and stream with a direction and magnitude that depends on the head relations. Certain stream reaches were simulated in model layers 2, 3, or 4 where the stream elevation was substantially below that of the surrounding terrain, for example in an incised canyon (fig. 5). Streams were simulated using the streamflow-routing (STR1) module for MODFLOW by Prudic (1989).

The formula for calculating the flux of water between the ground-water system and streams is based on Darcy's law and is given by Prudic (1989) as

$$Q_l = CSTR(H_s - H_a) \qquad (2)$$

where

Q_l is leakage to or from the aquifer through the streambed, (L^3/T),

H_s is head in the stream, (L),

H_a is head in the aquifer, (L), and

CSTR is conductance of the streambed (L^2/T), which is the hydraulic conductivity of the streambed multiplied by the area of the streambed divided by its thickness.

The rate of ground-water flow to or from streams is proportional to the difference between the head in the stream and the head in the aquifer, and to the streambed conductance. If the head in the aquifer is greater than the head in the stream, then Q_l is negative, indicating flow from the aquifer to the stream; if the head in the aquifer is less than the head in the stream, then the flow is from the stream to the aquifer.

Cells in the model representing stream-aquifer relations (stream cells) are shown in figure 5. These include all major perennial streams and most perennial tributaries. Some stream cells actually represent multiple tributaries where the scale of the cell is large compared to the spacing of the streams. Parts of the Crooked River that flow on low-permeability bedrock are very poorly connected to the regional ground-water system and are not represented in the model. The movement of ground water to or from streams is a function of the head in the stream, H_s, also known as stream stage. Stream stage is the elevation of the water surface in the stream, and a single value must be chosen to represent the stream across the entire cell. Stream stages used in this simulation were determined by picking an approximate median stream elevation within the cell using USGS 1:24,000-scale topographic maps.

The streambed conductance, *CSTR*, controls the rate at which water moves to or from a stream in response to a given head gradient. Direct measurements of streambed conductance are rare and these terms are usually derived empirically during model calibration. As generally conceptualized, the streambed-conductance term is used to simulate a low-permeability streambed material that impedes the movement of water to or from the stream (McDonald and Harbaugh, 1988). This is a reasonable representation of losing streams in the upper Deschutes Basin, where sediment on the bottom of a stream and in fractures below the stream impede water leakage from the stream. It is not, however, a reasonable representation of many of the gaining reaches where water flows to the stream from springs emerging from open fractures at or above the elevation of the stream. In this case, there is no low-permeability layer impeding the exchange of water and the rate is controlled primarily by the permeability of the surrounding rock. Streambed-conductance terms were initially calculated using a streambed thickness of 10 feet, stream widths of 20 to 50 feet (depending on the stream size), and a vertical hydraulic conductivity of 0.5 to 5.0 ft/d. The hydraulic-conductivity value was then adjusted during model calibration.

Evapotranspiration can remove water from both the unsaturated and saturated zones. Evapotranspiration from the unsaturated zone is calculated and accounted for by the DPM. Evapotranspiration from the saturated zone occurs where certain plants (phreatophytes) transpire water directly from the water table. This occurs generally in areas where the water table is relatively close to land surface and within the rooting depth of plants. Evapotranspiration (ET) from the water table is represented by a head-dependent flux boundary condition in the model.

Evapotranspiration from the water table is simulated using the evapotranspiration (EVT) module for MODFLOW (McDonald and Harbaugh, 1988). Evapotranspiration is calculated assuming that when the head in the aquifer (the water-table elevation) is at or above a specified elevation known as the ET surface (generally taken to be land-surface elevation), evapotranspiration from the water table will occur at a specified maximum rate. When the water-table elevation falls below a specified depth, known as the extinction depth (generally corresponding to the maximum rooting depth of plants), evapotranspiration from the water table stops. When the water-table elevation is between the ET surface elevation and the extinction depth, evapotranspiration varies linearly from the maximum rate to zero depending on the water-table elevation.

The maximum evapotranspiration rate used in this simulation was based on information from the DPM. The DPM uses information on vegetation, soils, elevation, and climate to calculate the total potential evapotranspiration of an area as well as the actual evapotranspiration from the unsaturated zone. The difference between these two figures is the portion of the potential evapotranspiration not satisfied by evapotranspiration from the unsaturated zone. This residual evapotranspiration is the amount that could potentially be satisfied by evapotranspiration from the water table and is the figure used for the maximum evapotranspiration rate in the EVT module. The maximum evapotranspiration rate for the steady-state model was set at 2 ft/yr (feet per year). For the transient model, the maximum evapotranspiration rate varied with stress periods ranging from between zero and 1 foot during the winter, and up to 4 feet during the summer. The extinction depth used in the simulation to represent the maximum rooting depth of plants was 5 feet, which is within the range of 2 to 5 feet used for various land-cover types in the DPM (Boyd, 1996).

Evapotranspiration from the water table as simulated by the EVT module only occurs where the water table is very close to land surface. This occurs in the upper Deschutes Basin in only a few settings. Very shallow water-table conditions occur over a wide area in the La Pine subbasin, and in the drainage of Indian Ford Creek. The water table can also be close to land surface in riparian zones along certain streams. Because the evapotranspiration process can lead to numerical instability, it is applied only to regions of the model where evapotranspiration from the water table is thought to represent a significant part of the hydrologic budget. Therefore, the evapotranspiration from the water table is only simulated in the Black Butte–Sisters area, alluvial areas northwest of Bend, and in the La Pine subbasin (fig. 5).

The final hydrologic-process boundary condition in this discussion is ground-water pumpage, which is simulated as a specified flux. Only irrigation and public-supply pumping is simulated in the model. Pumpage by individual domestic wells was not simulated because most of the pumpage is returned to the ground-water system through on-site sewage-disposal systems and the amount of consumptive use is negligible—less than 2 ft^3/s. Specified fluxes are removed from cells corresponding to the geographic locations and production depths of wells. Pumpage from wells with open intervals that span multiple model layers was proportioned among the layers based on the percentage of the open interval in each layer. Pumping rates applied during the simulation vary with time. Techniques used to determine the locations and rates of pumping are described in Gannett and others (2001). The pumping rates for irrigation wells were determined using information from the OWRD water-rights files, satellite imagery, and data from State and County agricultural agencies. Pumping rates for public-supply wells were determined using data provided by the municipalities and water companies. The geographic distribution of irrigation and public-supply pumpage in the model is shown in figure 8. Rates of pumping for each semiannual stress period are shown in figure 9.

Model Parameters

Horizontal Hydraulic Conductivity

The scarcity of information on the subsurface geology in the saturated zone and of aquifer-test data precludes mapping hydraulic conductivity on a cell-by-cell basis. A practical alternative is to represent hydraulic conductivity in a set of discrete subregions or zones within which conditions are considered uniform. The zones defined for the upper Deschutes Basin represent the hydraulic-conductivity distribution at a scale that can be supported with available geologic and hydrologic data. Lite and Gannett (2002) delineated seven hydrogeologic units in the upper Deschutes Basin that provide a general framework for the spatial distribution of hydraulic conductivity.

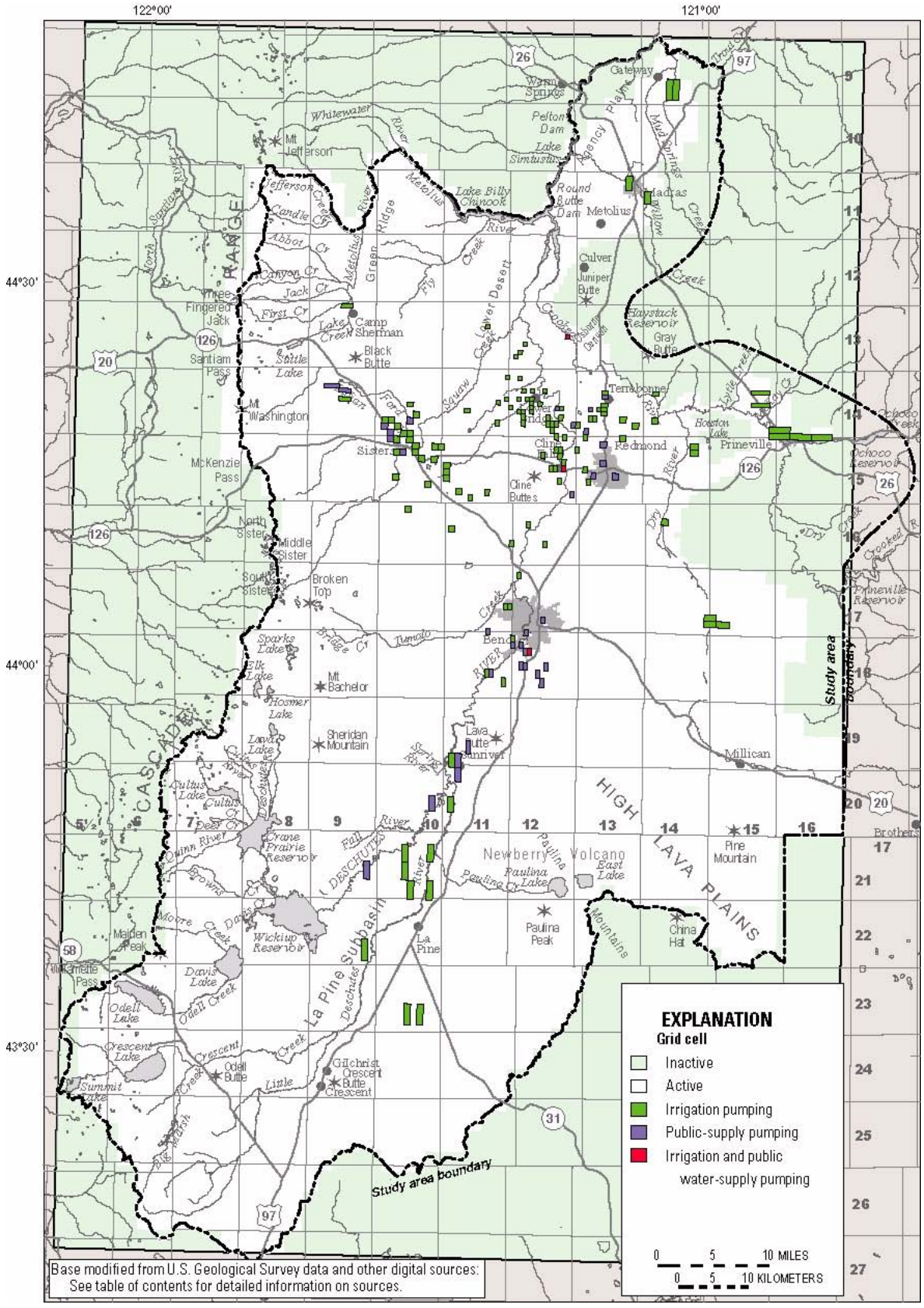

Figure 8. Distribution of irrigation pumpage and public water-supply pumpage on the model grid.

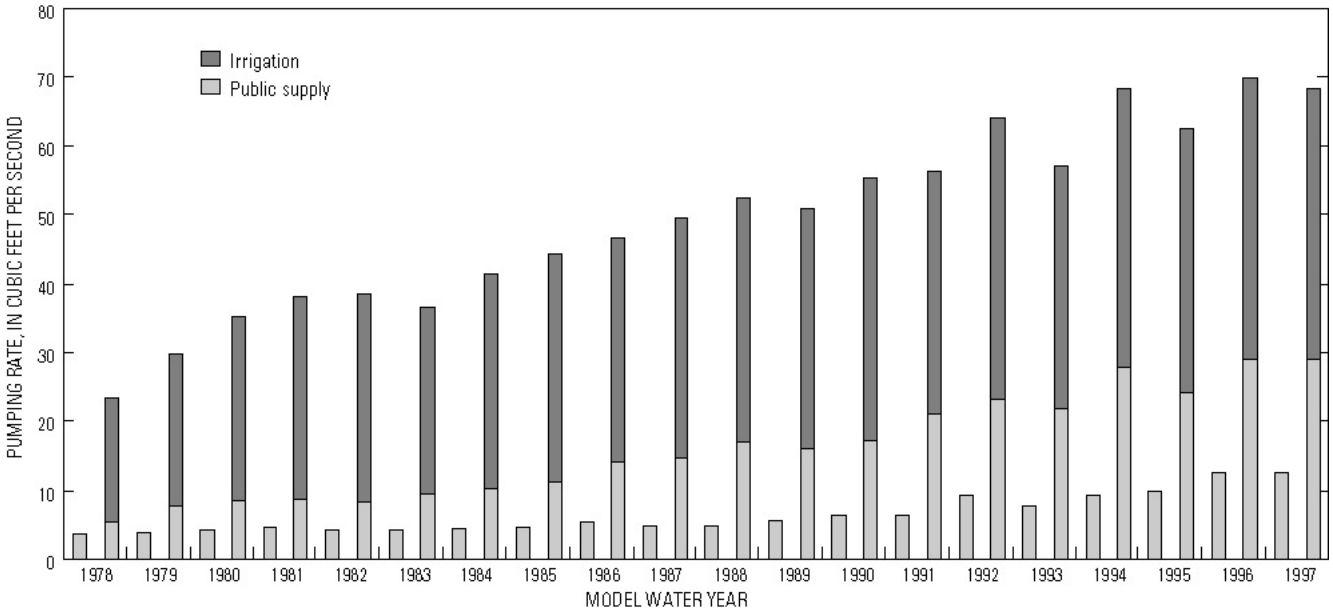

Figure 9. Rates of ground-water pumpage for irrigation and public-supply use for each semiannual stress period from 1978 to 1997.

These hydrogeologic units are based on stratigraphy and facies distribution within the basin as determined from surficial geologic maps, well logs, analysis of well cuttings, and geophysical data. The 7 hydrogeologic units were ultimately further divided into 17 zones based on several criteria, including the geographic density of hydraulic-head measurements, hydraulic gradients, recharge distribution, and analysis of residuals and sensitivity during calibration. Because the final zonation scheme was defined in part on hydraulic-head distribution, it is more detailed in the populated parts of the basin, where wells are plentiful. Hydraulic-conductivity zonation varies with depth in the model in places where geologic and hydrologic information are sufficient to support the level of detail. Model layer 1 includes a zone (6) to represent shallow alluvial deposits. Modifications to the hydraulic-conductivity zonation made during the model-calibration process are discussed in a later section. The final hydraulic-conductivity zonation for the model is shown in figure 10.

Vertical Hydraulic Conductivity

The spatial distribution of vertical hydraulic conductivity follows the same zonation as horizontal hydraulic conductivity. Vertical hydraulic conductivity is uniform within each zone, but the value of vertical hydraulic conductivity varies between zones.

In MODFLOW, the vertical hydraulic conductivities of two vertically adjacent cells are used to compute a vertical leakance term. The vertical leakance term (VCONT) is given by McDonald and Harbaugh (1988) as

$$VCONT = \frac{1}{\frac{(\Delta z_u)/2}{K_{z_u}} + \frac{(\Delta z_l)/2}{K_{z_l}}} \quad (3)$$

where

Δz_u is the thickness of the upper layer (L),

Δz_l is the thickness of the lower layer (L),

K_{z_u} is the vertical hydraulic conductivity of the upper cell (LT^{-1}), and

K_{z_l} is the vertical hydraulic conductivity of the lower cell (LT^{-1}).

Storage Coefficients

The spatial distribution of storage coefficients follows the hydraulic-conductivity zonation scheme. Storage coefficients are constant only within each layer in each zone and can vary between layers within zones. Although all layers were modeled as confined, meaning transmissivity remains constant with respect to head fluctuations, storage coefficients in the uppermost layers were set to values typical of unconfined or semiconfined aquifers. This allowed the upper layers to behave unconfined or semiconfined with respect to their storage characteristics.

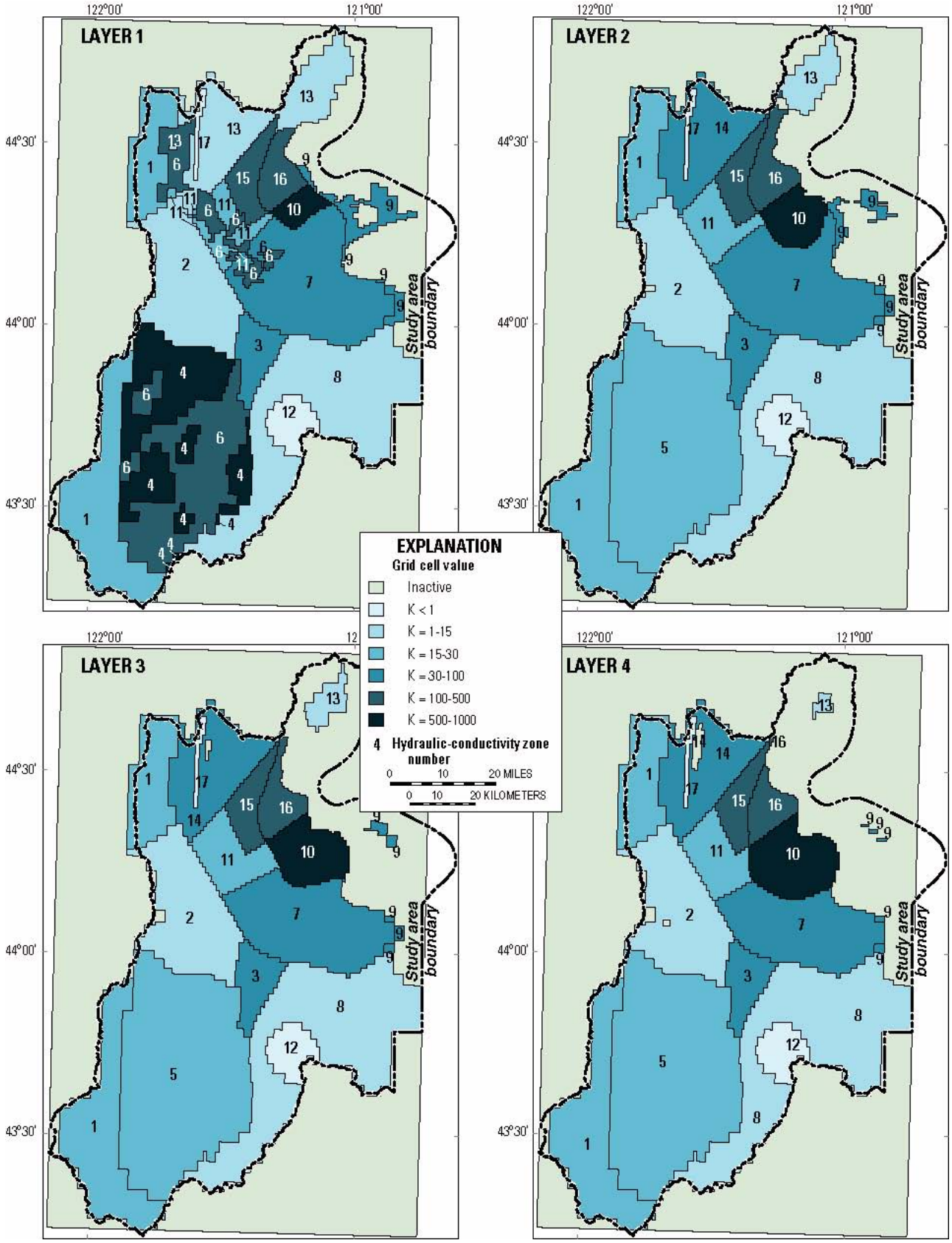

Figure 10. Hydraulic-conductivity zonation in all model layers. (K, hydraulic conductivity, in feet per day)

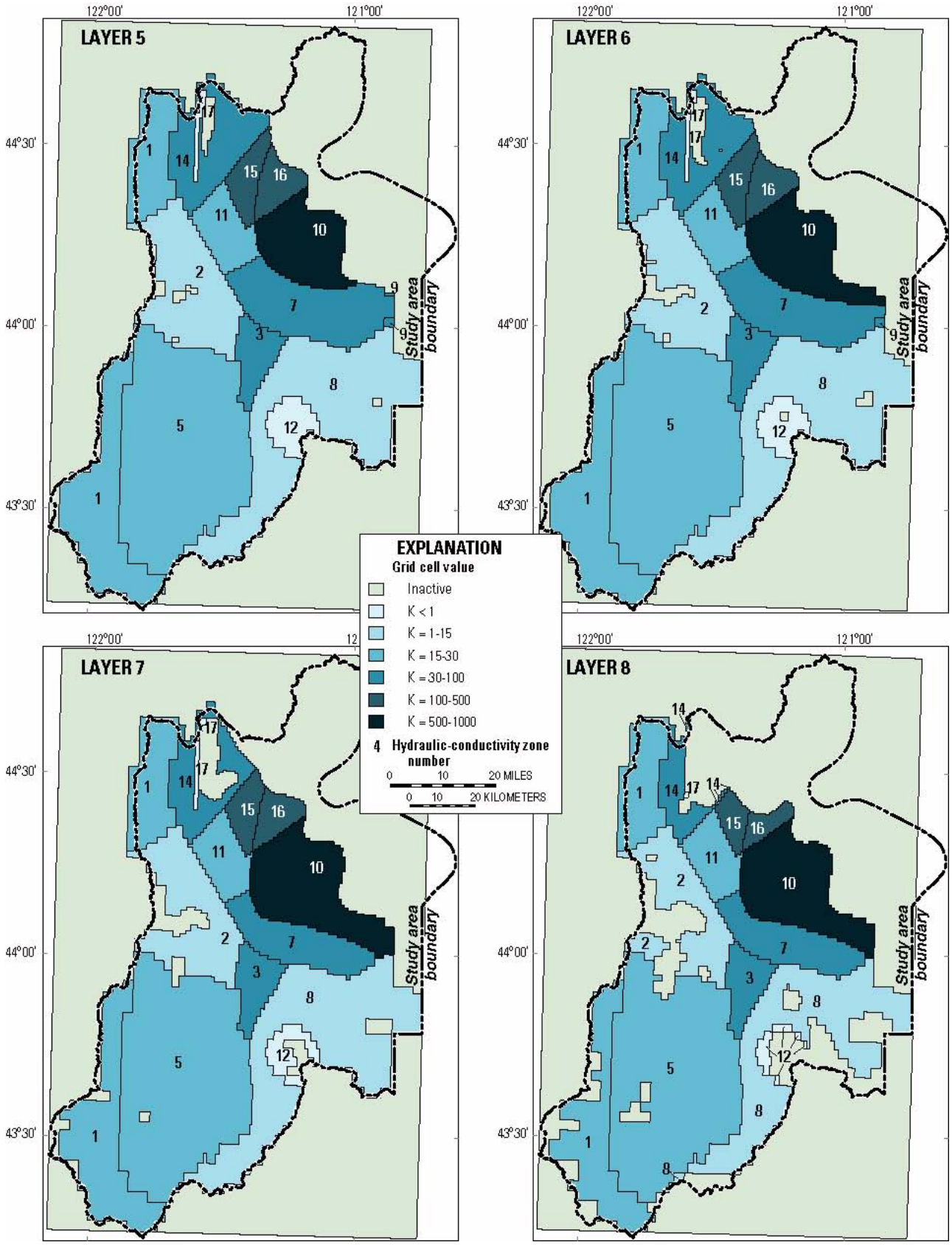

Figure 10. Hydraulic-conductivity zonation in all model layers—Continued. (K, hydraulic conductivity, in feet per day)

MODEL CALIBRATION

Model calibration is the process whereby model parameter structure and parameter values are adjusted and refined to provide the best match between measured and simulated values of hydraulic heads and flows. Traditionally, models are calibrated by a trial-and-error process in which model parameters are adjusted within reasonable limits from one simulation to the next to achieve the best model fit. Model fit is commonly evaluated by visual comparison of simulated and measured heads and flows or by comparing root mean square (RMS) errors of heads and flows between simulations.

Models can also be calibrated using inverse methods in which the optimal parameter values for a given parameter structure are determined using a mathematical technique such as nonlinear regression (Cooley and Naff, 1990; Hill, 1992, 1998). This technique is sometimes referred to as *parameter estimation.* The regression process finds the set of parameter values that minimizes the difference between simulated and measured quantities such as hydraulic heads and flows.

The upper Deschutes Basin ground-water model was calibrated in two steps: (1) steady-state calibration to average conditions during the period 1993 to 1995, and (2) calibration to transient conditions from 1978 to 1997. Inverse methods were used for the steady-state calibration, and traditional trial-and-error methods were used for the transient calibration. Inverse methods were not used for transient calibration because the combination of the sparse transient data set and relatively complicated model parameterization (developed using the rich steady-state data set) was not conducive to stable regression. The trial-and-error method provided satisfactory results for the transient calibration and met the overall goals of the project. The steady-state and transient calibration processes are discussed in the following paragraphs.

Steady-State Calibration

The upper Deschutes Basin regional steady-state ground-water model was calibrated to average conditions from 1993 to 1995. This period was chosen because much of the data collection for the project occurred during this time and because average conditions during this period were reasonably close to long-term average conditions. For example, the average rate of recharge from precipitation during the 1993–95 period is estimated to be about 3,500 ft^3/s, while the 1962–97 average is estimated to be about 3,800 ft^3/s (fig. 7). There is no evidence to suggest that the regional ground-water system in the upper Deschutes Basin is not in long-term equilibrium with the natural climate cycles and human activity. For example, no long-term water-level declines due to pumping were observed in the data, and (with few exceptions) ground-water discharge measurements show trends that can be related only to climate.

Steady-State Calibration Data

Head observations for calibration consisted of water-level measurements from 983 wells. Head observations were not evenly distributed throughout the model domain but were clustered geographically in the populated areas of the study area (fig. 4) and vertically toward the upper parts of the flow system. Just over one-half of the head observations are in the upper two layers of the model, and 91 percent are in the upper five layers. Head observations were related to specific cells (horizontally and vertically) based on the well location and on the depth of the well's open interval. Head observations from wells in which open intervals span multiple layers were compared to simulated heads in the associated layers according to methods described by Hill (1992). Although the steady-state model was calibrated to average conditions during the 1993 to 1995 time period (which approximates average long-term conditions), head measurements made outside of this time period were used during steady-state model calibration. This was necessary because obtaining water-level measurements during the calibration period was not possible in approximately one-half of the wells because of accessibility problems. In these cases, water levels measured by the driller or the USGS at an earlier time were used. This was acceptable hydrologically because time-series water-level data showed that water-level fluctuations in most of the model area were on the order of a few feet, rarely exceeding 10 feet, and within the range of the measurement error from topographic maps (Caldwell and Truini, 1997). In addition, the temporal fluctuation is small in relation to the overall range in heads and large hydrologic gradients throughout most the modeled area. Head data were scrutinized carefully, and anomalous values due to measurement or location errors, pumping effects, or the obvious influence of immediately adjacent canals were removed from the calibration data set.

Calibration of this model benefited from a particularly rich set of flow observations. Flow observations were based on gain and loss estimates described in detail by Gannett and others (2001). Estimates of the average ground-water discharge to, or leakage from, 60 separate stream reaches were used in steady-state model calibration (fig. 11). Estimates along major streams, which account for the largest fluxes in the model, were based on gain-loss studies (seepage runs) conducted during the calibration period. Repeat measurements in subsequent years and comparison with gaging-station data indicated that the fluxes used for major streams were reasonably representative of average conditions. Estimates for some of the smaller streams and tributaries were based on gage data from both active and historic gages with periods of record ranging from a few years to decades. Some flux estimates in the upper Metolius River drainage were based, in part, on miscellaneous streamflow measurements. All flow observations were weighted to reflect their reliability.

Steady-State Calibration Procedure

The steady-state calibration was done using MODFLOWP, a version of MODFLOW modified by Hill (1992) to estimate parameters using nonlinear regression. In MODFLOWP, nonlinear least-squares regression is used to find the set of parameter values that will minimize the weighted sum of squared errors (SOSE) objective function (Hill, 1998):

$$S(\underline{b}) = \sum_{i=1}^{ND} w_i[y_i - y'_i(\underline{b})]^2 \qquad (4)$$

where

- $\underline{b}$ is a vector containing values for each of the parameters being estimated,
- ND is the number of observations (hydraulic head and flow measurements),
- y_i is the ith observation being matched by the regression,
- $y'_i(\underline{b})$ is the simulated value corresponding to the ith observation, and
- w_i is the weight assigned to the ith observation.

The differences between the observed and simulated values [$y_i - y'_i(\underline{b})$] are referred to as *residuals*. Residuals are weighted by the term w_i for two reasons. First, weighting allows meaningful comparisons of measurements with different units because the weighted values are dimensionless. Secondly, weighting can be used to reduce the influence of measurements with large errors or uncertainty and increase the influence of measurements with small errors. In MODFLOWP, the weight for a particular observation is formulated as the inverse of the variance of the measurement error.

The observation weights used in this study were developed in a manner similar to that suggested by Hill (1998). For hydraulic-head measurements, error was dominated by the accuracy of topographic maps used to determine land-surface elevation (and subsequently head). Other sources of error were considered negligible compared to map accuracy limitations. Map accuracy was taken to equal plus or minus one contour interval, which was usually either 10 or 20 feet. A standard deviation of measurement error was estimated for each measurement by assuming that the 95-percent confidence interval for the true head was equal to the head measurement plus or minus the contour interval of the topographic map used to determine the well elevation.

Flow observations (estimates of the flux of water moving between the ground-water and surface-water systems) were also weighted by estimating standard deviations of measurement errors. Unlike head observations, however, there was no single dominant source of error. Flow observations assumed to represent average conditions were estimated from a variety of data sources and were generally known with much less certainty than head observations. The weighting of flow observations was based on subjective estimates of 95-percent confidence intervals developed considering the data and methods used to derive the flow observation. For the steady-state calibration, the 95-percent confidence interval associated with a particular observation was based on a subjective evaluation of how likely the observed value represented average 1993–95 conditions. In situations where the value was based on repeated measurements during the 1993 to 1995 period, confidence intervals were as small as plus or minus 10 percent. Confidence intervals were larger where values were inferred from gage data. Confidence intervals were largest, in some instances exceeding the flow estimate, where values were estimated from miscellaneous streamflow measurements or gage data outside the 1993 to 1995 time period.

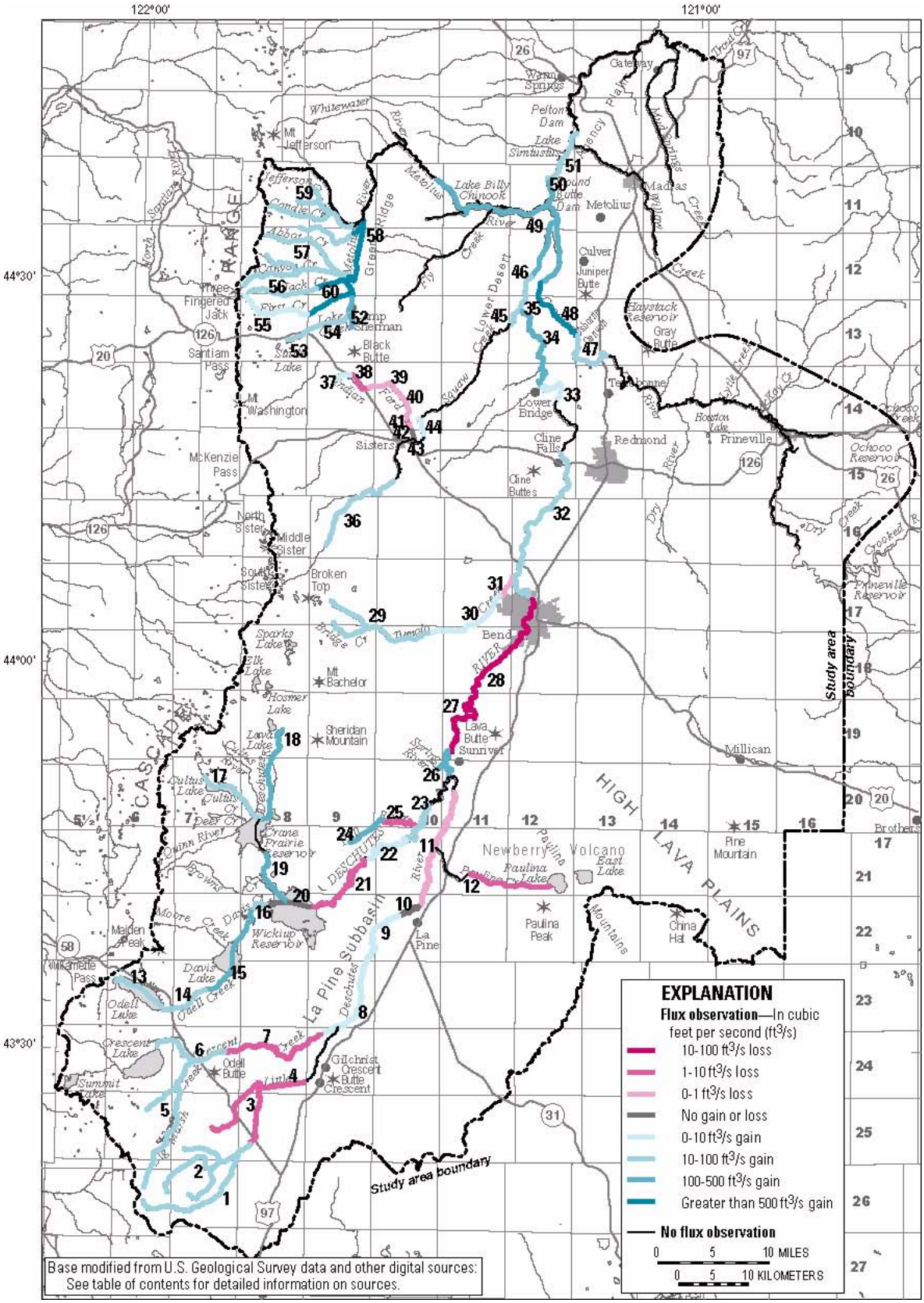

Figure 11. Stream fluxes used for steady-state calibration. (Numbers correspond to observation numbers in table 3, p. 45–46.)

Nonlinear regression was done using the MODFLOWP code of Hill (1992), which minimizes the objective function, equation (4), by nonlinear regression using a modified Gauss-Newton optimization method. The general basis of the technique is described by Cooley and Naff (1990) and the code and instructions are found in Hill (1992). Methods and guidelines for model calibration using inverse methods are presented by Hill (1998).

Steady-State Model Parameters

During steady-state model calibration, the parameter structure allowed adjustment of 32 parameters. The boundary fluxes along the Cascade Range crest in the Metolius River drainage and east of Newberry Volcano, pumpage rates, and evapotranspiration parameters were not adjusted during calibration. These model parameters were not set up for optimization and not adjusted during calibration for a variety of reasons. First, they were derived independently and considered reasonably reliable. Boundary flux and evapotranspiration parameters were potential sources of problems with the regression due to correlation with other parameters and nonlinearity. The parameters adjusted during calibration include hydraulic conductivity in 17 separate zones (fig. 10), streambed conductance values, recharge, modelwide vertical anisotropy, and additional vertical leakance parameters in 6 of the hydraulic-conductivity zones. The six vertical leakance parameters were set up for zones 3, 7, 8, 10, 11, and 16, where large vertical gradients existed and/or data were considered sufficient to support refinement of vertical hydraulic-conductivity estimates. The vertical leakance parameter allows adjustment of the vertical leakance (VCONT) between layers in subregions of the model in addition to the modelwide vertical anisotropy. This is done by adding another conductance term in the denominator of equation (3).

Numerous hydraulic-conductivity zonation schemes were tried during the calibration process. Zonation schemes were modified to reduce the sum of squared errors after optimization, reduce the number and size of geographic areas dominated by positive or negative residuals (model bias), minimize parameter correlation, and minimize the number of insensitive parameters. During this process, care was taken to remain faithful to the geologic data and overall geologic understanding.

Streams in the model were organized into seven groups, based on their geologic setting (table 1). Streambed conductance *(CSTR)* values within each of these groups could be adjusted up or down in unison.

Table 1. Stream groupings used for streambed conductance parameters

Parameter number	Streams included
KST1	Drainages in and on the margin of the Cascade Range south of Mt. Bachelor
KST2	Fall and Spring Rivers
KST3	Low gradient sections of the Deschutes and Little Deschutes Rivers and tributaries in the La Pine subbasin
KST4	Deschutes River, Sunriver to Bend
KST5	Upper Tumalo and upper Squaw Creeks
KST6	Deschutes, Crooked, and Metolius Rivers and tributaries in the ground-water discharge area near and below Lake Billy Chinook
KST7	Upper Metolius River and tributaries

Parameter Sensitivity

The ability to estimate values for particular parameters using nonlinear regression is affected by parameter sensitivity, which reflects the amount of information about a particular parameter provided by the available observation data. Changing values of parameters with low sensitivity has little effect on the sum of squared errors. Changing values of parameters with high sensitivities can have a relatively large effect on the sum of squared errors.

MODFLOWP calculates the scaled sensitivity of a simulated value to a single parameter (Hill 1998) as

$$ss_{ij} = \left(\frac{\partial y'_i}{\partial b_j}\right) b_j w_{ii}^{1/2} \qquad (5)$$

where

y'_i is the simulated value associated with the *i*th observation,

b_j is the *j*th estimated parameter,

$\frac{\partial y'_i}{\partial b_j}$ is the sensitivity of the simulated value associated with the *i*th observation with respect to the *j*th parameter and is evaluated at $\underline{b}$ (the set of parameter values at which the sensitivity is being evaluated), and

w_{ii} is the weight of the *i*th observation.

The combined scaled sensitivity of all simulated equivalents of the observations to an individual parameter is provided by the composite scaled sensitivity (Hill, 1998). The composite scaled sensitivity is calculated for each parameter by MODFLOWP (Hill, 1998) as

$$css_j = \left[\sum_{i=1}^{ND} (ss_{ij})^2 \Big|_{\underline{b}} / (ND) \right]^{1/2} \quad (6)$$

where

ND is the number of observations, and

ss_{ij} is the scaled sensitivity described above (evaluated at $\underline{b}$).

Composite scaled sensitivities are dimensionless and their magnitudes are a measure of the total amount of information on a particular parameter provided by all the observations. Generally speaking, the regression method employed by MODFLOWP has difficulty estimating values for parameters with composite scaled sensitivities that are considerably lower than those for other parameters in the model. Models commonly include some parameters that have low composite scaled sensitivities and cannot be estimated using regression methods. These parameters are usually set to reasonable values and are not included in the regression process.

The composite scaled sensitivities of all parameters in the upper Deschutes Basin model configured for optimization are shown graphically in figure 12. Parameters in figure 12 are grouped into those that were optimized and those that were not optimized. It can be seen that the nonoptimized parameters generally have low sensitivity. Low sensitivity parameters often destabilize the regression process, and can result in parameter value estimates that are physically unreasonable. Sensitivity is not the only factor, however, influencing the ability of the regression process to optimize certain parameters. It can be seen in figure 12 that some parameters with low sensitivity were successfully optimized, and others with larger sensitivities (for example, recharge) were not.

Final Parameter Values

The final values for horizontal and vertical hydraulic-conductivity parameters in the steady-state calibration, both optimized and set, are shown in table 2. Parameter values not determined using regression were set using trial and error to values that were within reasonable limits prior to final optimization of other parameters. Generally, only small adjustments were made. Hydraulic conductivity in zone 6 (K6 on fig. 12), which represents Quaternary alluvial deposits along the margin of the Cascade Range from the Metolius River to Bend and in the La Pine subbasin, was set to 194 ft/d (2.25×10^{-3} ft/s).

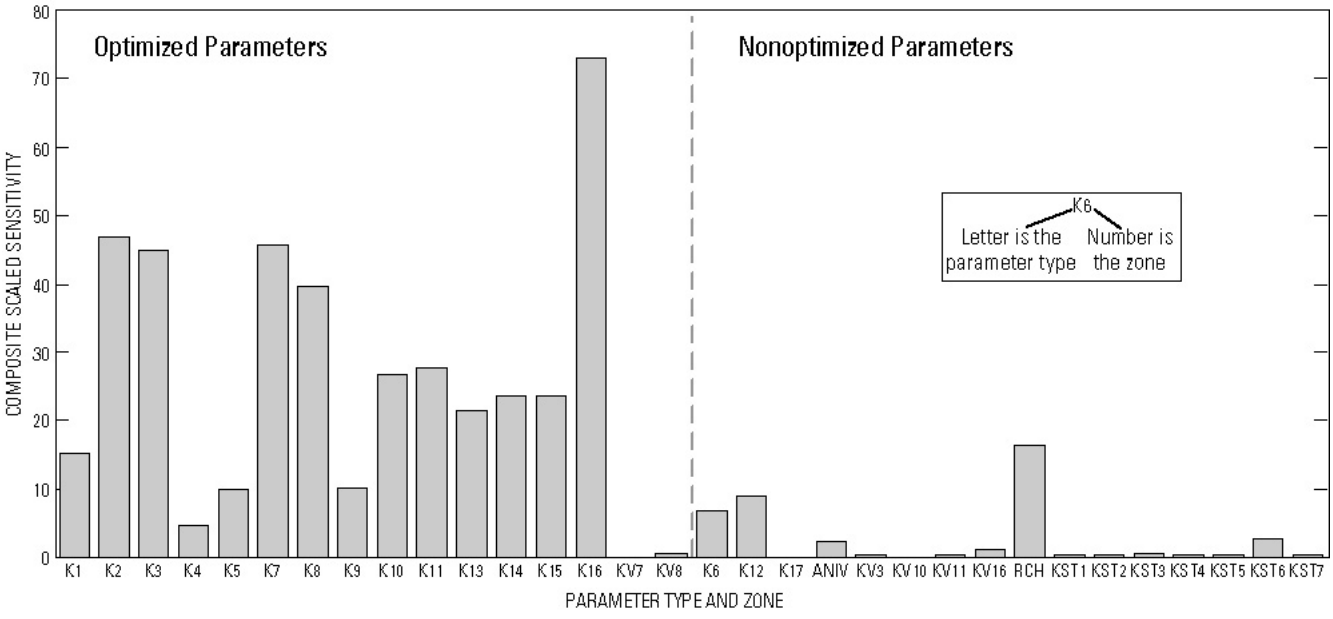

Figure 12. Composite scaled sensitivities of steady-state parameters. (Parameter types are as follows: K, horizontal hydraulic conductivity; KV, vertical leakance; ANIV, modelwide vertical anisotropy; RCH, recharge; KST, streambed conductance.)

Table 2. Final hydraulic-conductivity values

[K_{xy}, horizontal hydraulic conductivity; K_z, vertical hydraulic conductivity; parameters in bold type optimized]

Zone no.	K_{xy} ft/s	K_{xy} ft/day	K_z ft/s	K_z ft/day	K_{xy}/K_z
1	[a]**2.41×10^{-4}**	[a]**$2.09\times10^{+1}$**	2.41×10^{-7}	2.09×10^{-2}	1,000
2	[a]**6.48×10^{-5}**	[a]**5.60**	6.48×10^{-8}	5.60×10^{-3}	1,000
3	[a]**3.54×10^{-4}**	[a]**$3.06\times10^{+1}$**	3.03×10^{-7}	2.62×10^{-2}	1,170
4	[a]**8.99×10^{-3}**	[a]**$7.77\times10^{+2}$**	8.99×10^{-6}	7.77×10^{-1}	1,000
5	[a]**2.32×10^{-4}**	[a]**$2.00\times10^{+1}$**	2.32×10^{-7}	2.00×10^{-2}	1,000
6	2.25×10^{-3}	$1.94\times10^{+2}$	2.25×10^{-6}	1.94×10^{-1}	1,000
7	[a]**7.00×10^{-4}**	[a]**$6.05\times10^{+1}$**	[a]**1.66×10^{-8}**	[a]**1.43×10^{-3}**	[a]**42,200**
8	[a]**1.17×10^{-4}**	[a]**$1.01\times10^{+1}$**	[a]**3.37×10^{-9}**	[a]**2.91×10^{-4}**	[a]**34,754**
9	[a]**3.60×10^{-4}**	[a]**$3.11\times10^{+1}$**	3.60×10^{-7}	3.11×10^{-2}	1,000
10	[a]**1.14×10^{-2}**	[a]**$9.84\times10^{+2}$**	9.74×10^{-6}	8.42×10^{-1}	1,169
11	[a]**2.26×10^{-4}**	[a]**$1.95\times10^{+1}$**	1.19×10^{-7}	1.03×10^{-2}	1,904
12	6.60×10^{-6}	5.70×10^{-1}	6.60×10^{-9}	5.70×10^{-4}	1,000
13	[a]**1.69×10^{-4}**	[a]**$1.46\times10^{+1}$**	1.69×10^{-7}	1.46×10^{-2}	1,000
14	[a]**1.07×10^{-3}**	[a]**$9.25\times10^{+1}$**	1.07×10^{-6}	9.25×10^{-2}	1,000
15	[a]**2.79×10^{-3}**	[a]**$2.41\times10^{+2}$**	2.79×10^{-6}	2.41×10^{-1}	1,000
16	[a]**3.68×10^{-3}**	[a]**$3.18\times10^{+2}$**	2.20×10^{-6}	1.90×10^{-1}	1,674
17	1.00×10^{-7}	8.64×10^{-3}	1.00×10^{-10}	8.64×10^{-6}	1,000

[a] Parameter optimized.

Hydraulic conductivity in zone 12 (K12 on fig. 12), which represents the central part of Newberry Volcano, was set to 0.57 ft/d (6.6×10^{-6} ft/s). This is an order of magnitude lower than the final value used for the central Cascade Range, but near the middle of the range given by Ingebritsen and others (1992) for near-surface rocks in the Cascade Range. The hydraulic conductivity of zone 17 (K17 on fig. 12), which represents a low-permeability barrier along the Green Ridge fault zone, was set to 8.6×10^{-3} ft/d (1.0×10^{-7} ft/s).

The modelwide vertical anisotropy, the ratio of horizontal to vertical hydraulic conductivity (ANIV on fig. 12), was set to 1,000. The KV (vertical leakance) parameters act to further limit vertical conductance of certain zones. KV parameter values for zones 7 and 8 were determined by regression, and for zones 3, 10, 11, and 16 were set by trial and error.

Recharge rates were kept at the values determined by the DPM except in the southern part of the Cascade Range and the La Pine subbasin, where rates were reduced by 25 percent (a total of about 400 ft^3/s) to better fit heads and flows. Recharge rates and hydraulic-conductivity values are often correlated parameters in many ground-water models, meaning that the observed head distribution can be simulated by a variety of values as long as the ratio of recharge and hydraulic conductivity remains the same. Such correlation was not generally an issue in the upper Deschutes Basin model because recharge rates were independently constrained by ground-water discharge measurements.

Streambed conductances were based on an assumed streambed thickness of 10 feet and streambed hydraulic-conductivity values ranging from 0.1 to 50 ft/d (with one reach set at 250 ft/d). Nearly all reaches had hydraulic conductivities less than 10 ft/d. Streambed conductances were adjusted manually to achieve a good fit between simulated and observed stream gains and losses. Values were most commonly adjusted downward in losing reaches to better simulate the impediment of stream leakage by streambed materials and sediment-filled fractures. Stream reaches with large hydraulic-conductivity values were typically spring areas where ground water discharges from coarse sediments and open fractures in lava along streambanks and canyon walls.

All final parameter values (table 2) fall within or close to expected ranges, with the possible exception of the vertical hydraulic conductivity of zones 7 and 8. The regression process tended to set the KV parameter values for these two zones such that vertical anisotropies were on the order of 10^4, which is an order of magnitude higher than in other zones. Although anomalous, these values are not unreasonable. First, this area (particularly zone 7) is characterized by very high vertical head gradients, which suggests low vertical hydraulic conductivity. Anisotropies of 10^4 were necessary to simulate the observed gradients. Although high, these anisotropies are similar to or less than those found in some modeling studies in the Columbia River Basalt Group (Tanaka and others, 1974; Mac Nish and Barker, 1976). It is unclear what geologic conditions may cause high vertical anisotropies in these zones; however, sparse subsurface data suggest this region of the model contains a higher proportion of layered lava sequences than elsewhere. The final value of hydraulic conductivity for zone 6 (194 ft/d) is about twice the value of 88 ft/d estimated for the La Pine subbasin from aquifer tests (Century West Engineering Corporation, 1982).

Steady-State Calibration Model Fit

A number of statistical and graphical analyses of model fit, as described by Hill (1998), are presented in this section. Comparisons of simulated and measured heads and flows are included as well. Statistical and graphical techniques to evaluate model fit generally involve the analysis of residuals. A residual is the difference between a measured quantity, for example a head elevation, and its simulated equivalent [see equation (4)]. Of particular interest is the overall magnitude of the residuals and the degree to which they are random, independent, and normally distributed. Some of these characteristics are important in identifying model error and in evaluating confidence intervals on estimated parameter values. A number of statistical and graphical analyses of residuals are presented in this section along with more traditional comparisons of simulated and observed heads and flows using maps and graphs.

Statistical Measures of Model Fit and Parameter Uncertainty

The calculated error variance is an overall measure of the magnitude of residuals. The calculated error variance is simply the sum of squared errors from equation (4) divided by the number of observations minus the number of parameters (see equation 14 of Hill, 1998). The square root of the calculated error variance is known as the *standard error of regression.* If the model fit is consistent with the data accuracy, and the weighting appropriately reflects the data accuracy, both the calculated error variance and the standard error of regression should equal 1.0 (Hill, 1998). Values larger than 1.0 suggest model error. In practice, the calculated error variance is almost always greater than 1.0. The calculated error variance and standard error of regression for the steady-state calibration described herein are 55.47 and 7.45, respectively. Sources of error are discussed later in the report.

A more intuitive measure of overall model fit is the product of the standard error of regression and the statistics used to determine weights (usually standard deviations or coefficients of variation). These values are referred to by Hill and others (1998) as fitted standard deviations or fitted coefficients of variation. The weights used for head observations in the steady-state model calibration are based on the assumed error in topographic maps used to determine well elevations. The standard deviation of measurement error for most wells was 10.2 feet. Multiplying this figure by the standard error of regression yields a fitted standard deviation for heads of 76 feet.

It is desirable for weighted residuals to be independent, random, and normally distributed. Weighted residuals that are not so may be an indication of model error. Moreover, calculation of certain statistics, such as confidence intervals on parameter values, requires residuals to have these properties. Independence and randomness of weighted residuals can be assessed by plotting them against weighted simulated values (Cooley and Naff, 1990, p. 170; Hill, 1994, p. 3). Residuals from the steady-state calibration are plotted in figure 13. If weighted residuals are random, they should be equally distributed above and below the horizontal zero axis. In addition, weighted residuals should show no trends as a function of weighted simulated value; in other words, there should be no distinct slope or curve to the data. Weighted residuals plotted in figure 13 generally meet both these criteria with the exception of a cluster of points on the right-hand side of the graph with weighted residuals that are all negative. These correspond to head observations in the La Pine subbasin, primarily in zone 5. The predominantly negative residuals indicated that simulated heads are systematically too high in this area. Various parameterization schemes were tried and none satisfactorily resolved the problem, but usually resulted in problems matching stream fluxes or heads elsewhere. Efforts to devise a solution were hampered by the lack of deep subsurface geologic information, particularly in the area just north of the La Pine subbasin (zone 3). The high simulated heads in the La Pine subbasin do not significantly affect overall simulation results, but may be problematic for detailed analysis in that area.

Certain inferential statistics, such as confidence intervals on parameter estimates, require that residuals be normally distributed. The degree to which weighted residuals are normally distributed can be assessed by a normal probability plot (Draper and Smith, 1998). If ordered residuals are normally distributed, they will fall approximately on a straight line on such a plot. Figure 14 is a normal probability plot of head and flow residuals for the steady-state model. The plot shows both head and flow residuals are generally linear but that there is slight curvature, particularly at the tails of the plot. There are, however, very few outliers.

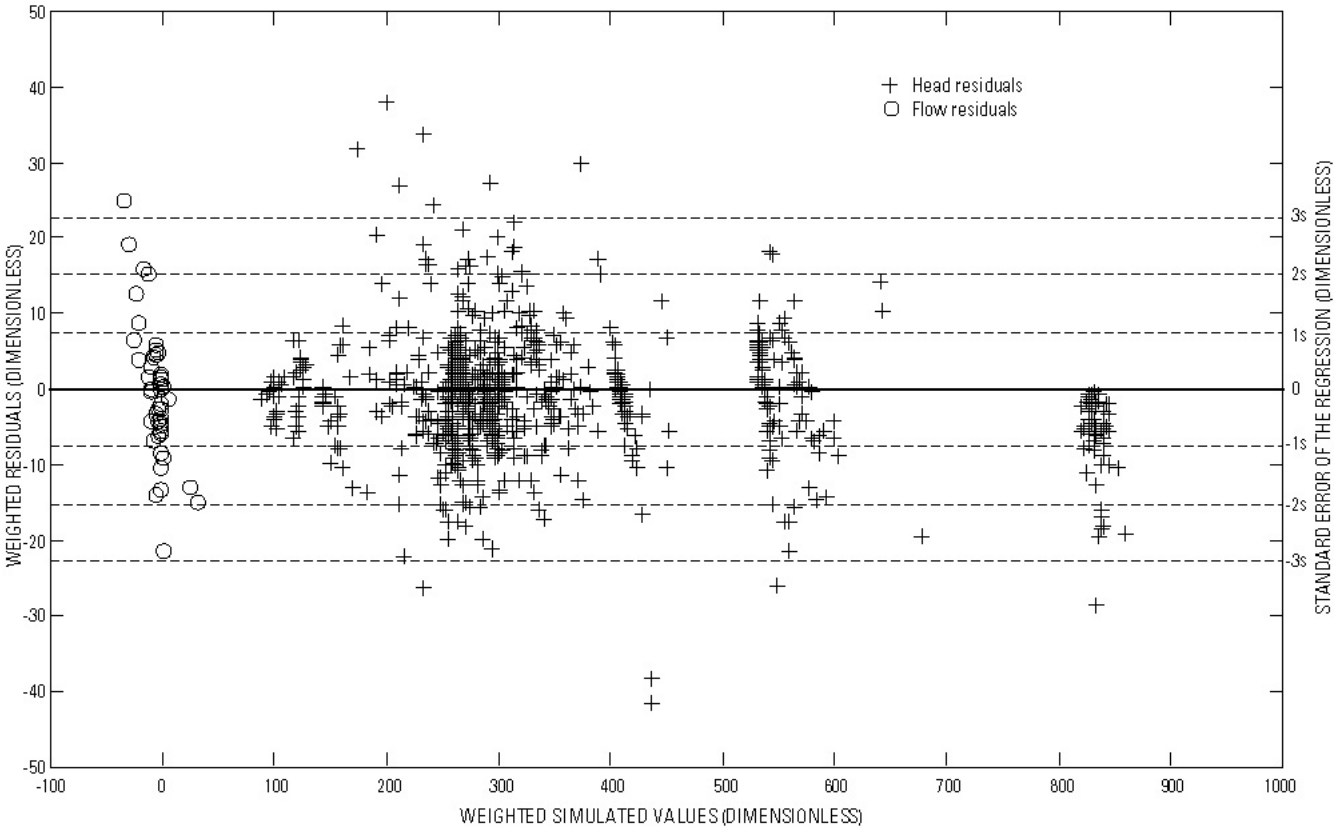

Figure 13. Weighted residuals as a function of weighted simulated values.

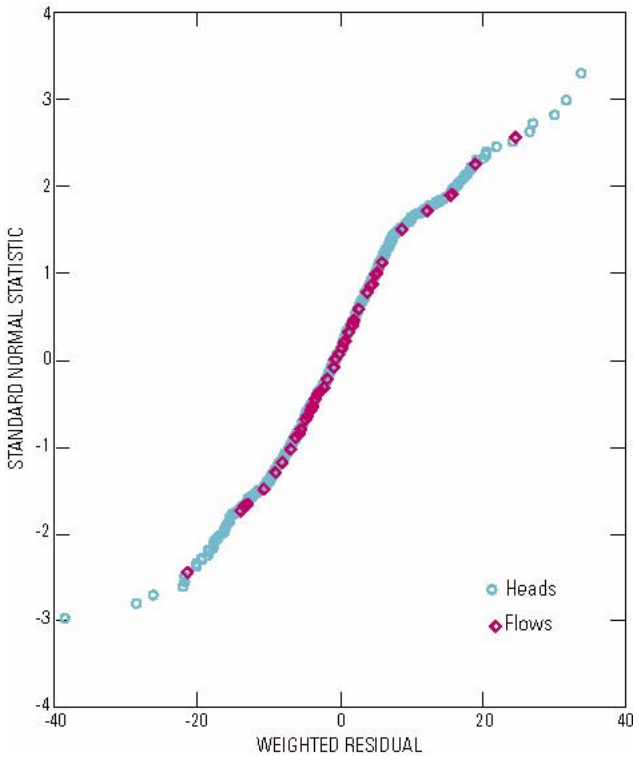

Figure 14. Normal probability plot of ordered weighted residuals.

An associated statistic for testing the normality of the distribution of residuals is the correlation coefficient between the ordered weighted residuals and the order statistics from a normal probability distribution function, denoted as R^2_N (Hill, 1992, 1998). Values of R^2_N close to 1.0 indicate that weighted residuals are independent and normally distributed. If R^2_N is significantly less than 1.0, the weighted residuals are not likely independent and normally distributed. Critical values of R^2_N below which residuals are not likely independent and normally distributed (at 0.05 and 0.1 significance levels) are given by Hill (1998, appendix D). The critical values are a function of the number of observations, with the values increasing with the number of observations. The largest number of observations for which Hill (1998) gives critical values of R^2_N is 200, and the steady-state model has 1,043 observations. The critical R^2_N for 200 observations is 0.987 so the value for 1,043 observations would be slightly higher but still less than 1.0. The R^2_N value for the steady-state model calibration is 0.977, slightly below the critical value for 200 observations at the 0.05 significance level.

By this measure, the weighted residuals are not likely to be truly independent and normally distributed.

Numerical models of complex ground-water systems are usually nonlinear. The degree of nonlinearity can be evaluated by the modified Beale's measure (Cooley and Naff, 1990). The modified Beale's measure is calculated from MODFLOWP output using the program BEALEP (Hill, 1994). The program also calculates critical values for evaluating the modified Beale's measure. These critical values indicate that the upper Deschutes Basin model would be considered effectively linear if the modified Beale's measure is less than 0.05 and would be considered highly nonlinear if the modified Beale's measure is greater than 0.6. The modified Beale's measure for the calibrated steady-state model is 0.3, indicating that it is moderately nonlinear. Principal causes of nonlinearity are head-dependent boundaries such as streams and evapotranspiration processes.

In order to provide information on parameter uncertainty, MODFLOWP calculates 95-percent linear confidence intervals for parameter estimates (fig. 15). Confidence intervals represent the precision with which the parameters are estimated given the available data. Parameter confidence intervals from a model can be compared to the range of reasonable parameter values, determined independently of the model using aquifer tests, specific-capacity tests, and the literature, to assess the reasonableness of the estimated values. The expected ranges for values in this model are described in the preceding discussion of hydraulic conductivity and by Gannett and others (2001). The relatively small range of the confidence intervals on figure 15 indicates that the available data provide sufficient information to narrowly constrain the parameter estimates. The closeness of the estimated parameter values and confidence intervals to the expected values indicates that the estimates are consistent with independent hydrogeologic information. The confidence intervals for the hydraulic-conductivity parameters for zones 4 and 5 are larger than for other hydraulic-conductivity parameters likely because of sparse or poorly distributed observations in those zones. These larger confidence intervals are consistent with the low composite scales sensitivities for these parameters on figure 12.

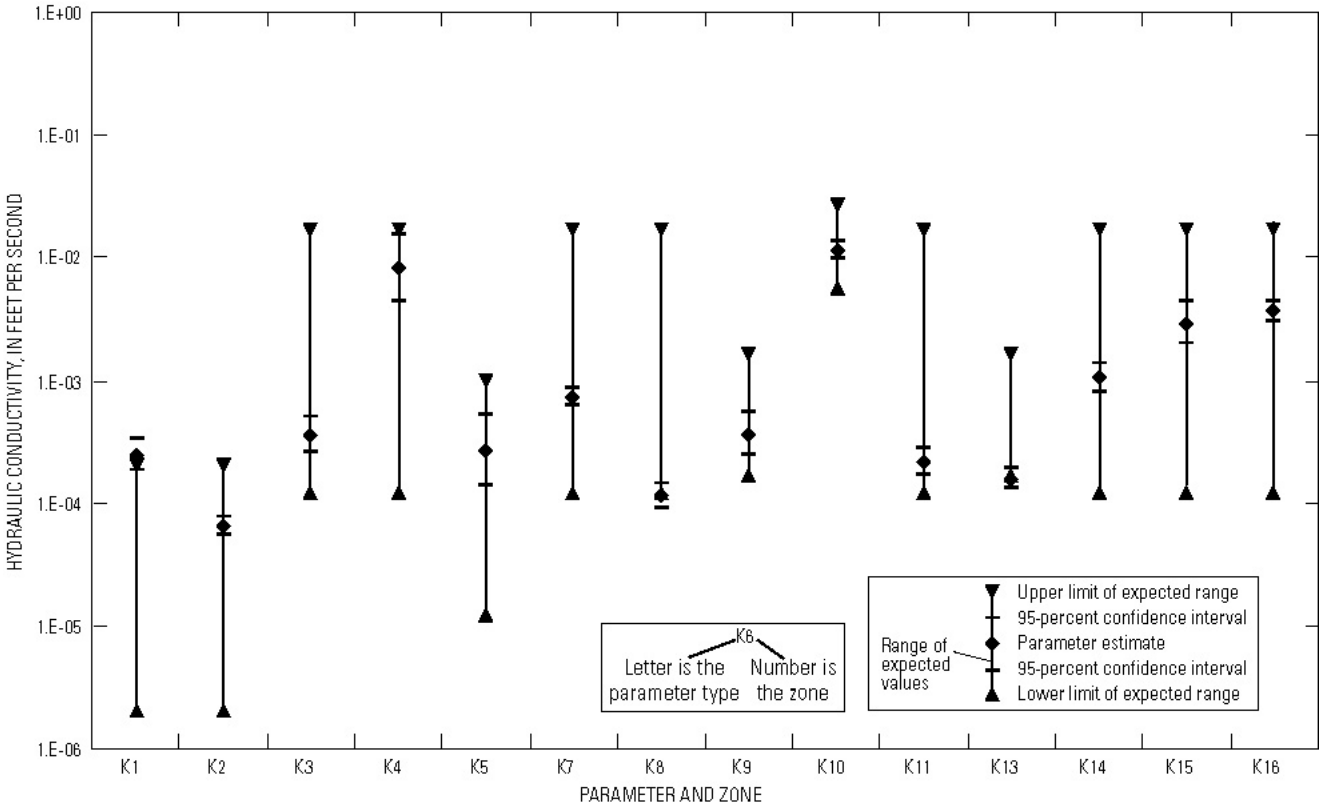

Figure 15. The final values, 95-percent confidence intervals, and ranges of expected values for optimized steady-state hydraulic-conductivity parameters.

The method used to calculate the 95-percent confidence intervals assumes that the model is linear in the vicinity of the optimized parameter values and that residuals are independent and normally distributed. As previously discussed, the requirements of model linearity and independent normally distributed residuals are not strictly met; however, measures indicate that the model is not highly nonlinear and that residuals are reasonably close to being independent and normally distributed. Because the assumptions are not strictly met, the computed linear confidence intervals shown in figure 15 must be considered approximate indicators of parameter uncertainty and used with caution.

Parameter correlation can be a problem in ground-water models. Two parameters can be highly correlated when available information is insufficient to determine unique values for each. Coordinated changes in correlated parameter values will result in the same heads and flows. MODFLOWP calculates a matrix of parameter correlation coefficients using the methods described by Hill (1998). Parameter correlation coefficients range from -1.0 to +1.0. Correlation coefficients with absolute values close to 1.0 indicate a high degree of correlation. In such cases the effects of parameter correlation need to be evaluated. Correlation coefficients with absolute values less than about 0.95 are considered acceptable (Hill, 1998). All correlation coefficients for the steady-state calibration were well within the acceptable range, with the largest being 0.86.

Comparison of Simulated and Observed Steady-State Heads

Model calibration also can be assessed qualitatively by visually comparing simulated hydraulic heads and flows with measured values. Figure 16 shows the simulated head distribution, representing mean heads for the 1993–95 period, contoured by computer (using the program of Harbaugh, 1990) as well as contours drawn by hand from field measurements for each model layer. Hand-drawn head contours are based primarily on field measurements from wells and from elevations of major springs and gaining streams. At certain locations in some layers, head contours were constrained by field measurements in overlying and underlying layers. The variation in hydraulic head with depth was an issue when hand contouring measurements from wells. In areas with high vertical gradients, the measured head at any particular location can vary depending on the vertical location within the layer. Moreover, the open intervals of some wells span multiple layers, and the measured head is a function of the heads in all the water-bearing zones penetrated. In general, data for each layer (including the multilayer measurements) were fairly consistent, and hand-drawn contours are well constrained where there are abundant data points. The placement of contours is much less certain where they are constrained by only one or two data points or where data are widely spaced. In figure 16, contours based on field measurements are drawn only where sufficient data were available. The hand-contoured area and number of contours present diminished with depth as data become sparse. Hand-drawn contours are solid where well constrained and dashed where data are sparse or ambiguous. Hand-drawn head contours closely follow or overlie simulated head contours where the simulated contours are entirely consistent with field data.

Contours of the simulated head distribution are generally consistent with contours hand drawn based on field measurements. The direction and magnitude (slope) of simulated head gradients match measured regional gradients well. There are some areas, however, where simulated head contours consistently differ from those drawn from field measurements. Simulated heads are generally higher than measured heads in the La Pine subbasin, as described earlier in the discussion of figure 13. This is most noticeable in layer 1, but occurs in lower model layers as well. Another area where simulated heads appear to be consistently different from measured heads is in layers 2 through 5 north of Cline Buttes between Redmond and Sisters. The simulated 2,600 foot contour in these layers generally forms an east-west arc gently convex toward the south. Field measurements suggest that the 2,600 foot contour is more curved toward the south, becoming v-shaped with the apex close to Cline Buttes.

In areas where head data are insufficient to draw contours, a direct comparison between simulated and actual head distributions is not possible. In such areas, for example the Cascade Range and Newberry Volcano, simulated heads are generally consistent with what would be expected given the topography, precipitation distribution, and inference from streams and sparse well data.

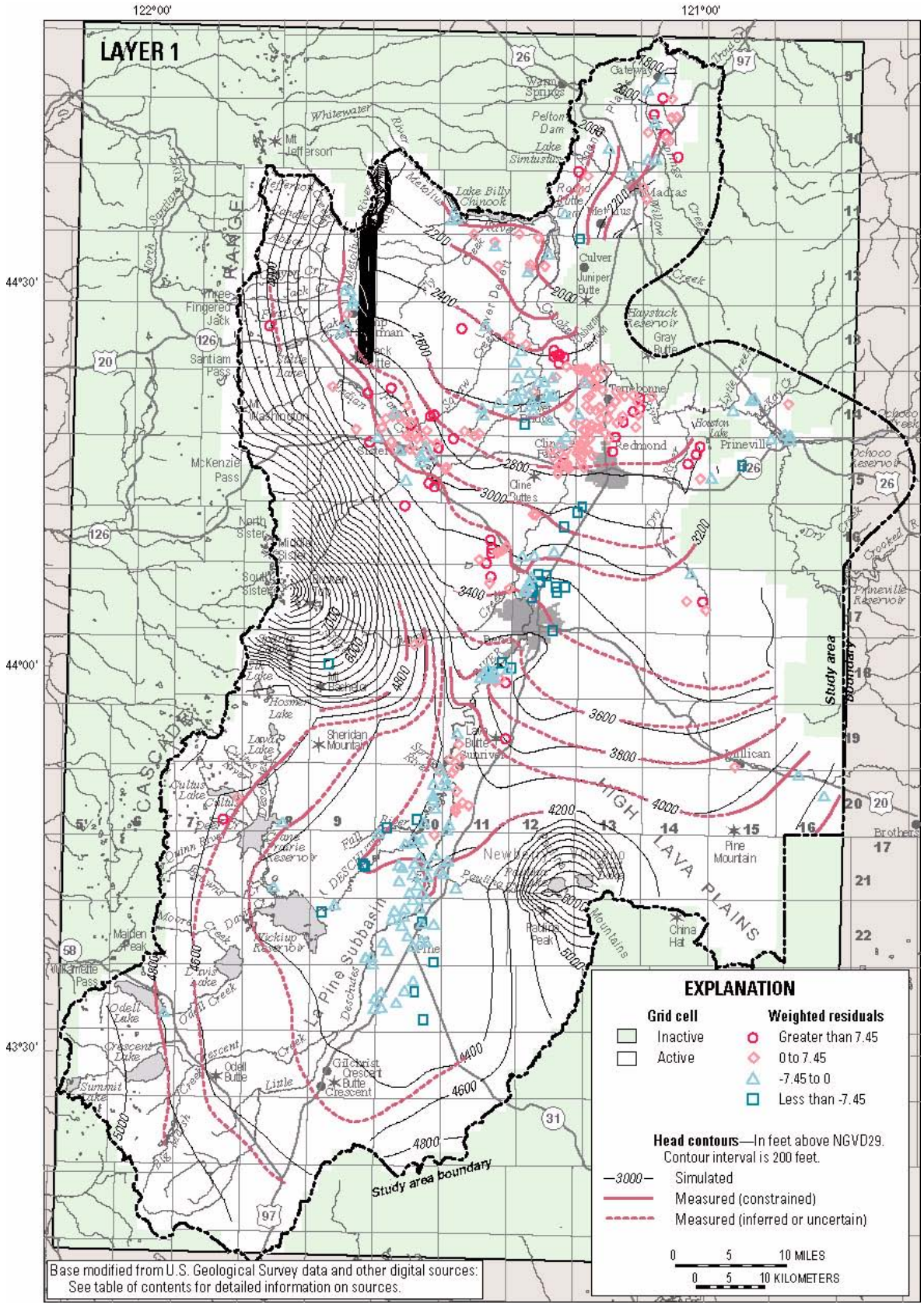

Figure 16. Lines of equal measured head and lines of equal simulated head for all model layers.

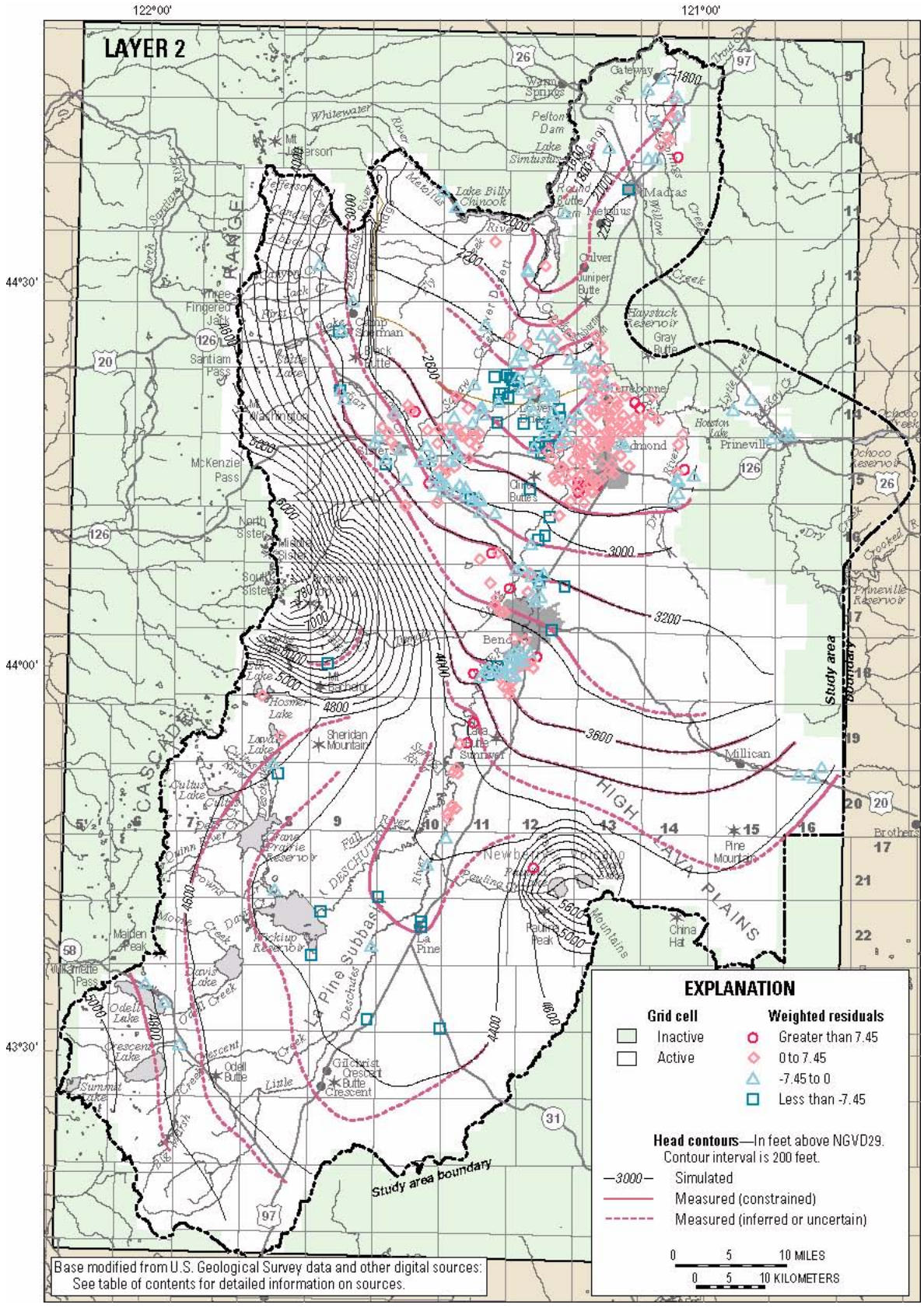

Figure 16. Lines of equal measured head and lines of equal simulated head for all model layers—Continued.

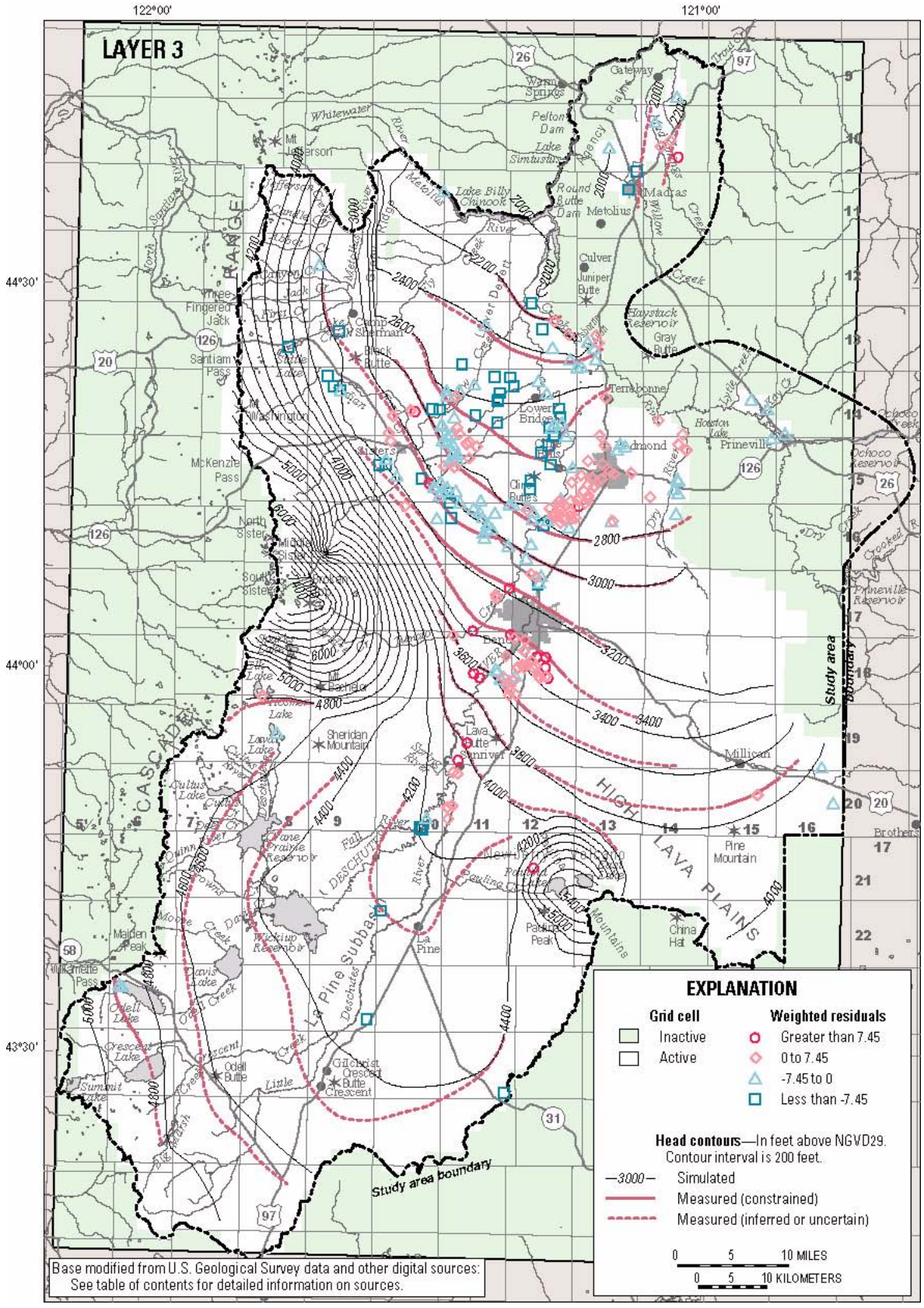

Figure 16. Lines of equal measured head and lines of equal simulated head for all model layers—Continued.

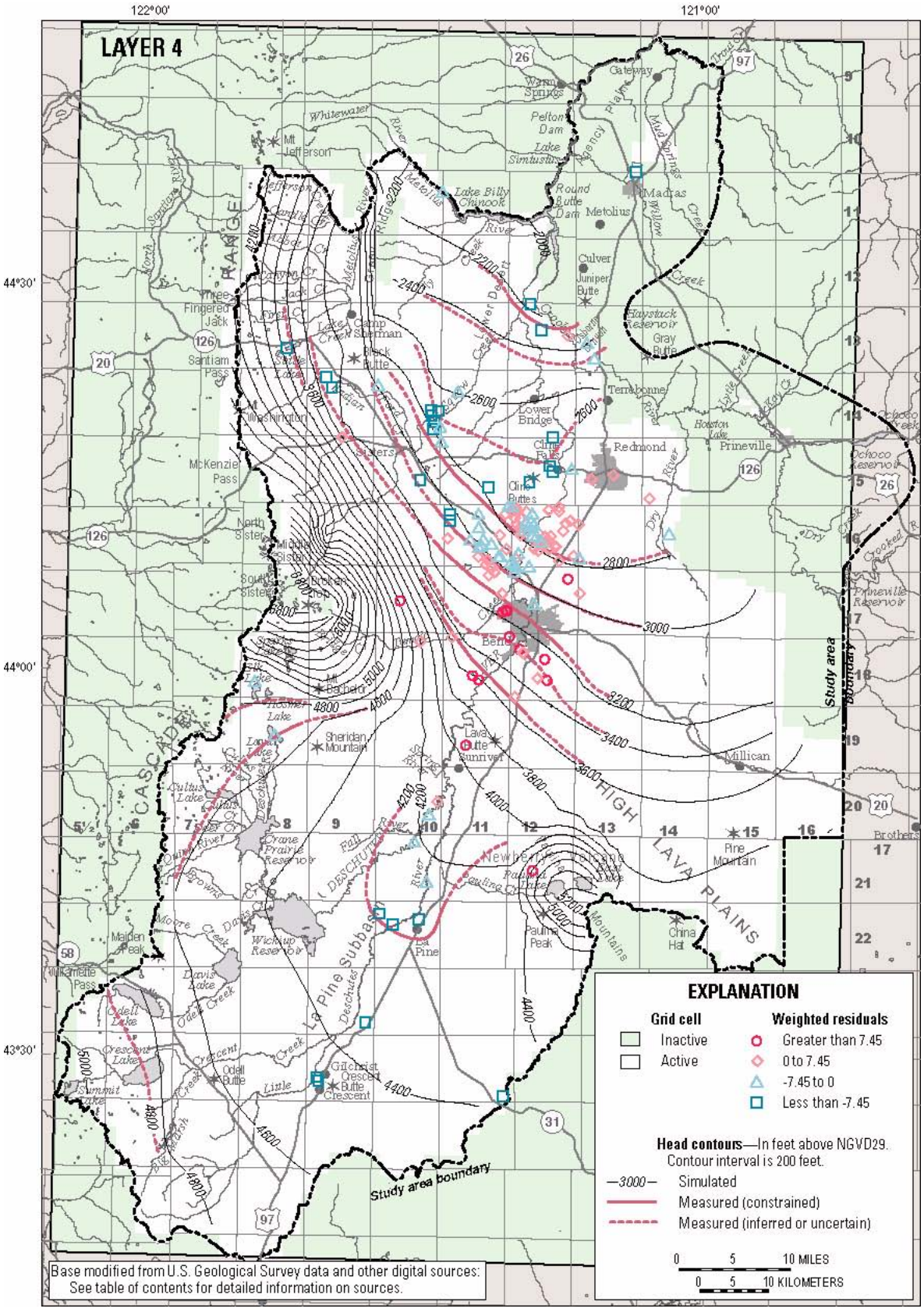

Figure 16. Lines of equal measured head and lines of equal simulated head for all model layers—Continued.

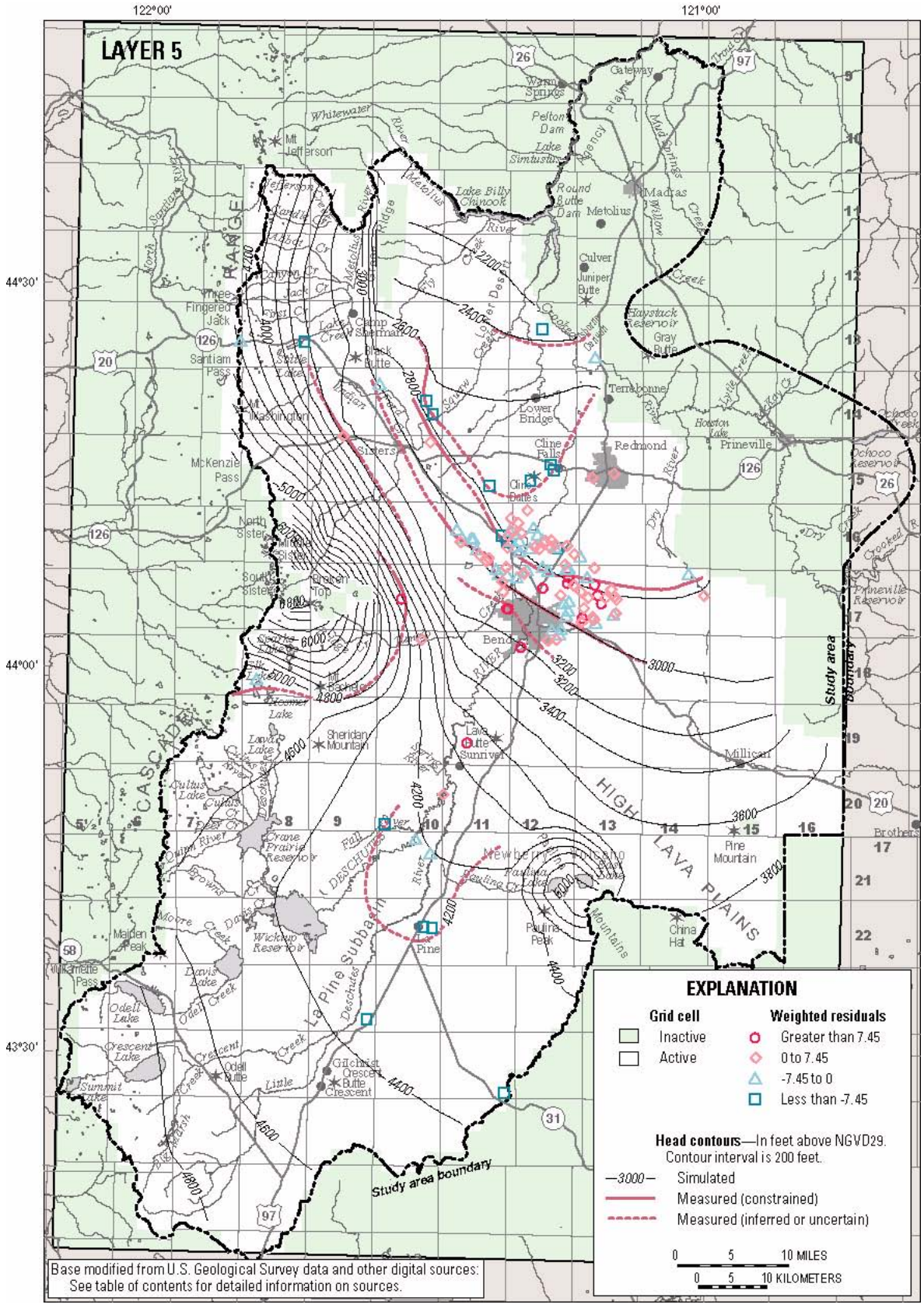

Figure 16. Lines of equal measured head and lines of equal simulated head for all model layers—Continued.

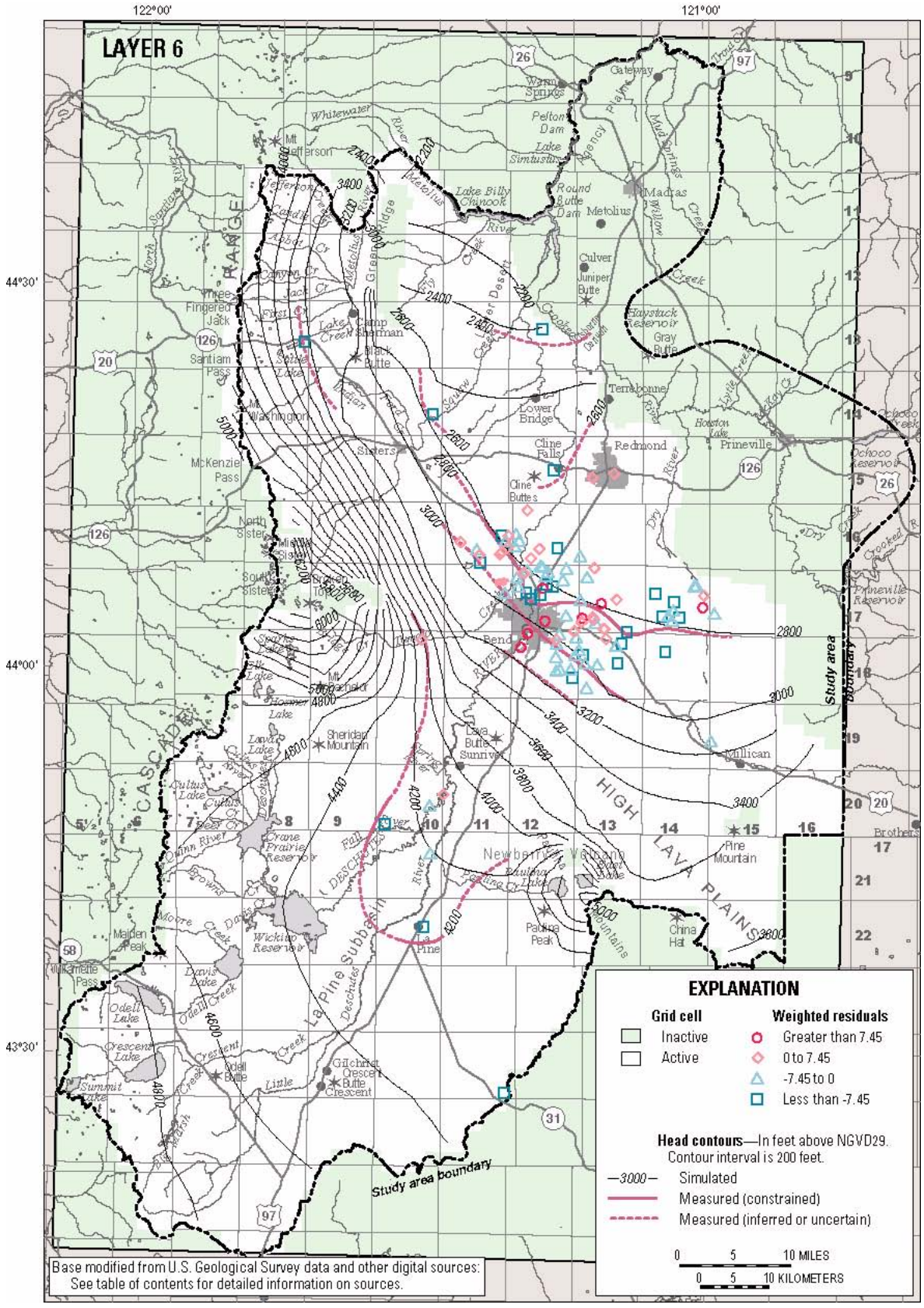

Figure 16. Lines of equal measured head and lines of equal simulated head for all model layers—Continued.

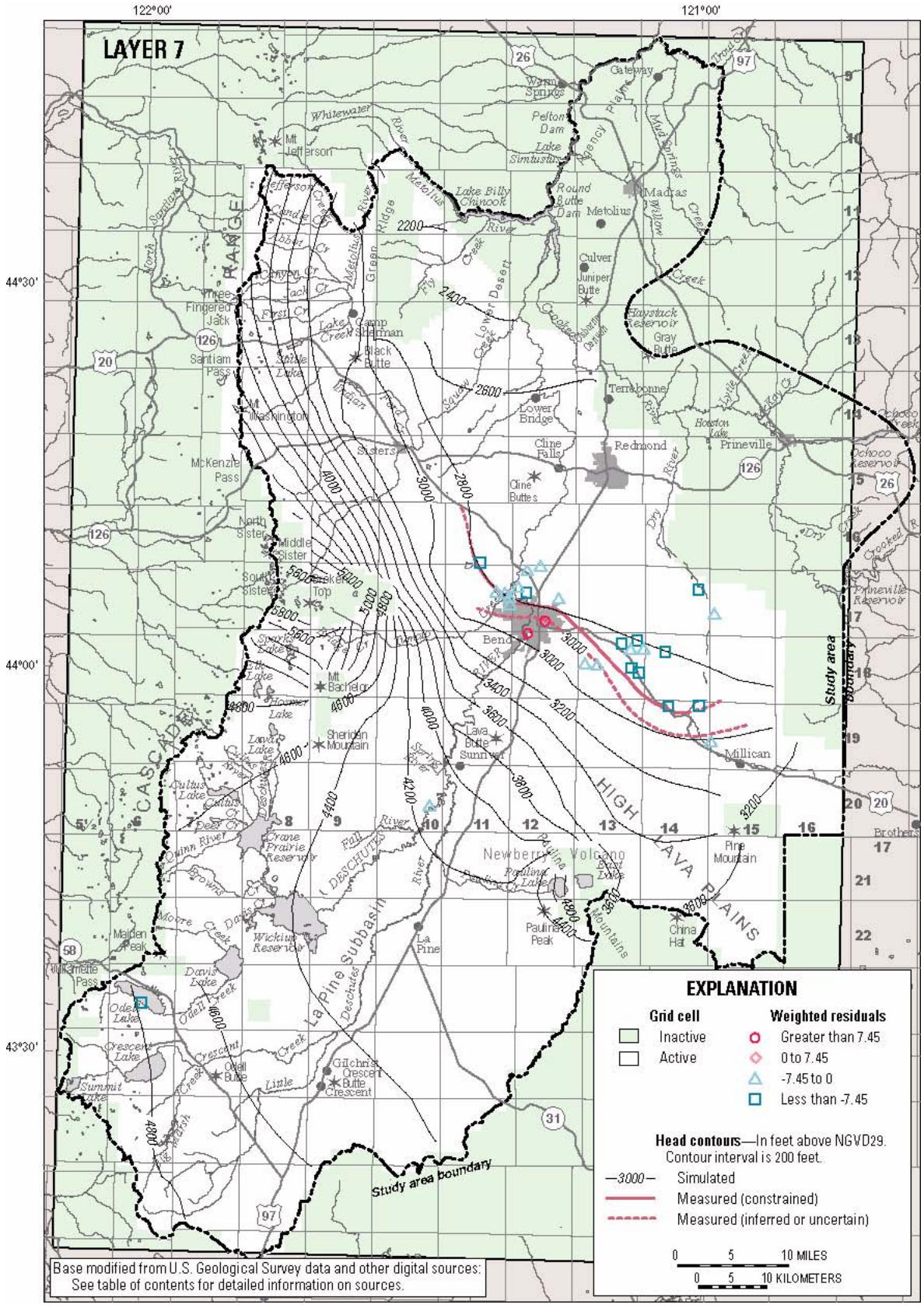

Figure 16. Lines of equal measured head and lines of equal simulated head for all model layers—Continued.

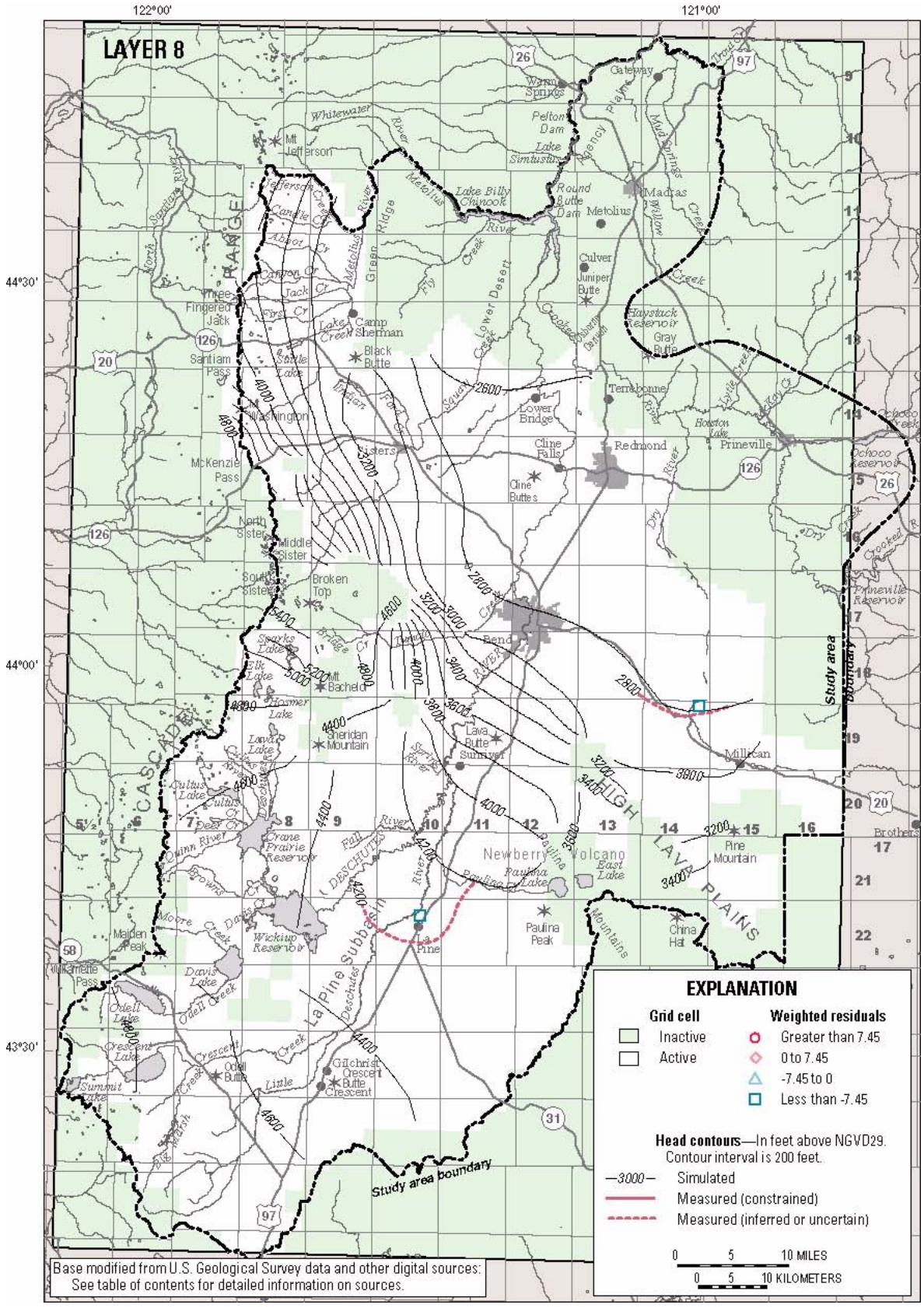

Figure 16. Lines of equal measured head and lines of equal simulated head for all model layers—Continued.

Comparison of Simulated and Observed Steady-State Ground-Water Flow to and from Streams

The reasonableness of simulated ground-water discharge to, or recharge from, streams can be assessed by comparing simulated values with estimates derived by independent methods. Estimates of the average rates and distribution of ground-water flow to and from the Deschutes, Crooked, and Metolius Rivers and most major tributaries in the upper Deschutes Basin were developed by Gannett and others (2001) based on a variety of data from seepage runs conducted by OWRD, gaging stations, and miscellaneous streamflow measurements. Ground-water flow estimates to or from 60 stream reaches were used in the steady-state model calibration. The locations of the 60 reaches are shown in figure 11. Estimated and simulated flows are given in table 3, and a comparison of estimated and simulated flows is shown in figure 17. These data are also shown as a scatter plot in figure 18.

The pattern of stream gains and losses represented by the 60 steady-state flow estimates contains spatial variability that cannot be reasonably simulated with a regional-scale model. The distribution of stream gains and losses is controlled by the interplay of geology, topography, streambed characteristics, and the hydraulic-head distribution in the ground-water system. Data describing the spatial variability of these factors (particularly subsurface geology) is not available in most parts of the upper Deschutes Basin (for example the Cascade Range) at the scales comparable to the resolution of the gain and loss estimates. In addition, topography, a critical factor in the interaction between ground water and streams, is greatly generalized in the regional-scale model.

The regional-scale model, therefore, does not include the level of complexity required to simulate the spatial variations in stream gains and losses represented by the available flow estimates. It is useful, therefore, to aggregate stream reaches and consider net flows of water moving between the ground-water and surface-water systems in subregional areas at scales that reflect model complexity and represent overall hydrologic settings.

Comparisons of estimated and simulated ground-water flows to and from streams aggregated in 13 hydrologic settings (table 4) show that the steady-state model, in general, reasonably simulates the observed magnitude and direction of ground-water flow to and from streams at regional and subregional scales. Estimated and simulated values are shown graphically in figure 19. Simulated ground-water flows to streams are within a factor of 1.4 of estimated values in most major discharge areas.

There are two settings where simulated flows are off by a factor of nearly 20. The largest differences between simulated and estimated flows to and from streams occur along the Little Deschutes River downstream of Crescent Creek in the flat part of the La Pine subbasin, where the simulated ground-water discharge of 88 ft^3/s greatly exceeds the estimated value of 5 ft^3/s. This is expected given that, as previously described, simulated heads are consistently higher than observed heads in that area. The excess discharge here is compensated for in the overall budget by simulated discharge to streams that is slightly lower than observed in the Cascade Range to the west, and simulated losses slightly larger than expected along the Deschutes River to the north. Flow residuals are also large in the area drained by tributaries to the upper Metolius River, where the simulated ground-water discharge of 13 ft^3/s is only about 5 percent of the observed ground-water discharge of 260 ft^3/s. Simulated discharge to the Metolius River main stem is reasonably close to the estimated value.

The rate and distribution of ground-water discharge to major inflow areas along the main stems of the Deschutes, Crooked, and Metolius Rivers, including the area near their confluence**,** are, in general, close to the measured or estimated values. Critical stream reaches along which simulated ground-water discharge rates are close to estimated rates include the main stem of the Metolius River from the headwaters to Jefferson Creek, the Deschutes River between Lower Bridge and the gage near Culver, the Crooked River from Osborne Canyon to the gage below Opal Springs, and Lake Billy Chinook downstream to Lake Simtustus. A significant part of the total ground-water discharge in the upper Deschutes Basin occurs along these reaches, so the close fit between simulated and estimated rates of ground-water discharge is noteworthy.

Table 3. Measured or estimated steady-state stream gains and losses due to ground-water exchange, and simulated equivalents

[Observation locations are shown by number on figure 11; RM, river mile; all values are cubic feet per second; Res., reservoir]

Observation number	Stream reach	Measured or estimated stream flux	Estimated 95% confidence interval on measured or estimated flux			Simulated stream flux
			Estimated 2 sigma	Lower	Upper	
1	Little Deschutes River—above RM 86	-19.7	10	-29.7	-9.7	0.0
2	Little Deschutes River—RM 86–80	-11.8	10	-21.8	-1.8	0.0
3	Little Deschutes River—RM 80–71	2.6	10	-7.4	12.6	-6.6
4	Little Deschutes River—RM 71–64.5	2.0	10	-8.0	12.0	-4.0
5	Big Marsh Creek	-21.0	10	-31.0	-11.0	-47.5
6	Crescent Creek—above RM 18.5	-23.7	10	-33.7	-13.7	-12.0
7	Crescent Creek—RM 18.5–2.2	1.5	10	-8.5	11.5	-24.3
8	Little Deschutes River—RM 57.5–43	-2.3	10	-12.3	7.7	-32.1
9	Little Deschutes River—RM 43–33.5	-2.9	10	-12.9	7.1	-25.7
10	Little Deschutes River—RM 33.5–26.7	0.0	1	-1.0	1.0	-7.9
11	Little Deschutes River—RM 26.7–13.7	0.6	10	-9.4	10.6	-22.4
12	Paulina Creek—RM 13–5.2	6.1	1	5.1	7.1	12.7
13	Odell Lake	-41.0	20	-61.0	-21.0	-23.6
14	Odell Creek—Lake outlet to gage	-41.0	10	-51.0	-31.0	-21.1
15	Odell Creek and Davis Creek above RM 3	-191.0	25	-216.0	-166.0	-102.0
16	Davis Creek below RM 4 (west arm Wickiup Res.)	-15.0	5	-20.0	-10.0	-7.9
17	Cultus River above Crane Prairie Res.	-63.0	20	-83.0	-43.0	-7.9
18	Deschutes River above Crane Prairie Res.	-151.0	20	-171.0	-131.0	-14.9
19	Deschutes River between Crane Prairie Res. and Wickiup Res.	-229.0	50	-279.0	-179.0	-146.0
20	Wickiup Res.	0.0	50	-50.0	50.0	-20.1
21	Deschutes River—Wickiup Res. to RM 217.6	1.5	10	-8.5	11.5	-7.2
22	Deschutes River—RM 217.6–208.6	-6.0	10	-16.0	4.0	-6.4
23	Deschutes River—RM 208.6–199.7	-24.0	10	-34.0	-14.0	-46.2
24	Fall River above RM 5	-119.0	20	-139.0	-99.0	-140.0
25	Fall River—RM 5–0.4	7.0	5	2.0	12.0	-34.0
26	Deschutes River—RM 191.5–189 (includes Spring River)	-271.0	50	-321.0	-221.0	-63.8
27	Deschutes River—RM 198–181.4	23.8	10	13.8	33.8	28.4
28	Deschutes River—RM 181.4–164.4 (Benham Falls to Bend)	89.0	10	79.0	99.0	157.0
29	Tumalo Creek above RM 11 (Columbia Southern diversion)	-68.0	20	-88.0	-48.0	0.0
30	Tumalo Creek—RM 11–3.2	-1.0	5	-6.0	4.0	0.0
31	Tumalo Creek—RM 2.3–0.3	0.2	1	-0.8	1.2	0.0
32	Deschutes River - RM 164.4–145.3 (Bend to Cline Falls)	-15.0	3	-18.0	-12.0	-10.4
33	Deschutes River—RM 138–134 (near Lower Bridge)	-10.0	2	-12.0	-8.0	-22.5
34	Deschutes River—RM 134–124.9 (below Lower Bridge)	-170.0	20	-190.0	-150.0	-210.0
35	Deschutes River—RM 124.9–123.3	-102.0	10	-112.0	-92.0	-31.1
36	Squaw Creek above RM 26.8 (gage)	-65.0	10	-75.0	-55.0	-109.0
37	Indian Ford Creek above RM 10.7 (Black Butte Ranch springs)	-6.1	3	-9.1	-3.1	0.0
38	Indian Ford Creek—RM 10.7–8.0	1.7	2	-0.3	3.7	0.0
39	Indian Ford Creek—RM 8.0–3.6	0.6	1	-0.4	1.6	0.0
40	Indian Ford Creek—RM 3.6–2.1	0.6	1	-0.4	1.6	0.0
41	Indian Ford Creek—RM 2.1–1.3	2.8	1	1.8	3.8	0.0
42	Indian Ford Creek—RM 1.3-–0.8	0.5	1	-0.5	1.5	0.0
43	Indian Ford Creek—RM 0.8 to mouth	0.0	1	-1.0	1.0	0.0
44	Squaw Creek—RM 19.0–16.5	-6.6	1	-7.6	-5.6	0.0

Table 3. Measured or estimated steady-state stream gains and losses due to ground-water exchange, and simulated equivalents —Continued

[Observation locations are shown by number on figure 11; RM, river mile; all values are cubic feet per second; Res., reservoir]

Observation number	Stream reach	Measured or estimated stream flux	Estimated 2 sigma	Estimated 95% confidence interval on measured or estimated flux: Lower	Upper	Simulated stream flux
45	Squaw Creek—RM 1.7 to mouth (includes Alder Springs)	-94.0	10	-104.0	-84.0	-124.0
46	Deschutes River—RM 123.0–120.0 (Culver gage)	-25.0	5	-30.0	-20.0	-88.8
47	Crooked River—RM 20.4–13.8	-70.0	15	-85.0	-55.0	-204.0
48	Crooked River—RM 13.8–6.7 (Opal Springs gage)	-1,006.0	200	-1,206.0	-806.0	-990.0
49	Lake Billy Chinook	-420.0	100	-520.0	-320.0	-558.0
50	Deschutes River Round Butte Dam to Lake Simtustus	-200.0	75	-275.0	-125.0	-22.4
51	Lake Simtustus	-51.0	15	-66.0	-36.0	-14.4
52	Metolius River—RM 41.2 (headwaters) to 38.1	-257.0	50	-307.0	-207.0	-244.0
53	Suttle Lake	-31.0	10	-41.0	-21.0	0.0
54	Lake Creek—Suttle Lake outlet to mouth	-36.0	10	-46.0	-26.0	-5.0
55	First Creek—upper part of drainage	-1.5	5	-6.5	3.5	0.0
56	Jack Creek—upper part of drainage	-46.0	10	-56.0	-36.0	0.0
57	Canyon Creek—entire drainage above RM 0.5	-60.0	10	-70.0	-50.0	-6.2
58	Abbot Creek—entire drainage above RM 1.5	-12.0	5	-17.0	-7.0	-2.1
59	Candle Creek—entire drainage above RM 2.0	-73.0	25	-98.0	-48.0	-0.1
60	Metolius River—RM 38.1–28.8 (Jefferson Creek)	-724.0	100	-824.0	-624.0	-512.0

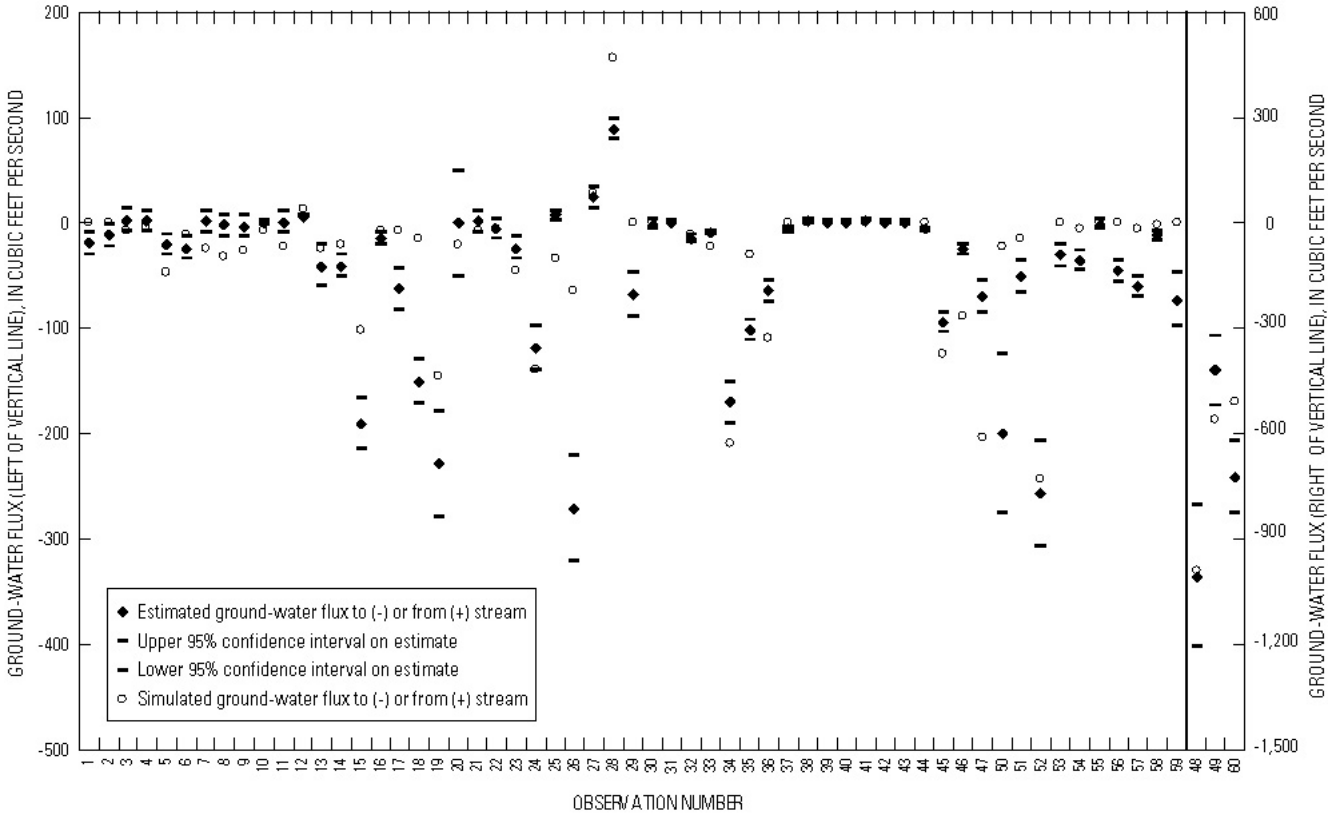

Figure 17. Measured or estimated steady-state stream fluxes, 95-percent confidence intervals on measured or estimated stream fluxes, and simulated steady-state stream fluxes. (The left-hand axis corresponds to observations left of the bold vertical line, and the right-hand axis corresponds to observations with larger values to the right of the bold vertical line.)

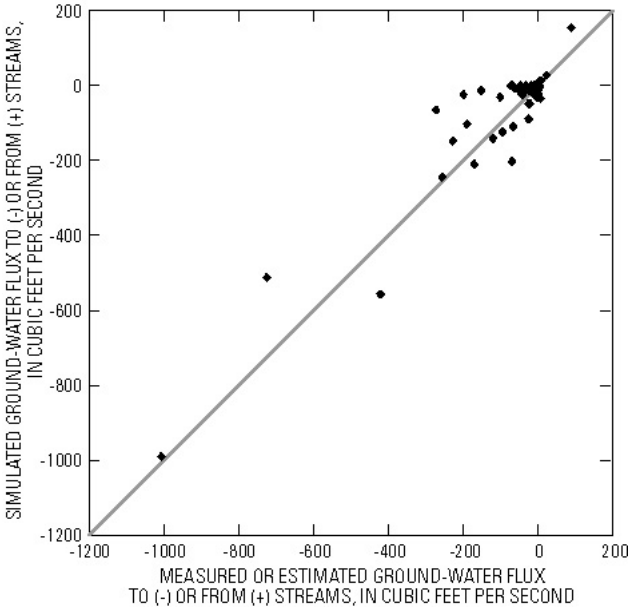

Figure 18. Simulated stream fluxes as a function of measured or estimated stream fluxes.

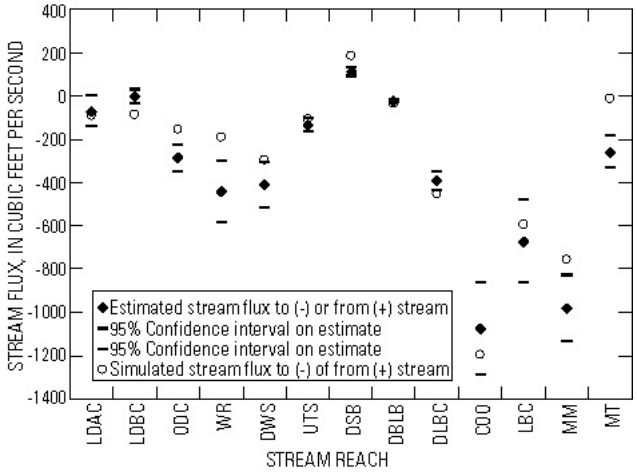

Figure 19. Measured or estimated steady-state stream fluxes, 95-percent confidence intervals on measured or estimated stream fluxes, and simulated steady-state stream fluxes for aggregated stream reaches. (Stream-reach abbreviations explained in table 4.)

Table 4. Measured or estimated gains and losses to aggregated stream reaches, and simulated equivalents

[All values are cubic feet per second; RM, river mile]

Stream reaches	Figure 19 designation	Measured or estimated stream flux	95% Confidence interval on measured or estimated flux		Simulated stream flux
			Lower	Upper	
Little Deschutes River and tributaries above Crescent Creek	LDAC	-70	-140	0	-94
Little Deschutes River below Crescent Creek	LDBC	-5	-36	26	-88
Odell and Davis Creek drainages	ODC	-288	-348	-228	-155
Wickiup Reservoir and tributaries from the north	WR	-443	-583	-303	-189
Deschutes River and tributaries from the west between Wickiup Reservoir and Sunriver	DWS	-412	-517	-307	-298
Upper Tumalo and upper Squaw Creeks	UTS	-133	-163	-103	-109
Deschutes River between Sunriver and Bend	DSB	113	93	133	185
Deschutes River between Bend and Lower Bridge	DBLB	-25	-30	-20	-33
Deschutes River between Lower Bridge and the Culver gage	DLBC	-391	-436	-346	-454
Crooked River between Osborne Canyon and the Opal Springs gage	COO	-1,076	-1,291	-861	-1,194
Lake Billy Chinook and downstream down to and including Lake Simtustus	LBC	-671	-861	-481	-595
Metolius River main stem above RM 28.8	MM	-981	-1,131	-831	-756
Metolius River tributaries above Jefferson Creek	MT	-260	-335	-185	-13

Steady-State Model Water Budget

The steady-state model water budget is evaluated by looking at the instantaneous rates of the various budget components (table 5). The water balance in the model closes to within about 0.02 percent. The recharge, boundary flux, and pumpage components of the budget are specified. Stream leakage and evapotranspiration are head-dependent quantities and are calculated by the model. Total stream-leakage figures in table 5 do not match the total measured (or estimated) stream fluxes given in tables 3 and 4 because not all stream cells are represented in tables 3 and 4. Moreover, the gain and loss observations in tables 3 and 4 are net values integrated over many cells, whereas the budget values are the gross sums of all individual cells. The comparison of measured and simulated stream fluxes presented earlier indicates that simulated stream leakage is reasonable.

Table 5. Steady-state model simulated water budget

[All values in cubic feet per second; ---, not applicable]

Budget component	In	Out
Recharge (precipitation)	3,106	---
Recharge (canal)	492	---
Recharge (on-farm)	68	---
Recharge (total)	3,666	---
Subsurface inflow	847	---
Stream leakage	403	4,464
Evapotranspiration	---	420
Pumpage	---	31
Total	4,916	4,915

It is more difficult to evaluate the simulated evapotranspiration rate of 420 ft^3/s. Gannett and others (2001) estimated that evapotranspiration from the water table in the La Pine subbasin was probably less than 80 ft^3/s. The simulated value of 420 ft^3/s includes evapotranspiration from a much larger area that includes the upper Indian Ford Creek and Metolius River drainages, where shallow ground water is common. Because heads are systematically too high in the La Pine subbasin, as previously described, it can be assumed that evapotranspiration is overestimated in that area.

Transient Calibration

The upper Deschutes Basin regional ground-water model was also calibrated to transient conditions for the 20-year period between 1978 and 1997. This period was chosen for several reasons. First, it was a period of rapid growth in population in the basin. It is also a period of sufficient length to include decadal-scale climate variations that are known to be the principal force driving head and discharge fluctuations. Lastly, this period includes time-series water-level measurements collected by the USGS in the late 1970s as part of an earlier project.

The initial conditions for the transient simulation were based on climate conditions for the 4 years prior to the calibration period. The first stress period for the transient calibration is the winter of 1978 (November 1977 through April 1978). Conditions during the 4 years prior to the beginning of the transient calibration period were slightly wetter than the average conditions during the 1993–95 water years used for steady-state calibration by a factor of about 1.15. The starting heads for the transient calibration were derived from a steady-state simulation using the 1993–95 average recharge rate multiplied by 1.15.

Transient Calibration Data

Time-series head data and ground-water discharge data reflecting the dynamic behavior of the regional ground-water system were used for transient calibration. During the calibration period, head and discharge exhibited decadal and seasonal variations in recharge from precipitation, and seasonal variations in recharge from canal operation. The driving boundary conditions have been described in previous sections.

There are approximately 103 wells with time-series water-level data in the upper Deschutes Basin study area (Caldwell and Truini, 1997). The frequency of measurements varies from 2 hours to once or twice per year, with some wells having multiple-year gaps in records. The duration of record for wells varies from less than a year to over 50 years. Of available wells with time-series data, 64 were evaluated during transient calibration. A number of factors were considered while selecting wells for use in transient calibration. The overall goal was to have good geographic coverage, all hydrologic settings represented, and, where possible, consistent records throughout the calibration period. Wells were generally not used if they were monitored for only a short period of time or included too many nonstatic (pumping or recovering) water levels. Wells that appeared to be responding to influences that cannot be represented in a regional-scale model, such as large influences of nearby canals or pumping wells, were not included.

Information on temporal variations in ground-water discharge to streams (stream fluxes) was derived solely from stream-gage data. Stream-gage data can be used to estimate temporal variations in ground-water discharge only where certain conditions exist. Where a gage is on a stream that is entirely spring fed, the gage provides a direct record of ground-water discharge. For some streams, late season flows can be considered to be largely or entirely ground-water discharge. In these situations, the gage record can be used to estimate year-to-year variations but are not useful for evaluating seasonal variations. Where two gages exist on a stream, the ground-water inflow to the intervening reach can be estimated by comparing the gages, provided tributary inflows and diversions can be quantified. All of these situations occur in the upper Deschutes Basin.

The maximum ET rate was varied each stress period according to residual ET calculated by the DPM, as explained in the preceding section on boundary conditions. Public water-supply pumping was varied each stress period, with values based on data from water providers and population records. Irrigation pumping for the transient calibration was based on the 1993–95 steady-state values but varied according to climate-driven variations in consumptive use. Pumping for individual irrigation wells was included only for stress periods postdating the issuance of the associated water right.

Transient Calibration Procedure

Transient calibration was achieved using traditional trial-and-error methods. Regression methods were not employed because the model parameterization scheme, which was developed using the steady-state data set, was not well suited for allowing meaningful, stable, nonlinear regression using the transient data set. Transient data were much fewer than steady-state data and had a different spatial distribution. Trial-and-error methods for the transient calibration provided satisfactory results and met the overall project goals.

The same model parameter structure was used for the transient calibration as was used for the steady-state calibration. The only difference was the addition of storage coefficients. The storage coefficient parameterization followed the hydraulic-conductivity zonation. After experimentation it was determined that satisfactory transient calibration could be achieved using all of the parameter values from the steady-state calibration and adjusting only storage coefficients. Storage coefficients were adjusted by layer in each of the hydraulic-conductivity zones. In general, best results were achieved when storage coefficients decreased with depth (table 6).

Table 6. Final storage coefficient values

[na, zone not present in the layer]

	Storage coefficient							
Zone	Layer 1	Layer 2	Layer 3	Layer 4	Layer 5	Layer 6	Layer 7	Layer 8
1	0.004	0.002	0.002	0.00004	0.00004	0.00004	0.00004	0.000004
2	0.008	0.002	0.002	0.00004	0.00004	0.00004	0.00004	0.000004
3	0.15	0.0015	0.0015	0.00015	0.00015	0.00015	0.00015	0.00015
4	0.01	na	na	na	na	na	na	na
5	na	0.01	0.01	0.01	0.01	0.01	0.01	0.001
[a]6	0.3	na	na	na	na	na	na	na
[b]6	0.03	na	na	na	na	na	na	na
7	0.04	0.02	0.002	0.0006	0.0002	0.0002	0.00005	0.00005
8	0.01	0.0005	0.0005	0.0005	0.0005	0.0005	0.0001	0.0001
9	0.01	0.001	0.001	0.001	0.001	0.001	0.001	0.0001
10	0.05	0.05	0.05	0.05	0.05	0.01	0.0005	0.0005
11	0.02	0.004	0.004	0.004	0.002	0.002	0.0004	0.0004
12	0.001	0.001	0.001	0.001	0.001	0.001	0.001	0.0001
13	0.08	0.08	0.08	0.08	0.08	0.04	0.008	0.0008
14	0.05	0.05	0.05	0.01	0.01	0.005	0.001	0.0001
15	0.01	0.001	0.001	0.001	0.001	0.001	0.001	0.0001
16	0.002	0.001	0.001	0.001	0.001	0.001	0.001	0.0001
17	0.01	0.001	0.001	0.001	0.001	0.001	0.001	0.0001

[a] Metolius River drainage.
[b] All other areas.

Storage coefficients ranged from 0.3, for coarse, near-surface alluvial deposits, to 4×10^{-6}, for materials greater than 1,000 feet below the top of the saturated zone in the Cascade Range (zones 1 and 2). Specific storage values ranged from approximately 10^{-3} to 10^{-8} and also decreased with depth. This change in storage coefficients with depth is to be expected in volcanic terranes where the system is unconfined or semi-confined near the surface and becomes increasingly confined with depth. Moreover, specific storage values can be expected to decrease with depth as well, as rocks become increasingly altered and have less porosity. The final storage coefficient values are within reasonable and expected ranges, and are consistent with aquifer-testing results described in preceding sections (also see Gannett and others, 2001, table 1). The spatial distribution of final storage coefficient values is consistent with geologic information, with larger values generally occurring in parts of the Deschutes Formation where volcaniclastic and alluvial deposits are prominent in the section. Lower values were generally related to regions dominated by fine-grained sediments or thick lava sequences without coarse interbeds.

Comparison of Simulated and Observed Transient Heads

Time-series water-level data from 103 wells were available for the modeled area. As previously discussed, not all of these wells were suitable for use in model calibration because water levels in some wells responded to stresses that cannot be simulated in a regional-scale model. Water levels fluctuate in the upper Deschutes Basin in response to a variety of driving forces that work at different temporal and spatial scales. Long-term climate cycles are the dominant driving force, affecting the entire region and working on a decadal time scale. Annual recharge cycles also work over the entire region. Canal leakage and irrigation, also important driving forces, affect only parts of the model area and have an annual cycle that is out of phase with the timing of natural recharge. Which of these two seasonal processes dominates is largely a function of location. Other forces include stream-stage variations and ground-water pumping. These work at a variety of scales, generally small relative to other stresses. The model simulates the fluctuations caused by climate cycles, natural recharge from precipitation, and canal leakage and irrigation. Stream-stage variation is not explicitly represented in the model, so water-level fluctuations resulting from variations in stream stage are not simulated. Although ground-water pumping is included in the model, drawdown effects are averaged over entire model cells, so large fluctuations close to pumping wells are not simulated.

As was discussed in the previous section on steady-state calibration, observed water-level elevations are not matched exactly, particularly in regional-scale models with large head gradients. In the upper Deschutes Basin, the water-table elevation ranges over at least 4,500 feet. Elevations of head measurements from wells used in the model calibrations range from 1,797 to 5,586 feet. A comparison of measured and simulated heads (fig. 16) shows that the general geometry and elevation of the water table is simulated well at the regional scale. At any particular well, however, simulated and measured heads will differ. Fitted error statistics (Hill, 1998) for head residuals in the steady-state calibration indicate that the fitted standard deviation for heads is about 76 feet. This means that about 68 percent of the simulated heads are within 76 feet of the measured values, and that approximately 95 percent are within 152 feet. This error must be kept in mind when evaluating the head fluctuations simulated by the transient model.

Measured temporal head fluctuations in the upper Deschutes Basin during the calibration period range from less than 1 foot to as much as 30 feet. Most measured fluctuations are in the 5 to 10 feet range. This range of fluctuations is small compared to the steady-state head residuals. It is unlikely, and unexpected, that the transient calibration would improve on the fit to absolute head elevations. The principal goal in transient calibration is to match observed head fluctuations. Therefore, when assessing the transient calibration with respect to heads, comparing simulated and observed fluctuations is more important than comparing absolute head elevations. To aid in comparing water-level fluctuations, graphs in this section have separate vertical axes for measured and simulated water levels. The axes have the same vertical scale but may be offset; the amount of offset can be determined by comparing the vertical axes on the graph.

For the purposes of discussing simulated water-level fluctuations, the modeled area is divided into 12 subareas (fig. 20). The subareas are geographically distinct regions within which wells generally show similar water-level fluctuation patterns. Each subarea contains 2 to 10 wells with time-series water-level data. In the following paragraphs, the subareas are discussed in an approximate north to south order.

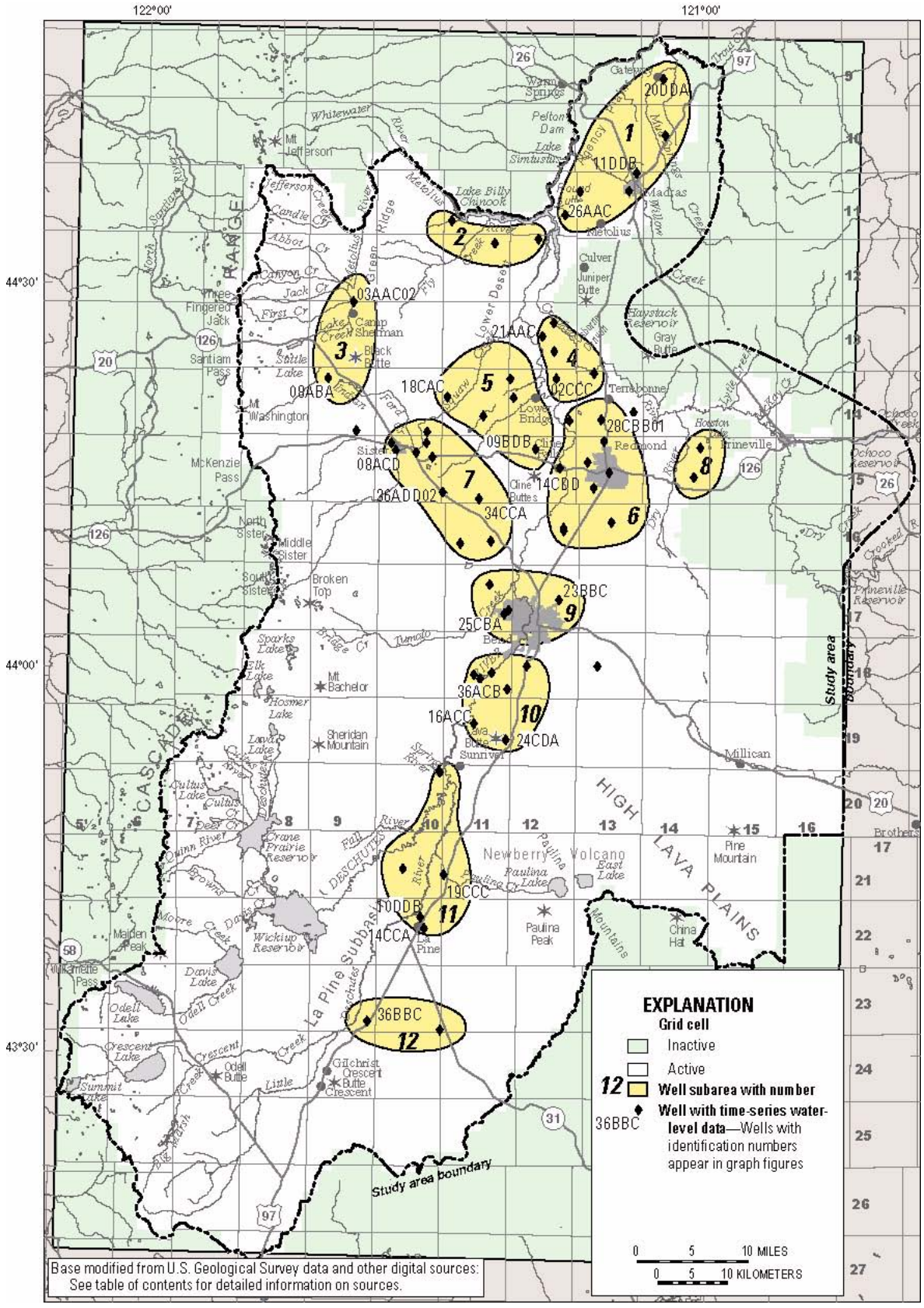

Figure 20. Subareas used for discussion of water-level fluctuations.

(1) Madras/Gateway Area

The Madras/Gateway area represents the entire model area north and east of Round Butte Dam (fig. 20, area 1). There are six wells with time-series water-level data in this area, representing the top four layers in the model. The general climate-driven pattern of water levels in this area, exemplified by well 09S/14E-20DDA (fig. 21), is a slight decline starting in the early 1980s followed by an abrupt rise starting in late 1996 or early 1997. Three wells in the area (typified by well 11S/12E-26AAC, fig. 21) do not follow this pattern but, contrary to climatic trends, exhibit a rising water level from the mid-1980s to the mid-1990s. The cause for this anomalous rise is not known, but it may be related to long-term effects of the filling of Lake Billy Chinook (Gannett and others, 2001). Because there is no process or boundary condition within the model to cause the anomalous rise, such as the filling of Lake Billy Chinook, it was not possible to simulate the rise. Simulated and observed water-level fluctuations match reasonably in wells such as 09S/14E-20DDA and 11S/13E-11DBB (fig. 21) where the fluctuations are driven by climatic factors.

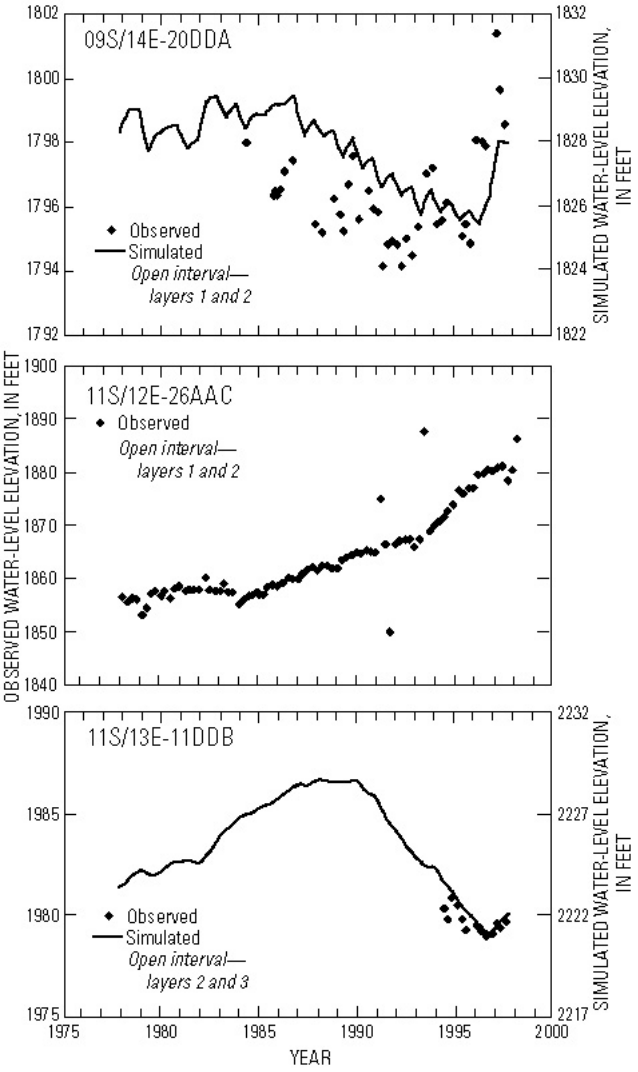

Figure 21. Simulated and observed water-level fluctuations in the Madras/Gateway area.

(2) Lower Desert Area

The Lower Desert area includes the region just south of the Metolius River arm of Lake Billy Chinook (fig. 20, area 2). There are three wells in this area with time-series water-level data, all of which exhibit anomalous behavior related to Lake Billy Chinook (see Caldwell and Truini, 1997, p. 22). Two of the wells exhibit the anomalous long-term rise contrary to climatic conditions described in the last section. The third well, for which only about 3 years of data are available, shows anomalous fluctuations likely related to either pumping or stage changes in the lake. Because of the anomalous behavior of these wells, comparisons with simulated fluctuations is not considered meaningful.

(3) Black Butte/Upper Metolius River Area

The Black Butte/upper Metolius River area extends from the uppermost Metolius River to south of Black Butte (fig. 20, area 3). The two wells with time-series data, 14S/09E-08ABA and 13S/09E-03AAC02 (fig. 22), represent model layers 1, 3, and 4. Data from the wells start in 1993 and 1994, respectively, so only the latter part of the calibration period is represented. Water levels in the area were generally declining until early 1995, when a snowmelt event caused a slight rise in water level. Water levels rose sharply during the winters of 1996 and 1997. Simulated water levels show both the early decline and subsequent water-level rises. The timing and magnitude of the measured and simulated fluctuations match reasonably well in the Black Butte/upper Metolius River area. Well 14S/09E-08ABA is particularly important, because it is one of the few wells representative of conditions in the Cascade Range, the principal recharge area.

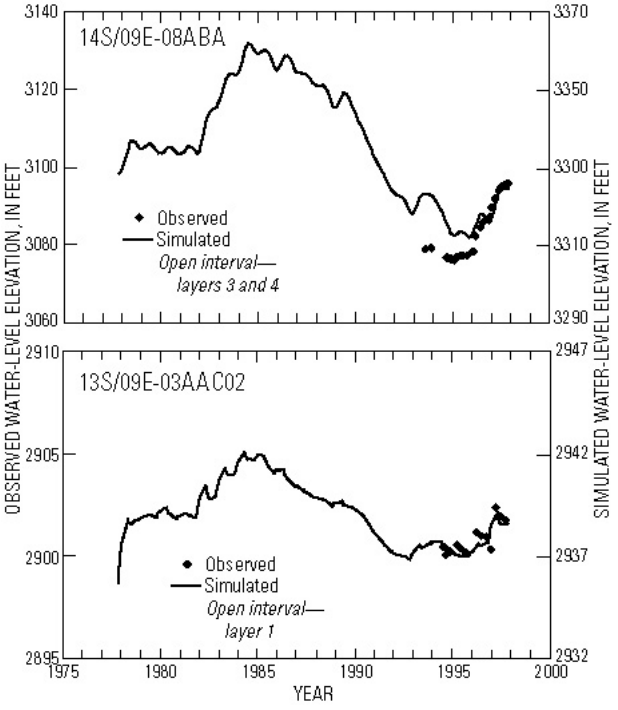

Figure 22. Simulated and observed water-level fluctuations in the Black Butte/upper Metolius River area.

(4) Peninsula Area

The Peninsula area includes the region between the Deschutes and Crooked Rivers north of Lower Bridge (fig. 20, area 4). Time-series water-level measurements are available for five wells in the area, but data only go back to 1993, so only the later part of the calibration period is covered. One well that has less than 2 years of data and an anomalous shallow water level is not considered further. Another well showed fluctuations dominated entirely by nearby canal leakage and so is also not considered useful for regional model calibration. The remaining three wells, which represent the top three model layers, showed slight declines (0.5 to 2.0 feet) between 1994 and 1996, followed by a general rise in water levels starting in late 1996 in response to wetter conditions (fig. 23). The wells also showed slight seasonal fluctuations of generally less than one-half a foot. Simulated head fluctuations match both the measured long-term decline and rise and also the seasonal variations. The simulated rise in water levels starting in 1996, however, is generally larger than that observed. The timing of fluctuations are simulated accurately in well 13S/12E-21AAC, but less so in well 14S/12E-02CCC.

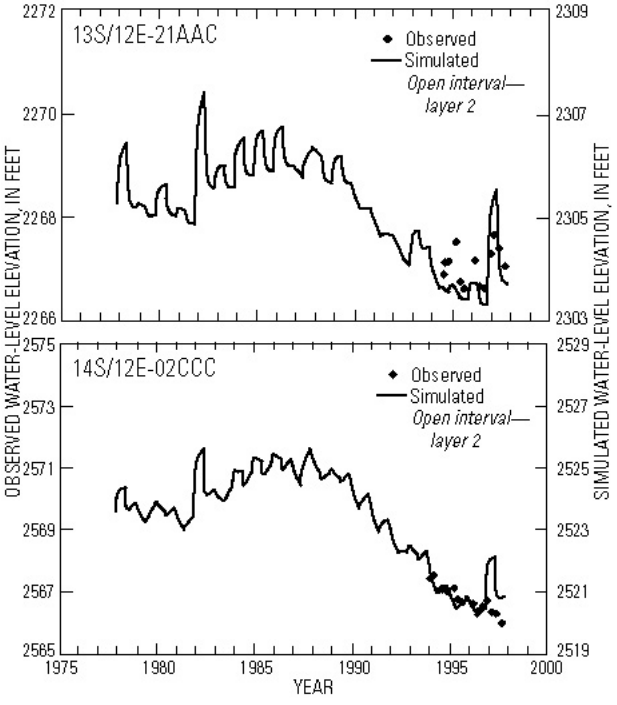

Figure 23. Simulated and observed water-level fluctuations in the Peninsula area.

(5) Lower Squaw Creek/Deep Canyon Area

The lower Squaw Creek/Deep Canyon area includes the region between the Deschutes River and Squaw Creek, extending south to about Cline Falls on the Deschutes River and to about Henkle Butte on Squaw Creek (fig. 20, area 5). Data were available for five wells in the area representing the top three model layers. All wells include measurements from 1993 to 1997, and three include some measurements from 1978 and 1979. There are no measurements in the area from the 1980s and early 1990s. As depicted by wells 15S/12E-09BDB and 14S/11E-18CAC (fig. 24), measurements show that water levels in the area declined approximately 5 feet between the late 1970s and mid-1990s. The decline continued until 1996, when water levels stopped declining and started to rise in response to the prevailing wet conditions. Simulated water-level fluctuations also show the long-term decline followed by the rise in response to wetter conditions. Simulated fluctuations generally match observed fluctuations well in both timing and magnitude in the lower Squaw Creek/Deep Canyon area.

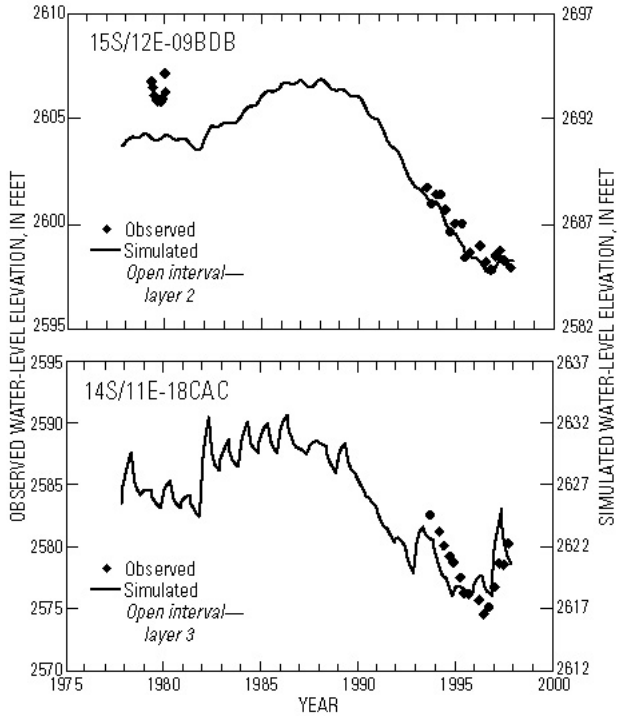

Figure 24. Simulated and observed water-level fluctuations in the lower Squaw Creek/Deep Canyon area.

(6) Redmond Area

The Redmond area, as used herein, refers to the region between the Deschutes River and Dry River that extends from Terrebonne south to about Long Butte (fig. 20, area 6). There are 11 wells with water-level fluctuation data available in this area representing the top four model layers. One of the wells, 15S/13E-18ADD (fig. 25) provides a continuous record of water-level trends throughout the calibration period. This well shows that the water table in the area rose slightly between the late 1970s and late 1980s, and then declined until late 1996 or 1997. Other wells in the area with shorter data sets, 15S/12E-14CDD and 14S/13E-28CBB01, show the end of the decline with more detail, and also show seasonal fluctuations. Simulated water levels match both the timing and magnitude of long-term water-level fluctuations in the Redmond area.

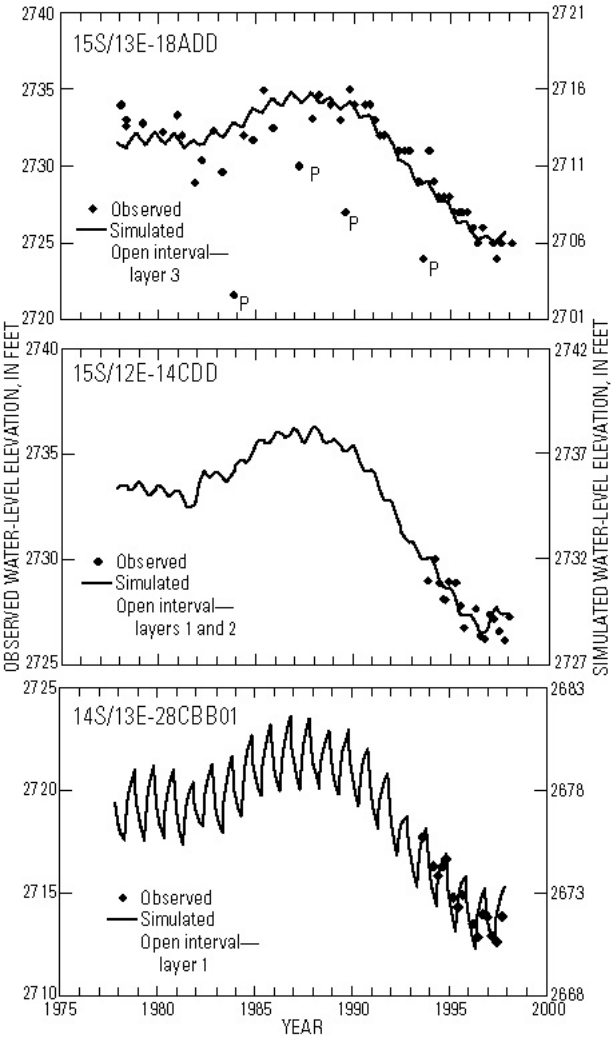

Figure 25. Simulated and observed water-level fluctuations in the Redmond area. (A "p" indicates measurements affected by pumping.)

Simulated and observed water-table fluctuations also match at shorter time scales. The simulated water levels in well 14S/13E-28CBB01 (fig. 25) match both seasonal fluctuations, which occur locally in response to irrigation and canal operation, and the longer term climatic signal (the year-to-year variation) in the observed data. The seasonal fluctuations observed in well 15S/12E-14CDD are out of phase with the irrigation-caused fluctuations, and are likely due to fluctuations in river stage. Because river-stage variations are not included in the model, simulated water levels in well 15S/12E-14CDD do not show this seasonal fluctuation, but only the longer-term climate-driven fluctuation. This well is largely unaffected by canal operation and irrigation.

(7) Sisters/Tumalo Area

The Sisters/Tumalo area extends from the region around the City of Sisters and McKinney Butte southeast to Tumalo (fig. 20, area 7). There are 10 wells in this area with time-series data representing mostly the top three model layers. One well is open to layers 5 and 6. Well 15S/10E-08ACD (fig. 26) has continuous record throughout the calibration period. Three of the wells have some data from the late 1970s and mid-1990s, but no data from the 1980s and early 1990s. Wells with long-term data show that water levels in the area were declining during the late 1970s. Water levels rose from the early 1980s until about 1986, which marked the start of a decline that lasted until about 1996. Water levels began to rise again in 1996 in response to the return to wet climatic conditions.

Simulated water levels match the timing of climate-driven changes in observed water levels reasonably well, usually within a year (fig. 26). However, the simulated water levels show a long-term downward trend that is steeper than actually observed. This mismatch is seen in a few other places in the model, but seems to be restricted to the upper few layers. The reasons for the mismatch early in the calibration period could be due to initial conditions. The initial conditions chosen gave the best overall model fit and were consistent with climatic conditions immediately prior to the calibration period. The initial conditions are, however, steady state and may not reflect the spatial variability of true initial conditions throughout the modeled area. As typified by wells 15S/10E-36AAD02 and 15S/11E-34CCA, the match between simulated and observed water-level trends during the 1990s is generally quite good in the Sisters/Tumalo area.

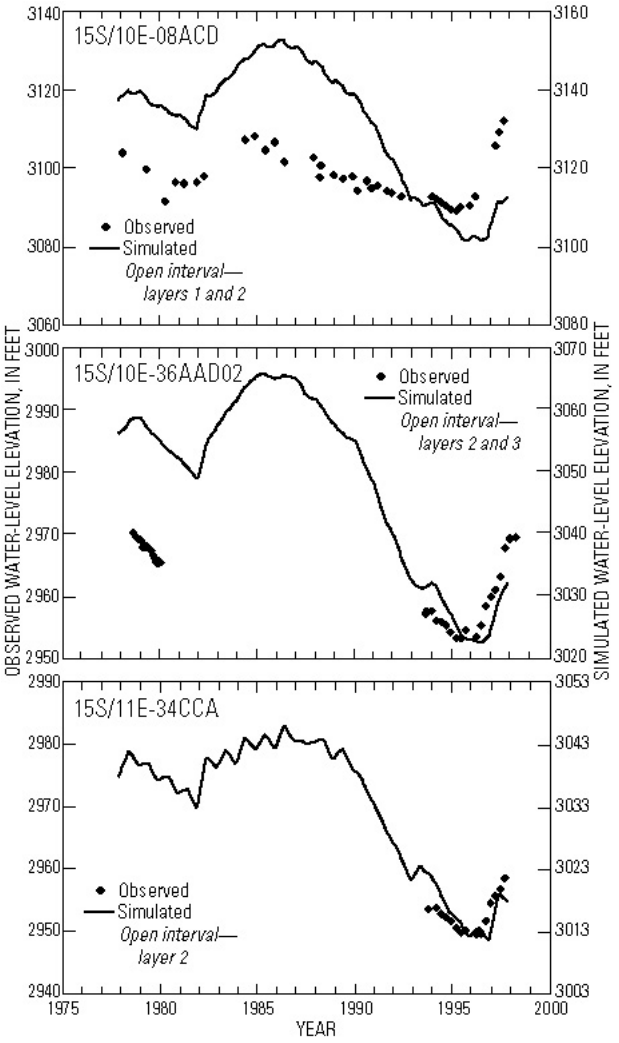

Figure 26. Simulated and observed water-level fluctuations in the Sisters/Tumalo area.

(8) Powell Butte Area

The Powell Butte area includes the region around and north of the town of Powell Butte (fig. 20, area 8). There are two wells in this area with time-series data from 1994 into 1997. Measurements in the area show stable or slightly declining water levels with seasonal fluctuations of 1 to 2 feet. Neither of the wells appears to have responded to the wet winters of 1996 and 1997. Simulated water levels show larger than measured seasonal fluctuations and a rise in water levels in response to the wet winters. Because both of these wells are near the margin of the pre-Deschutes Formation rocks, and on the model boundary, their value in assessing model calibration is unclear.

(9) Lower Tumalo Creek/Bend Area

The lower Tumalo Creek/Bend area refers to the vicinity of the City of Bend, Awbrey Butte, and lower Tumalo Creek (fig. 20, area 9). There are four wells with time-series data representing model layers 1, 2, 4, 5, and 7. No wells have continuous observations throughout the calibration period. There are measurements spanning the mid-1990s from all four wells, and some measurements from the late 1970s from two wells, 17S/11E-25CBA and 17S/12E-23BBC (fig. 27). Water levels in the area were declining during the late 1970s. No data are available for the 1980s and early 1990s, but based on data from other areas, water levels probably rose during the first one-half of the 1980s and then started to decline until the mid-1990s. Simulated water levels match the general trends observed in the measurements. The decline in simulated water levels between the late 1970s and the early 1990s is steeper than measured in the shallow layers (well 17S/11E-25CBA) and less steep than measured in the deep layers (well 17S/12E-23BBC). There are also slight short-term (year-to-year) variations in the measurements, probably due to pumping and/or nearby canal operation not present in the simulated water levels.

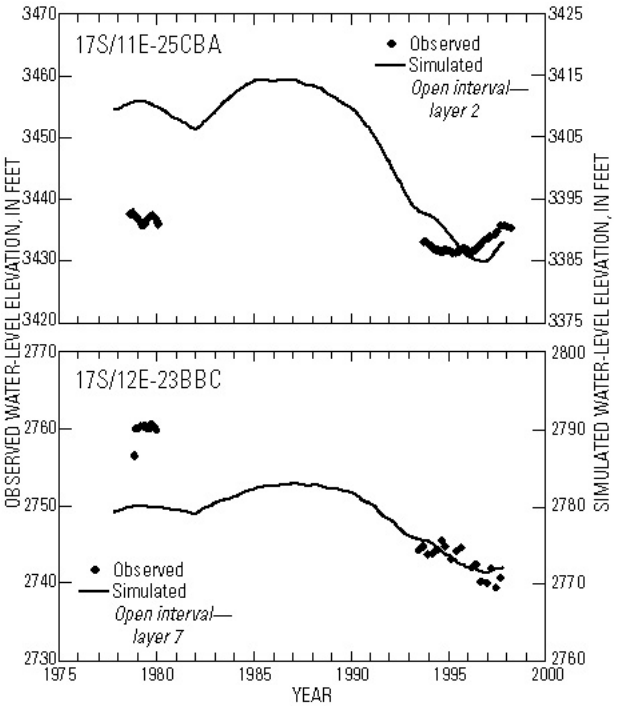

Figure 27. Simulated and observed water-level fluctuations in the lower Tumalo Creek/Bend area.

(10) Benham Falls Area

The Benham Falls area includes the region around Benham Falls and Lava Butte, and extends north to Lava Island (fig. 20, area 10). There are six wells with time-series data in this area representing the top four model layers. None of the wells has continuous record through the calibration period, all have measurements from the early to mid-1990s, and three also have measurements in the late 1970s. Measurements indicate that water levels in the area were stable or showed only very slight declines between the late 1970s and the 1990s (fig. 28).

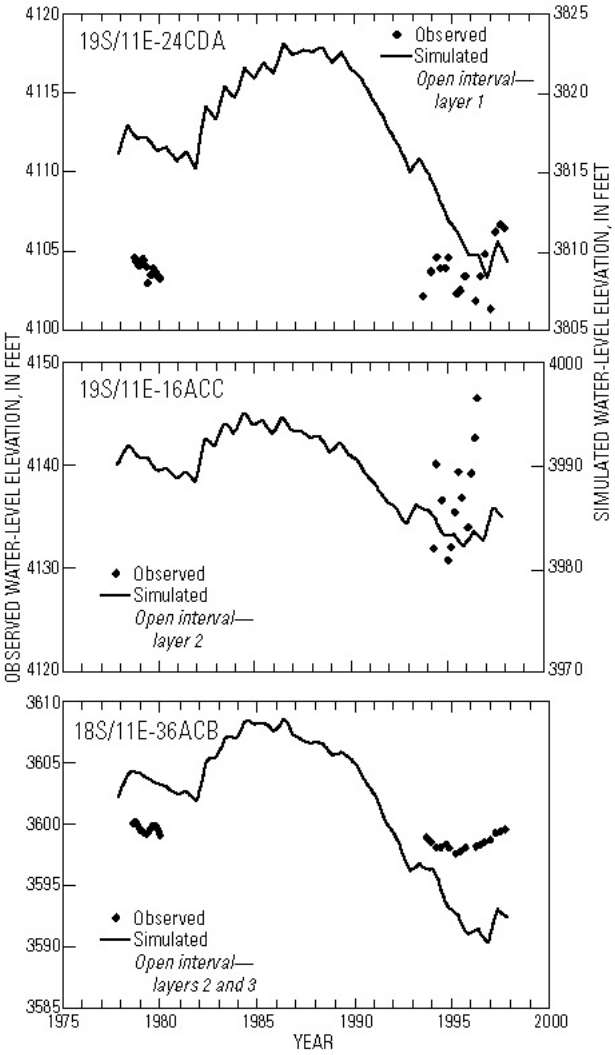

Figure 28. Simulated and observed water-level fluctuations in the Benham Falls area.

This is in contrast to many other regions, where water levels have fluctuated to a much larger degree in response to climate cycles. The stable water levels likely result from the moderating influence of the Deschutes River, which leaks water across this region at a long-term rate that is comparatively constant relative to climate variations. Wells in this area do, however, exhibit seasonal fluctuations of up to 6 to 10 feet (wells 19S/11E-24CDA and 19S/11E-16ACC), with fluctuations generally largest closest to the river. Gannett and others (2001) show that water-level fluctuations in well 19S-11E-16ACC result from variations in river stage caused primarily by releases from Wickiup Dam.

The match between simulated and observed water-level fluctuations in the Benham Falls area is poor. In general, simulated water levels show climate-driven decline in water levels of about 5 to 10 feet that is not observed in the data (fig. 28, wells 19S/11E-24CDA and 18S/11E-36ACB). The model is probably not reflecting the moderating effect of leakage from the Deschutes River on long-term fluctuations. In addition, simulated water levels do not show the seasonal fluctuations in the measured water levels. This is expected because the stream-stage variations that drive water-table fluctuations in this area are not present in the model. Simulated water levels do show the water-level rise caused by the onset of wet climatic conditions seen in the measured data.

(11) Central La Pine Subbasin

There are five wells with time-series data in the central La Pine subbasin (fig. 20, area 11). Three wells represent model layer 1, one well is open to model layers 5 and 6, and one well is open to model layer 8. One well has measurements for the entire calibration period, and a second has measurements from the mid-1980s to the mid-1990s. Long-term data from well 21S/11E-19CCC (fig. 29) show water-level trends similar to those observed elsewhere in the basin. Water levels rose from the early to mid 1980s, and then started a decline that lasted until the mid-1990s. The return to wet weather in 1996 caused water levels to start rising again. The character of water-level fluctuations in the La Pine subbasin varies with depth. Seasonal fluctuations that are prominent in shallow wells, such as well 21S/11E-19CCC, are virtually lacking in deep wells, such as 22S/10E-10DDB. The magnitude of longer term climate-driven fluctuations appears to be subdued at depth as well.

Simulated water-level fluctuations match those observed in most regards. The magnitude of the long-term, climate-driven trends are reasonably matched in both shallow and deep wells. In well 22S/10E-10DDB (fig. 29), open to model layer 8, the maximum and minimum simulated water levels appear to lag the observations by about 1 year. This lag does not appear to be present in well 22S/10E-14CCA, which is open to model layers 5 and 6. Both the timing and magnitude of long-term fluctuations are simulated at shallow depths (well 21S/11E-19CCC). The magnitude of annual fluctuations is also simulated well at shallow depths. The match between the timing of simulated and observed annual water-level fluctuations at shallow depths is variable. This is due to the limitations of the semiannual stress periods in the model.

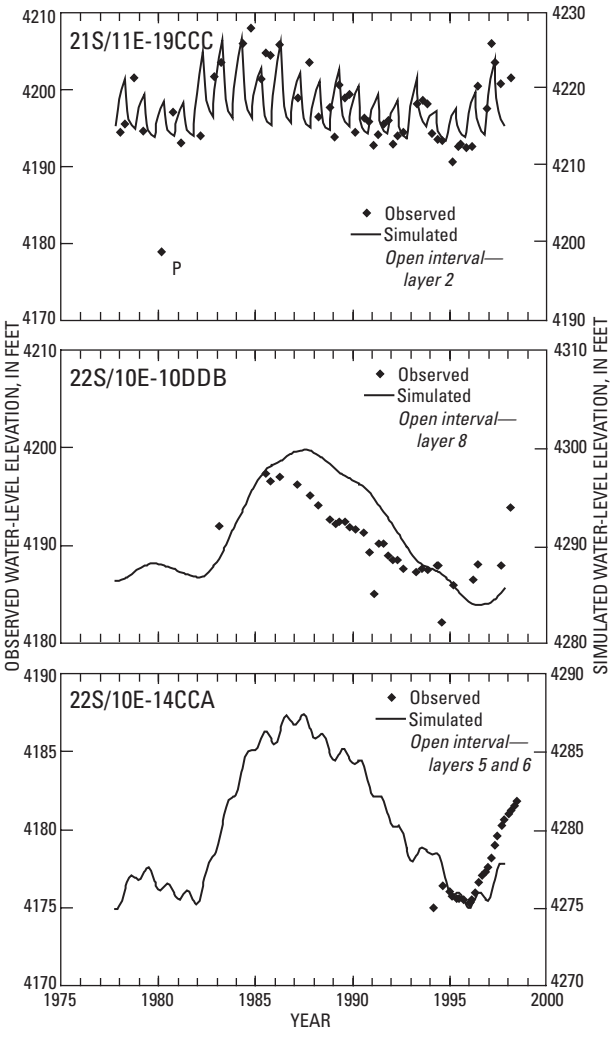

Figure 29. Simulated and observed water-level fluctuations in the central La Pine subbasin.

(12) Southern La Pine Subbasin

There are two wells with time-series data in the southern part of the La Pine subbasin (fig. 20, area 12). One is open to model layer 2, and the second is open to model layers 2 through 5. Measurements are available for both wells only for the mid-1990s, and no data are available on long-term water-level trends in the area. It is likely that long-term trends mirror the climate-driven trends seen elsewhere in the basin. Both wells in the area show apparent climate-driven water-level rise on the order of 2 feet during 1996 and 1997 as typified by well 23S/09E-36BBC (fig. 30). Neither well shows any annual fluctuation.

Simulated and observed water-level fluctuations do not match well in this part of the model. Simulated water levels exhibit annual fluctuations not observed in the measurements. Moreover, simulated water levels show a greater year-to-year variation than observed. Data from elsewhere in the La Pine subbasin show that shallow wells exhibit pronounced annual water-level fluctuations and that fluctuations in deeper wells are much more subdued. The observed water levels in this area are similar to those in deep wells elsewhere in the La Pine subbasin, while the simulated water levels are similar to those measured in shallow wells elsewhere in the subbasin. In other words, the model is not properly simulating the variation in water-level fluctuations with depth in this area. This should not be a problem with the use of the model, since this area is on the periphery of the model and far from critical stream reaches and areas of likely water use.

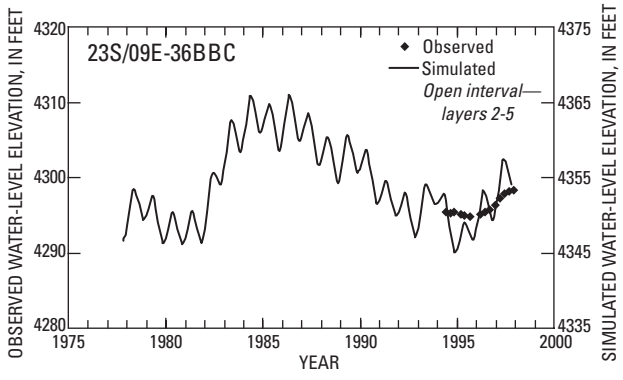

Figure 30. Simulated and observed water-level fluctuations in the southern La Pine subbasin.

Summary of Simulated Water-Level Fluctuations

Water-level fluctuations in the upper Deschutes Basin are primarily driven by climate cycles, canal leakage and irrigation, and variations in stream stage. Water-level fluctuations can also be caused by pumping. The upper Deschutes Basin ground-water model simulates fluctuations caused by climate cycles, annual recharge cycles, and canal leakage and irrigation. Water-level fluctuations caused by stream-stage variations are not simulated.

Climate-driven water-level fluctuations are simulated with reasonable accuracy over most of the model area. The timing of the simulated water-level response to the change to wet conditions starting in 1996 matches the observed response within months, in most cases, and generally within a year. The timing and magnitude of simulated water-level fluctuations caused by annual pulses of recharge from precipitation match those observed reasonably well, given the limitations of the time discretization in the model. Water-level fluctuations caused by annual canal leakage are simulated very well over most of the area where this occurs. Time discretization was not a problem in simulating canal-leakage effects because the stress periods in the model were designed to approximate the irrigation season.

There are some areas in the model where simulated long-term water-level declines exceed the observed decline (fig. 26). This can be the case even where the simulated and observed short- and long-term fluctuations match well. This appears to be an artifact of the starting heads and of starting with steady-state conditions.

Comparison of Simulated and Observed Transient Ground-Water Discharge to Streams

Streamflow data were used to estimate temporal variations in ground-water discharge to seven stream reaches in the modeled area representing major ground-water discharge areas. The ability to accurately simulate ground-water discharge variations to some reaches was limited by the scale of the model grid relative to the scale of the stream network. This was a particular problem with streams above Crane Prairie Reservoir, where model cells are up to 10,000 feet on a side and streams are often less than a mile apart. In such areas, it is more meaningful to look at ground-water discharge to regions of the model than to evaluate individual stream reaches.

The ability to simulate the exact timing of observed annual variations in ground-water discharge was limited by the time descretization in the model. The semiannual stress periods in the model were the same each year of the simulation: November to April and May to October. The actual timing of recharge from winter storms and snowmelt varies from year to year. Comparison of simulated and observed year-to-year variations is less affected by this timing. Simulated temporal variations in ground-water discharge are compared with estimated variations based on stream-gage data in the following paragraphs.

Odell Creek

Temporal variations in ground-water discharge to the Odell Creek drainage were estimated from streamflow gage data from Odell Creek (USGS station number 14055600). Streamflow at this point contains both ground-water and surface-water components, including flow from Odell Lake. A hydrograph of daily and monthly mean flows (fig. 31) shows many individual storm peaks, in addition to the annual spring runoff peaks. Baseflow, the ground-water component of flow inferred from low-flow periods on the hydrograph, ranged between 50 and 200 ft^3/s during the calibration period. Simulated ground-water discharge to the Odell Creek drainage above the gage (fig. 31) closely approximates the baseflow inferred from the stream hydrograph in both magnitude and timing of variations.

Streams above and below Crane Prairie Reservoir

Streams above Crane Prairie Reservoir are considered together because the scale of the stream network in this area is small compared to that of the model grid. Because of the scale discrepancy, not all streams above Crane Prairie Reservoir could be included in the model. Cultus Creek and the Deschutes River were represented in the model because they spanned the region drained by ground-water fed streams in the area.

Measured monthly mean flows and simulated baseflow of Cultus Creek are shown in figure 32. The flow of Cultus Creek responds rapidly to snowmelt and then goes dry (or nearly so) each fall, indicating that it is dominated by surface runoff and shallow ground-water discharge. Simulated baseflow (fig. 32) exceeds actual baseflow (as inferred from monthly mean values for low-flow months), particularly during the fall. The amplitude of the simulated baseflow variation is significantly less than that measured. Patterns of long-term baseflow variation are similar. Cultus River, a ground-water dominated stream with a mean annual discharge of 63 ft^3/s, is roughly a mile from Cultus Creek. Because Cultus River is not explicitly represented in the model, Cultus Creek, as simulated, must represent at least part of the ground water that actually discharges to Cultus River. Therefore, it is reasonable that simulated baseflow to Cultus Creek should exceed that actually measured.

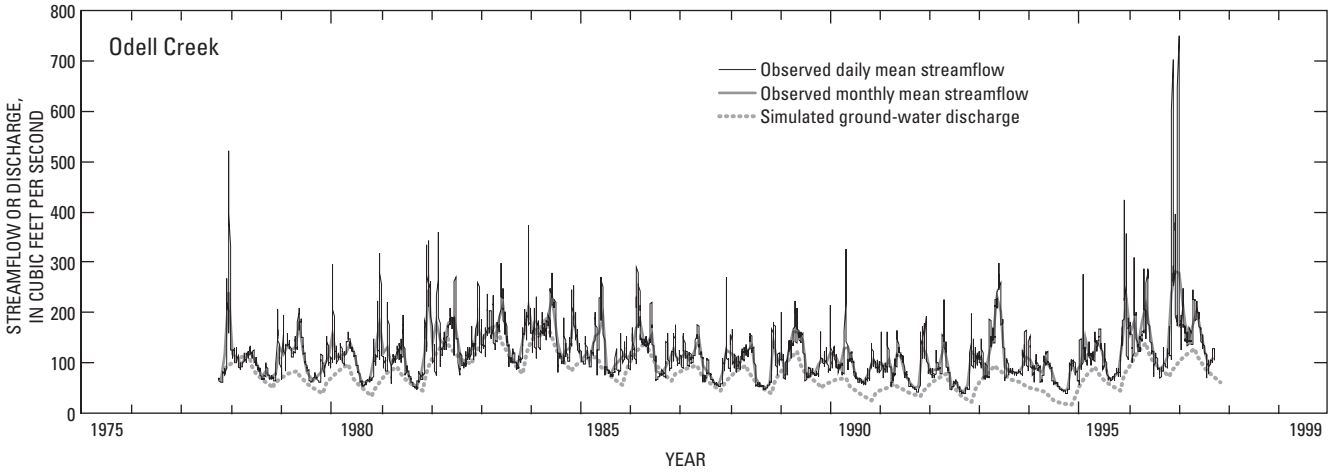

Figure 31. Daily and monthly mean flows of Odell Creek, and simulated ground-water discharge, 1977 to 1997.

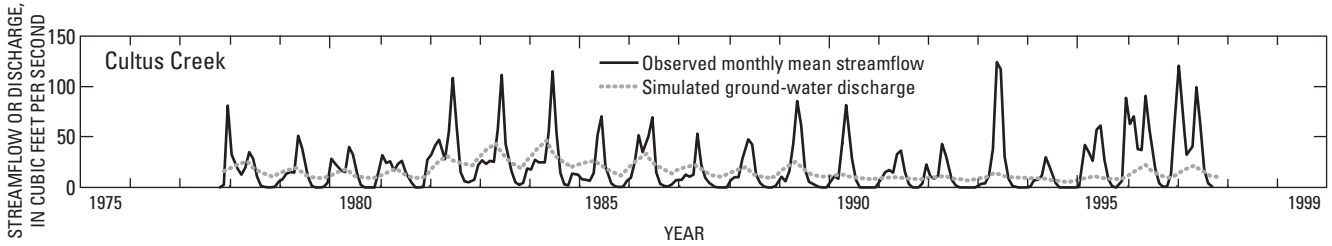

Figure 32. Monthly mean flow of Cultus Creek, and simulated ground-water discharge, 1977 to 1997.

Ground-water discharge in the vicinity of the uppermost Deschutes River can be evaluated from the streamflow gage below Snow Creek (USGS station number 14050000), just above Crane Prairie Reservoir. The hydrograph of daily and monthly mean flows (fig. 33) shows that the Deschutes River at this point is largely ground-water fed with little response to individual storms. The annual peaks caused by snow-melt are much larger than in other ground-water fed streams in the area, suggesting that the stream is fed in part by a relatively shallow ground-water system. Simulated ground-water discharge to the Deschutes River is lower than observed (fig. 33). Given that the Deschutes River must represent (in part) discharge to Cultus River as well, it is apparent that overall ground-water discharge in the area of the model above Crane Prairie reservoir is too low by roughly 50 to 100 ft^3/s. This limits the usefulness of the model for evaluating ground-water discharge fluctuations in this area.

Simulated ground-water discharge volumes below Crane Prairie Reservoir and above Davis Creek appear reasonable. Although there are no stream-gage data to estimate temporal variations in ground-water discharge to this reach of the Deschutes River, the simulated discharge compares favorably with the estimated average discharge from 1993 to 1995 used in the steady-state calibration (fig. 34).

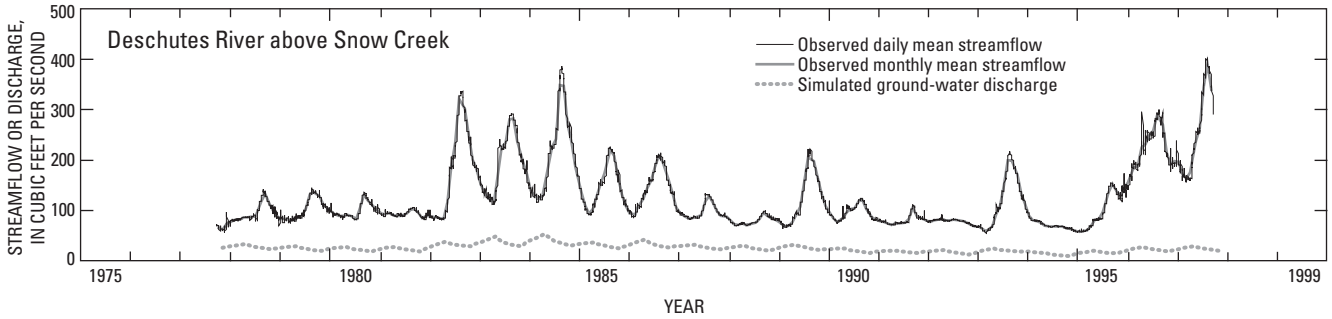

Figure 33. Daily and monthly mean flows of the Deschutes River above Snow Creek, and simulated ground-water discharge, 1977 to 1997.

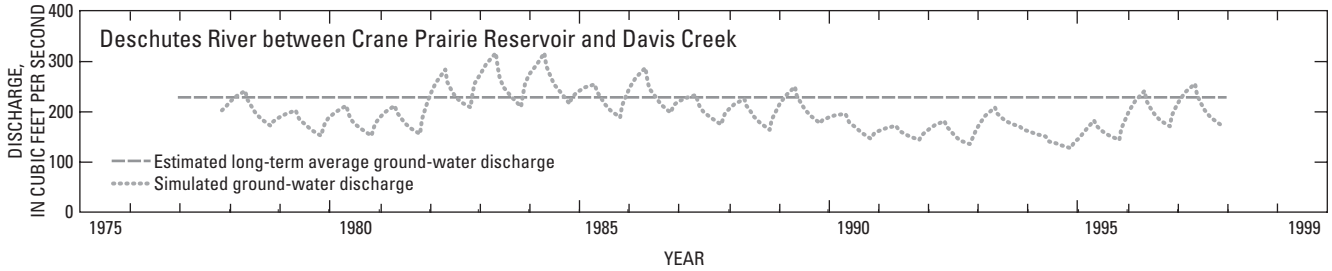

Figure 34. Simulated ground-water discharge to the Deschutes River between Crane Prairie Reservoir and Davis Creek, and estimated long-term ground-water discharge, 1977 to 1997.

Fall River

Fall River is entirely spring fed, so the gage record (USGS station 14057500) directly represents ground-water discharge. Simulated ground-water discharge to Fall River exceeds measured discharge by roughly one-third (about 50 ft^3/s) (fig. 35). The magnitude and timing of discharge variations, however, is considered good given the constraints of model grid scale and stress-period definition.

Metolius River Drainage

A hydrograph of monthly mean discharge of the Metolius River just upstream of Lake Billy Chinook (USGS station number 14091500) (fig. 36) shows that seasonal variations are small relative to the total discharge, as is typical of ground-water dominated streams. The Metolius River accounts for a large part of the total ground-water discharge in the upper Deschutes Basin. Much of the discharge is to springs along the main stem above Jefferson Creek and to lower parts of tributaries. Temporal variations in ground-water discharge to the Metolius River are difficult to estimate precisely because the only long-term gaging station on the river is low in the drainage, just upstream of Lake Billy Chinook. The streamflow at this point includes flow from both ground-water and surface-water dominated tributaries, some of which include glacial meltwater. It is clear, however, that a large proportion of the total flow of the Metolius River comes from ground water, and the flow seldom drops below 1,200 ft^3/s. October mean flows can be taken to represent regional ground-water discharge to the Metolius River. To correct for possible glacial contributions, the flow of Jefferson Creek and the Whitewater River (gaged since 1984 and 1983, respectively) can be subtracted from the flow of the Metolius River.

Simulated ground-water discharge matches October mean flows (corrected for Whitewater River and Jefferson Creek) reasonably well, particularly with respect to decadal-scale fluctuations (fig. 36). The notable departure between simulated ground-water discharge and October mean flows occurs in 1996 and 1997. The extremely wet winters of 1996 and 1997 caused a substantial increase in flow from the Metolius River drainage. It is apparent that during the fall of both 1996 and 1997 the flow of the Metolius River was still receding from the previous winter.

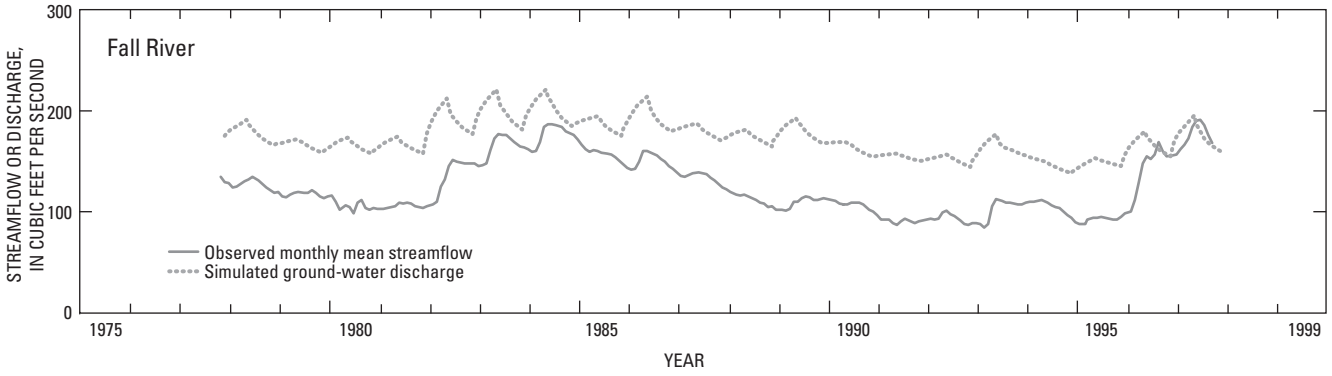

Figure 35. Monthly mean flow of Fall River and simulated ground-water discharge, 1977 to 1997.

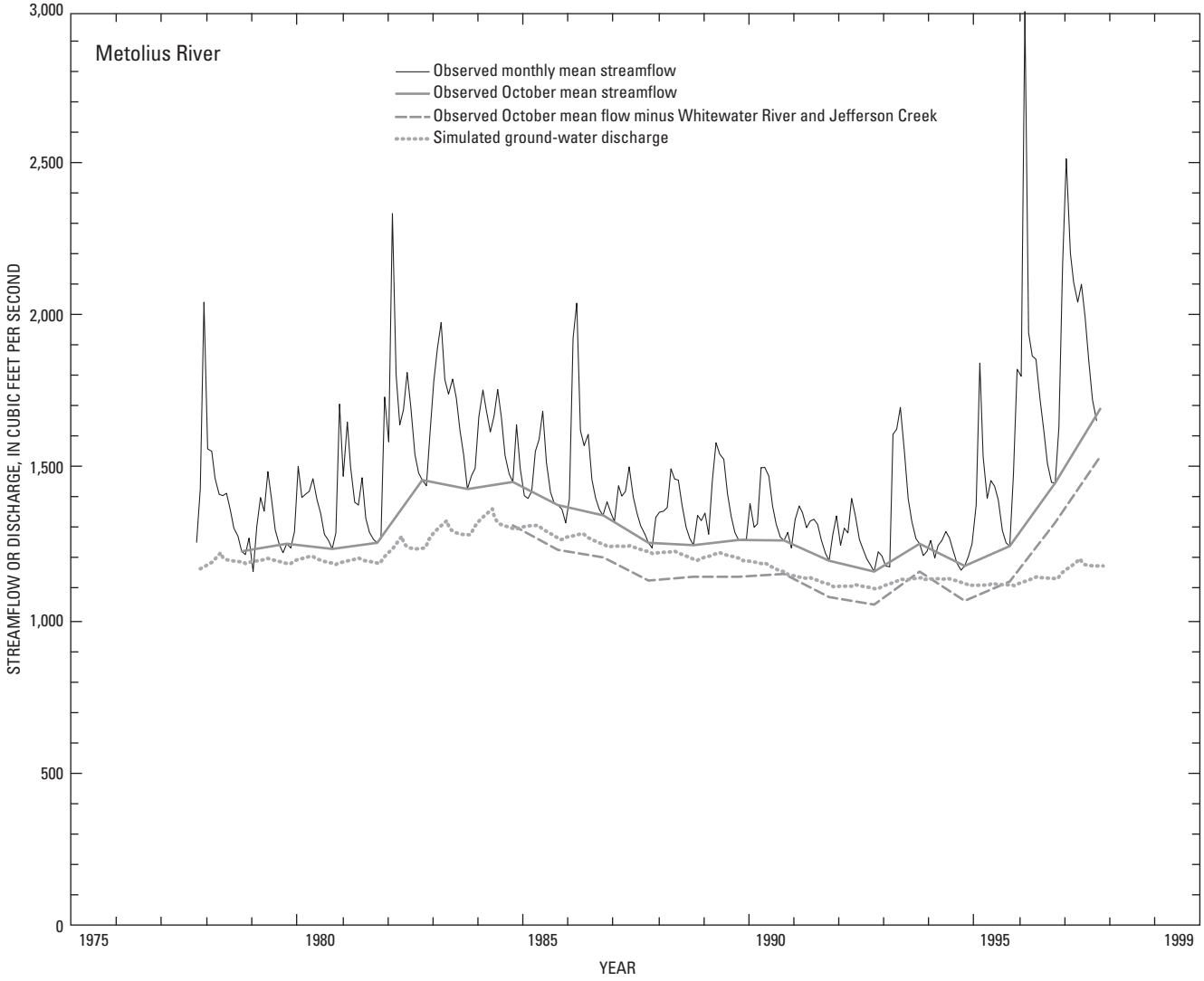

Figure 36. Monthly mean and October mean flow of the Metolius River, October mean flow of the Metolius River minus the October mean flows of Whitewater River and Jefferson Creek, and simulated ground-water discharge, 1977 to 1997.

Deschutes River—Bend to Culver

Temporal variations in ground-water discharge to the middle section of the Deschutes River can be evaluated by comparing data from gaging stations below Bend (USGS station number 14070500) and near Culver (USGS station number 14076500). During the summer months, tributary inflow to this reach is negligible, and the increase in flow of the river is attributable entirely to ground-water discharge (including discharge to the lower 2 miles of Squaw Creek). The amount of ground-water discharge can be determined by subtracting the flow at Bend from the flow at Culver during summer months. During the winter months, however, ungaged tributary inflow precludes the use of gage data to estimate ground-water discharge. Gage data, therefore, can be used to evaluate the year-to-year variations in ground-water discharge, but not seasonal variations.

The magnitude and timing of year-to-year variations in simulated fall ground-water discharge match observed variations in August mean ground-water discharge reasonably well (fig. 37). The total rate of simulated ground-water discharge exceeds observed discharge by roughly 100 to 150 ft^3/s. The larger discrepancy early in the simulation period is likely an artifact of starting conditions. The difference late in the simulation period is consistent with the steady-state calibration.

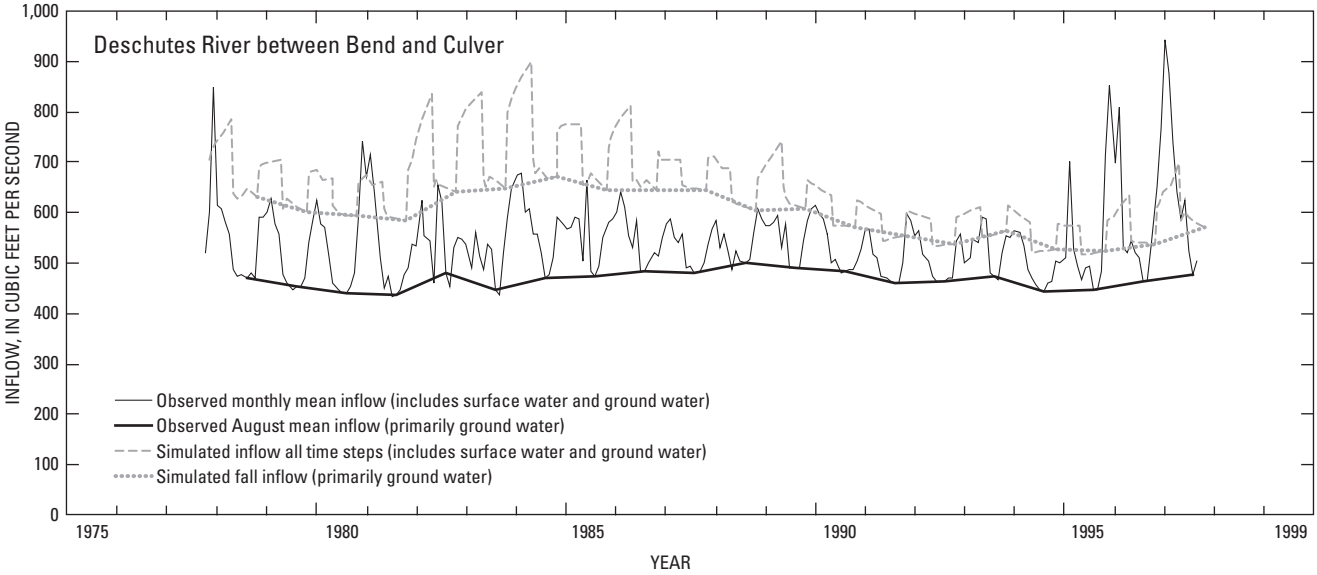

Figure 37. Measured monthly mean inflow to the Deschutes River between Bend and Culver, 1977 to 1997, and simulated inflow for all time steps. (Inflow includes both surface-water and ground-water components during winter months. Measured August mean inflow and simulated fall inflow is due almost entirely to ground-water discharge.)

Lower Crooked River

The lower Crooked River from Osborne Canyon to the mouth is one of the principal ground-water discharge areas in the upper Deschutes Basin, with ground-water discharge exceeding 1,000 ft^3/s. Ground-water discharge to the lower Crooked River was estimated using data from the streamflow gage below Opal Springs. During the late summer and early fall, the flow below Opal Springs consists almost entirely of ground-water discharge. The late summer/early fall flow of the Crooked River below Opal Springs has been used to evaluate long-term changes in ground-water discharge to the river (Sceva, 1968; Gannett and others, 2001). This can be done because long-term changes in ground-water discharge are large compared to variations in late-summer/early fall flow from upstream. Flow measurements below Opal Springs are of limited use in evaluating seasonal variations in ground-water discharge, however, because these variations are small compared to variations in flow from upstream. In order to evaluate short-term variations in ground-water discharge to the lower Crooked River, flow from upstream must be accounted for. Measurements of streamflow upstream of the ground-water discharge area are not available for the simulation period; however, insight can be gained from measurements available for a few years prior to the calibration period.

Streamflow just upstream of the ground-water inflow area (near Terrebonne) was measured from October 1968 to July 1973. These measurements can be subtracted from the flow at Opal Springs to evaluate short-term variations in ground-water discharge to the lower Crooked River. A comparison of monthly mean discharge between the two gages (fig. 38) shows that almost all of seasonal flow variation observed at the Opal Springs gage can be attributed to surface-water flow from upstream. Ground-water discharge, calculated as the difference between the two gages, shows much less variation. The short-term variations in the difference between the gages correspond exactly to the variations in streamflow. This suggests that the variations in the difference may not be due to variations in ground-water discharge, but are likely related to ungaged tributary inflow or systematic measurement error. A comparison of July mean flows at Terrebonne and Opal Springs (fig. 39) shows that even the year-to-year variations in discharge at Opal Springs are due predominantly to surface water upstream of the ground-water discharge area. In summary, variations in regional ground-water discharge to the lower Crooked River are small on a year-to-year basis and most pronounced at longer (decadal) time scales. This is to be expected given the scale of the ground-water system contributing to discharge at this point.

Simulated transient ground-water discharge to the lower Crooked River is consistent with inferences made from gage data (fig. 40). Simulated ground-water discharge shows small year-to-year variations and only slightly larger long-term (decadal) variation. The amount of simulated ground-water discharge is very close to the average late summer/early fall streamflow at Opal Springs during the calibration period.

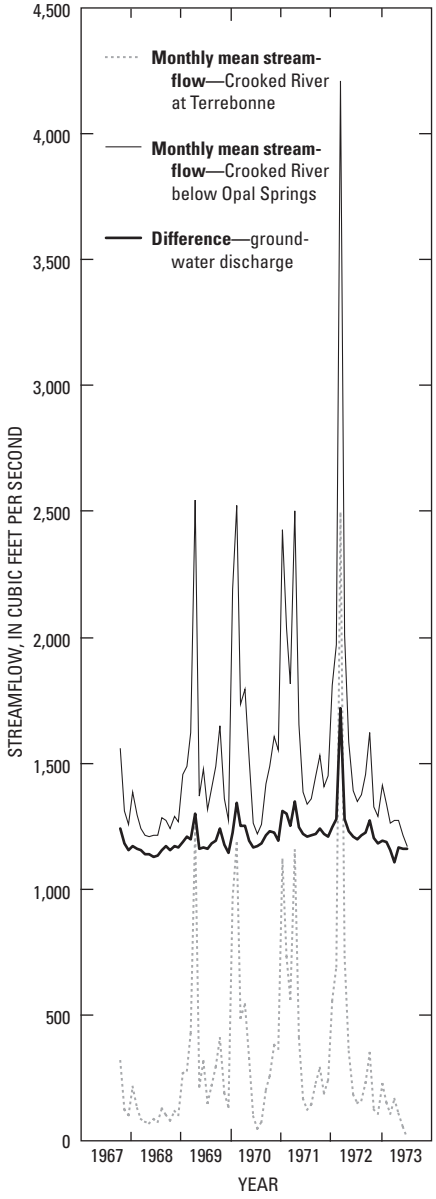

Figure 38. Monthly mean flows of the Crooked River below Opal Springs and at Terrebonne, and the difference between the two gages, 1967 to 1973.

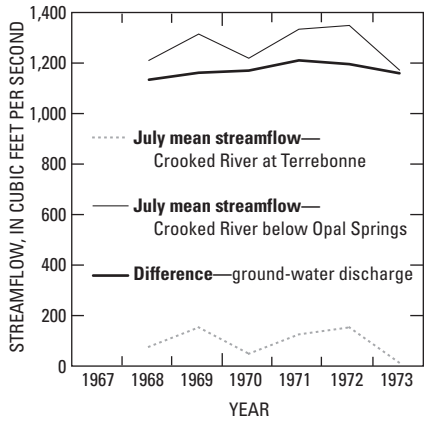

Figure 39. July mean flows of the Crooked River below Opal Springs and at Terrebonne, and the difference between the two gages, 1968 to 1973.

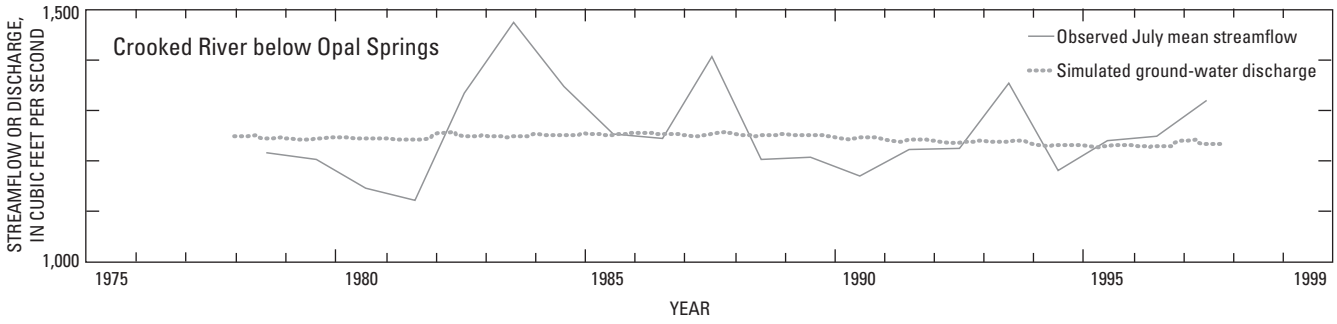

Figure 40. July mean flows of the Crooked River below Opal Springs and simulated ground-water discharge to the lower Crooked River, 1977 to 1997.

Summary of Transient Ground-Water Discharge to Streams

The transient model simulates the volumetric distribution and temporal variations in ground-water discharge to streams reasonably well. The match between simulated and measured volume of and variations in ground-water discharge is somewhat dependent on geographic scale. Simulated and observed discharge fluxes and variations are most similar for streams that receive regional ground-water discharge. At smaller scales (as would be represented by first-order tributaries), geologic heterogeneities, topographic complexity, and model discretization combine to reduce the accuracy of matches between observed and simulated discharge fluxes and variations. Nevertheless, simulated fluxes and variations are very close for certain small streams, such as Odell Creek.

The fit between observed and simulated discharge fluctuations is also somewhat dependent on temporal scales. Overall, the fit between simulated and observed discharge fluctuations is best at decadal time scales, which reflect long-term climate cycles (such as droughts). The ability of the model to match the timing of annual fluctuations is somewhat limited by the time discretization, particularly the semiannual stress periods, as previously discussed.

Transient Model Water Budget

The transient model water budget can be evaluated by observing the instantaneous rates of various budget components at the end of each stress period (table 7 and fig. 41). The most noticeable feature of the transient budget is the way the ground-water system attenuates the wide seasonal and interannual variations in recharge. Recharge varies interannually by a factor of nearly 5 while stream discharge varies by a factor of only about 0.2 (which is consistent with streamflow measurements). The large swings in recharge are moderated by storage. During the wet winters of 1982 to 1984, it can be seen that large amounts of ground water go into storage (as the water table rises), and the amount of ground water going into storage during the winter exceeds the amount coming out of storage the following summers. This situation is reversed during the dry winters of 1990 to 1992, when little water goes into storage and a much larger amount comes out of storage the following summers (as the water table drops). The variation in stream discharge over the calibration period is consistent with observed variations in discharge of the Deschutes River near Madras.

The transient model water budget shows a cumulative reduction in ground-water storage of about 3.5×10^{10} ft^3 (about 810,000 acre-ft) over the 1978 to 1997 transient calibration period. This is equivalent to about 0.31 feet of water over the model area and is consistent with the water-level declines observed over most of the study area between the late 1970s and mid-1990s.

Model Limitations

Numerical models of ground-water flow are only approximations of complex natural systems and, as such, have intrinsic error and uncertainty. Error stems largely from the fact that certain spatially variable properties, such as hydraulic conductivity and stream stage, must be represented as uniform values in discrete model cells. Simplification can also occur at larger scales within a model, as is the case here, where hydraulic conductivity is represented as uniform in zones composed of multiple model cells. Model uncertainty stems from random error in the field measurements used for model calibration, which is translated through model calibration to uncertainty in the calibrated parameter values.

Because of intrinsic error and uncertainty, the fit between simulated and observed hydraulic heads and fluxes, described in previous sections, is not perfect. For example, steady-state model head residuals have a fitted standard deviation of 76 feet, and a root-mean-square (RMS) error of 78 feet. The RMS error for heads in the transient calibration is 89.6 feet. This error affects the differences between simulated ground-water elevations and stream elevations and, consequently, the spatial distribution of simulated ground-water/surface-water exchanges. The comparison of simulated and measured stream gains and losses described in preceding sections, however, shows that the model fit is reasonably good, particularly at scales larger than a few to several miles. At smaller scales, the fit is not as good. The numerical model also has certain error with regard to transient phenomena. This can also be evaluated by assessing the fit between simulated and observed variations in hydraulic head and discharge to streams. In general, simulated and observed responses to regional stresses matched within a year or two. In the Redmond area, the model fit between simulated and observed responses to short-term stresses, such as canal operation and irrigation, was good.

Table 7. Transient model water budget for each stress period

[All values in cubic feet per second; Nov, November; Apr, April; Oct, October; ET, evapotranspiration]

Stress period	Season	Model water year	Recharge				Storage			ET	Stream leakage		Pumpage
			Precipitation	Canal	On-farm	Total	In from	Out to	Change		In from	Out to	
1	Nov–Apr	1978	7,605	104	13	7,722	124	3,627	3,503	48	352	5,362	4
2	May–Oct	1978	1,041	741	109	1,891	2,622	245	-2,377	622	373	4,848	14
3	Nov–Apr	1979	4,466	75	13	4,554	428	1,122	695	57	370	5,019	4
4	May–Oct	1979	1,279	790	109	2,179	2,304	242	-2,062	732	381	4,718	19
5	Nov–Apr	1980	5,093	104	13	5,210	289	1,622	1,334	42	371	5,050	4
6	May–Oct	1980	1,381	730	109	2,220	2,086	188	-1,898	624	382	4,702	22
7	Nov–Apr	1981	5,268	98	13	5,379	304	1,815	1,511	62	371	5,022	5
8	May–Oct	1981	1,500	675	109	2,284	2,007	157	-1,850	631	379	4,706	24
9	Nov–Apr	1982	10,814	88	13	10,915	57	6,362	6,305	48	328	5,729	4
10	May–Oct	1982	2,821	757	109	3,687	1,362	522	-840	516	349	5,181	24
11	Nov–Apr	1983	8,983	86	13	9,083	202	4,408	4,206	37	320	5,998	4
12	May–Oct	1983	1,655	787	109	2,552	2,600	427	-2,172	674	342	5,211	23
13	Nov–Apr	1984	9,438	82	13	9,533	170	4,708	4,538	28	316	6,121	4
14	May–Oct	1984	914	813	109	1,837	3,411	376	-3,035	758	342	5,272	26
15	Nov–Apr	1985	4,849	117	13	4,978	266	878	612	60	339	5,486	5
16	May–Oct	1985	870	791	109	1,770	3,111	244	-2,867	790	364	5,028	28
17	Nov–Apr	1986	8,017	100	13	8,129	177	3,702	3,525	51	327	5,718	5
18	May–Oct	1986	874	758	109	1,740	3,222	227	-2,996	850	365	5,067	30
19	Nov–Apr	1987	4,203	130	13	4,346	493	736	243	73	355	5,229	5
20	May–Oct	1987	1,725	768	109	2,602	2,270	325	-1,946	807	360	4,911	32
21	Nov–Apr	1988	4,539	105	13	4,657	428	1,063	635	73	359	5,155	5
22	May–Oct	1988	626	697	109	1,433	3,121	148	-2,973	806	353	4,766	35
23	Nov–Apr	1989	7,480	101	13	7,594	256	3,667	3,411	32	354	5,346	6
24	May–Oct	1989	621	765	109	1,496	3,102	197	-2,905	723	355	4,848	34
25	Nov–Apr	1990	2,531	120	13	2,664	1,306	236	-1,070	84	371	4,866	6
26	May–Oct	1990	880	714	109	1,703	2,649	159	-2,489	774	361	4,594	36
27	Nov–Apr	1991	2,507	91	13	2,612	1,297	422	-875	57	377	4,650	6
28	May–Oct	1991	1,624	682	109	2,415	1,686	159	-1,527	606	361	4,510	39
29	Nov–Apr	1992	3,660	96	13	3,770	843	1,111	268	64	387	4,663	9
30	May–Oct	1992	910	591	109	1,611	2,378	105	-2,272	652	372	4,410	44
31	Nov–Apr	1993	7,160	54	13	7,227	284	3,832	3,547	15	402	4,906	8
32	May–Oct	1993	2,766	724	109	3,600	929	486	-443	525	397	4,724	40
33	Nov–Apr	1994	1,407	103	13	1,523	1,984	53	-1,931	158	398	4,535	9
34	May–Oct	1994	636	627	109	1,372	2,606	128	-2,478	677	370	4,345	48
35	Nov–Apr	1995	5,111	79	13	5,204	533	2,278	1,745	30	409	4,675	10
36	May–Oct	1995	1,841	658	109	2,608	1,329	171	-1,158	471	387	4,491	44
37	Nov–Apr	1996	7,982	81	13	8,076	270	4,418	4,149	60	425	5,129	13
38	May–Oct	1996	1,167	749	109	2,025	2,397	291	-2,106	638	388	4,681	50
39	Nov–Apr	1997	8,990	95	13	9,098	83	4,953	4,870	63	378	5,374	13
40	May–Oct	1997	1,665	725	109	2,500	2,019	333	-1,686	576	402	4,809	49

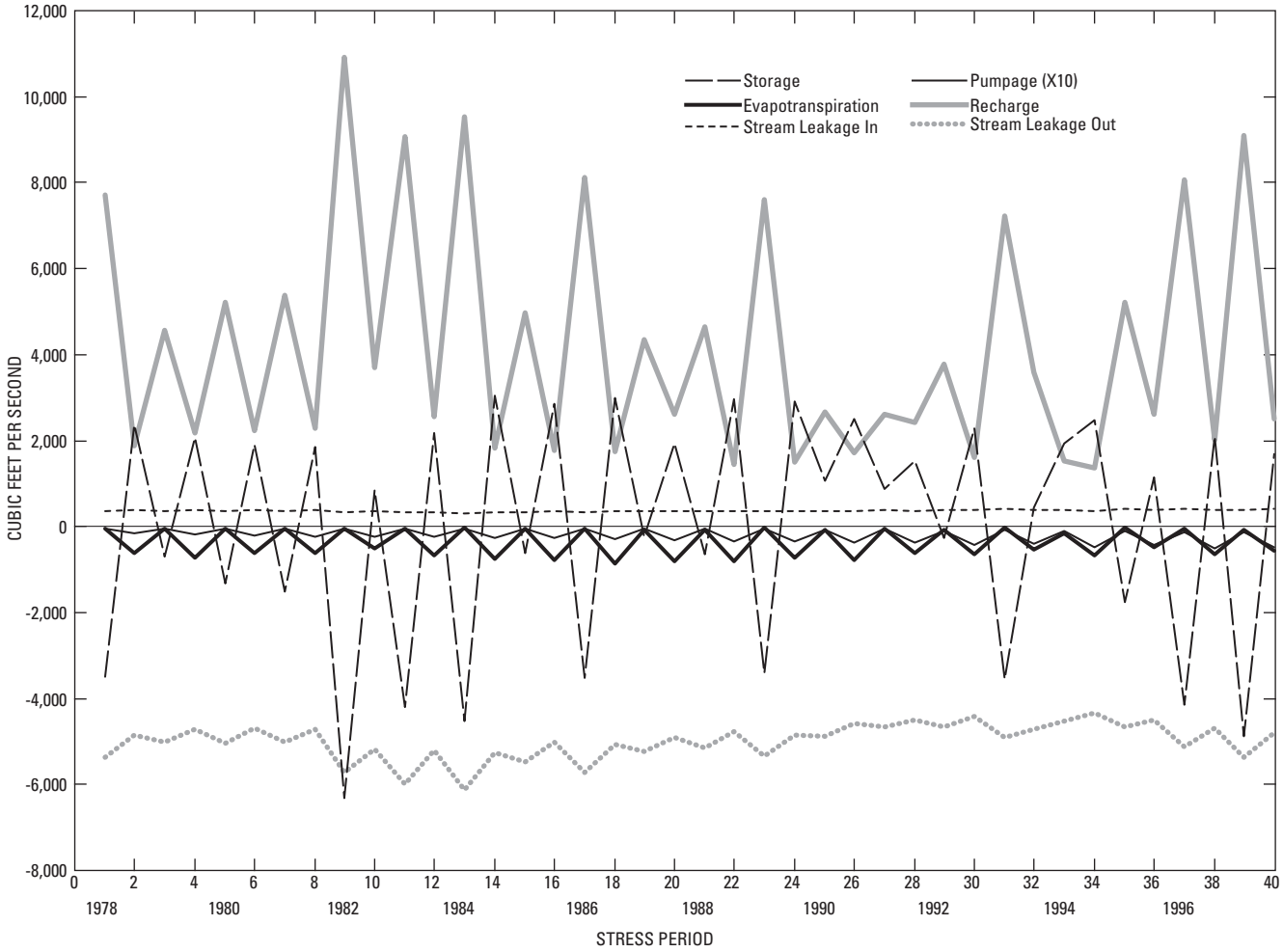

Figure 41. Variations in the transient model water budget by stress period.

Model error and uncertainty propagate into model predictions. Therefore, predictions of the location and timing of streamflow and head changes based on simulations must be considered general indicators of how the ground-water system will respond to stresses and should not be considered exact. A good sense of the accuracy and reliability of model predictions can be obtained by evaluating the match between simulations and observations as is done in the preceding calibration sections of this report.

EXAMPLE SIMULATIONS

The calibrated numerical model can be used to estimate the response of the regional ground-water system to new stresses, such as pumping wells or modifying recharge through canal lining. Both of these types of stresses involve changes in the hydrologic budget. In the case of pumping, ground water is removed from the system. In the case of canal lining, the recharge to the system is reduced. In both cases, the amount of pumping or reduced recharge must be offset by reductions in natural discharge from the ground-water system or increases in recharge elsewhere. Time is required for the ground-water system to compensate for these changes and reach a new equilibrium. During this time, changes in storage within the ground-water system occur as the water table changes to reflect the new equilibrium.

When analyzing the results of simulations, important factors to evaluate include the location and rates of changes in stream leakage and spring discharge, changes in the water-table elevation, and changes in ground-water storage.

Example simulations showing the effects of pumping and of canal lining are included in this section. When evaluating the results of these, or any simulations, it is important to remember that model predictions reflect the error and uncertainty in the model. Model predictions are best used as general guides to help understand how the ground-water system will respond to new stresses and should not be considered exact. A general sense of model accuracy and performance can be obtained from the comparison of observed and simulated heads and flows presented in the Model Calibration section of this report.

Simulating the Effects of Pumping

Example simulations were run to demonstrate the effects of pumping wells in three areas. Two of the areas are the population centers of Bend and Redmond. The third area is an arbitrary location between the Crooked and Deschutes Rivers near Osborne Canyon used to demonstrate the difference in the type of response close to a major discharge area. At each of these areas, both shallow and deep wells are simulated.

In all simulations, wells are pumped at a continuous rate of 10 ft^3/s for 50 years. The 50-year stress period is divided into 30 time steps. Successive time steps increase in length by a factor of 1.25, so they range in length from 5.7 days to 10 years. The simulations start with simulated steady-state conditions, and all stresses other than pumping are held constant.

When pumping of a well begins, virtually all the water comes from storage as the hydraulic head in the area immediately around the well drops, forming a *cone of depression*. With time, the cone of depression expands and starts to stabilize as sufficient ground water to offset the pumping is intercepted, and the proportion of pumped water coming from storage decreases. As the proportion of pumped water from storage decreases, the proportion of water from streams or other sources increases. At equilibrium, no water comes from storage and all pumped water comes from other sources. In the upper Deschutes Basin, the principal source of water to pumped wells once equilibrium has been attained is diminished streamflow.

The cone of depression from a pumping well can affect streamflow in both losing and gaining reaches. Along losing stream reaches where the ground-water elevation is sufficiently close to the stream elevation, lowering the ground-water head increases the head gradient between the ground-water system and the stream, causing increased stream leakage. If the ground-water head is far below the stream, the ground-water system and the stream are effectively uncoupled, and changes in head have little or no effect on stream loss. Along gaining reaches, the amount of ground-water discharge to the stream can be diminished by lowering the head in the ground-water system and reducing the head gradient, and ground-water flow, toward the stream.

The only other possible sources of water to pumped wells in the upper Deschutes Basin are reduced ET and increased inflow at basin boundaries. Lowering the water table in areas where phreatophytes utilize water directly from the water table can cause a reduction in ET. This process is simulated in the model but is generally inconsequential. Increased boundary fluxes due to head changes are not simulated in this model. However, locations of probable pumping in the upper Deschutes Basin are sufficiently distant from boundaries (compared to the proximity to streams) that the probable contribution from boundaries is likely minuscule. The model should be used with caution when evaluating the effects of pumping of wells very close to basin boundaries, however, such as very near or on the Cascade Range crest, because simulated drawdowns may be larger than they would be in reality.

Simulated Pumping in the Bend Area

The first pumping simulation is in model layer 2 in Bend (row 87, column 50) (fig. 42). In this simulation, water comes from storage, increased stream losses, and decreased gains. Gaging-station data discussed in preceding sections show gaining and losing reaches near Bend, indicating shallow ground water in hydraulic connection with the Deschutes River. After 2 years of pumping, about 2.3 ft^3/s or 23 percent of the pumping rate comes from diminished streamflow.

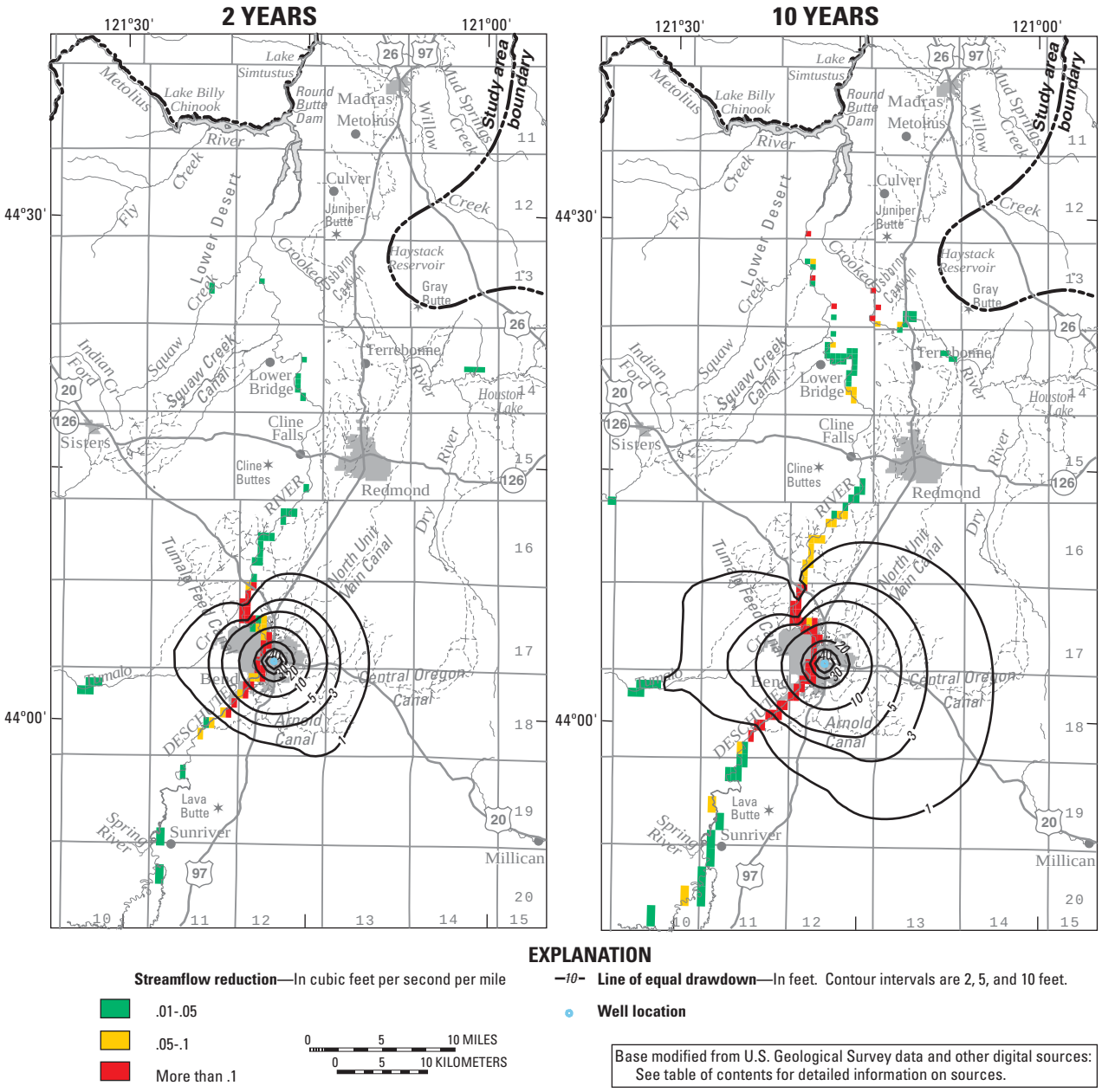

Figure 42. Simulated drawdown in model layer 2 and net reduction in ground-water discharge to streams after 2 and 10 years of pumping 10 ft^3/s from model layer 2 in the Bend area.

Most of the effect is to the Deschutes River in the vicinity of Bend (fig. 42). The diminished reaches include both those affected by increased leakage (stream losses) and decreased spring discharge (stream gains). After 10 years of pumping, about 5.8 ft^3/s, or 58 percent of the pumping rate, comes from diminished streamflow. The affected reaches are more widespread and include the confluence area, but are still concentrated in the Bend area. A graph depicting changes in the sources of water with time (fig. 43) shows that the amounts of water coming from storage and from diminished streamflow are equal after about 7 years and that 90 percent of the pumped water comes from diminished streamflow after about 42 years. Maximum drawdown in model layer 2 after 2 years is 76 feet (fig. 42). It is much less in model layer 1 (about 1 foot). The maximum drawdown in model layer 2 increases to only 80 feet after 10 years, but the effects are more widespread. Drawdown in model layer 1 is 4 feet after 10 years.

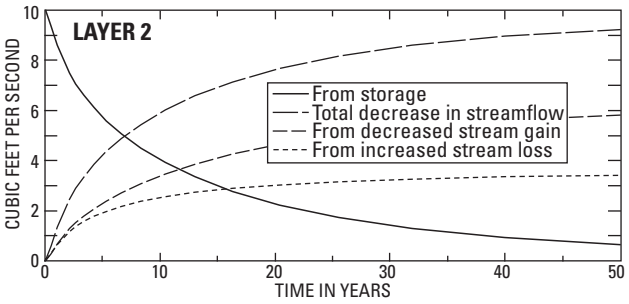

Figure 43. Variations with time in the amounts of ground water coming from storage and from diminished streamflow in response to pumping 10 ft^3/s from model layer 2 in the Bend area.

Simulated pumping of a deep well in Bend (model layer 7) shows how the response of the ground-water system can vary depending on well depth. After 2 years of pumping, most of the streamflow effects occur in the regional discharge area just above Lake Billy Chinook and in the area just above and below Benham Falls (fig. 44). The rate of streamflow depletion after 2 years is about 1.7 ft^3/s, or 17 percent of the pumping rate.

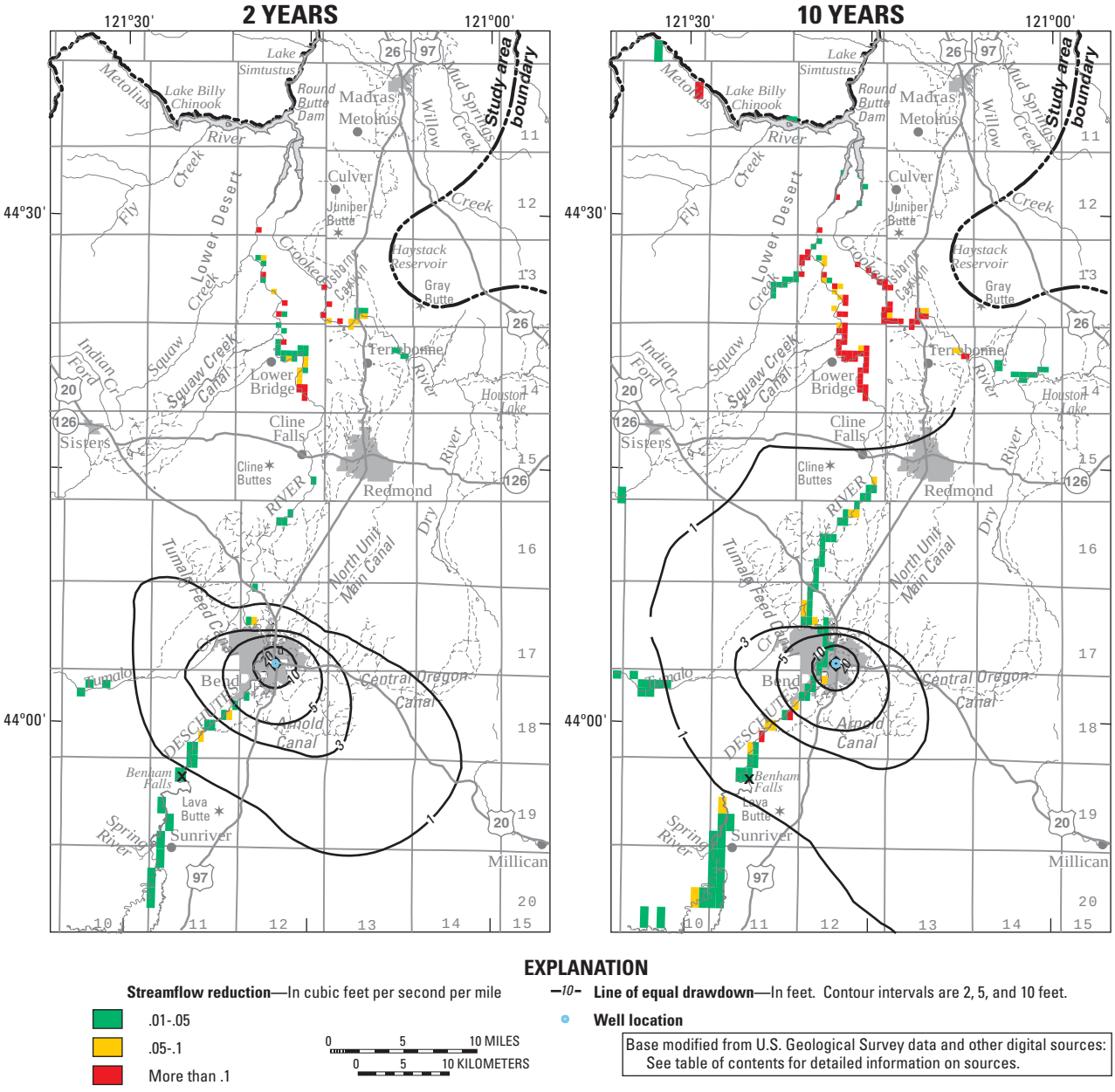

Figure 44. Simulated drawdown in model layer 7 and net reduction in ground-water discharge to streams after 2 and 10 years of pumping 10 ft^3/s from model layer 7 in the Bend area.

After 10 years of pumping, effects have spread to a few more stream reaches, but most effects are still seen along the Deschutes and Crooked Rivers in the regional discharge area upstream of Lake Billy Chinook (fig. 44). Stream gains and losses in the Bend area are relatively unaffected by deep pumping. The rate of streamflow depletion after 10 years of pumping is about 5.7 ft^3/s, or 57 percent of the pumping rate. As in the case of the shallower well, the amounts of water coming from storage and from diminished streamflow are equal at about 7 years (fig. 45). About 90 percent of the pumped water comes from diminished streamflow after about 35 years, sooner than the shallower simulation because the smaller storage coefficients in deeper model layers cause the cone of depression to expand and capture streamflow more quickly. Maximum drawdown in model layer 7 is about 30 feet after 2 years and does not increase after 10 years, but the cone of depression is more widespread.

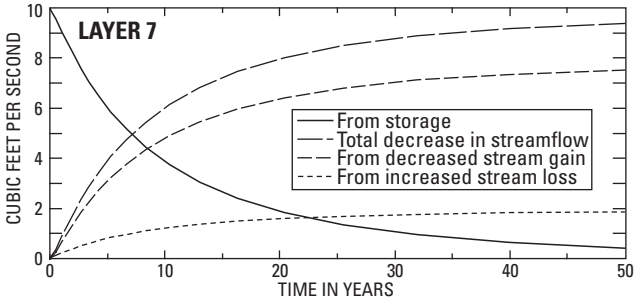

Figure 45. Variations with time in the amounts of ground water coming from storage and from diminished streamflow in response to pumping 10 ft^3/s from model layer 7 in the Bend area.

Simulated Pumping in the Redmond Area

Simulations suggest that streamflow depletion caused by pumping in the Redmond area (row 63, column 67) is concentrated in the ground-water discharge areas along the Deschutes and Crooked Rivers upstream of Lake Billy Chinook. Because vertical anisotropy is less than in the Bend area, the ground-water system responds similarly to simulated pumping of either shallow or deep wells (figs. 46 and 47). After 2 years of pumping, the rates of streamflow depletion are 1.6 and 1.9 ft^3/s (16 and 19 percent) for the shallow and deep wells, respectively. Most of the depletion is due to diminished spring discharge just above Lake Billy Chinook (figs. 46 and 47). After 10 years of pumping, streamflow depletion is about 5.8 ft^3/s (58 percent of the pumping rate) for both the shallow and deep simulations. Streamflow depletion is more widespread after 10 years, but most of the effect is still in the inflow area above Lake Billy Chinook. Both simulations in the Redmond area show that the amounts of ground water coming from storage and diminished streamflow are equal after about 7 years, and that 90 percent of the pumping rate comes from diminished streamflow after about 32 years (fig. 48). Simulated drawdowns are small in the Redmond area due to the high transmissivity; this is consistent with aquifer-test results. Simulated drawdown around the shallow well is only 4 feet after 10 years of pumping, and only 2 feet in the deep well after the same period (figs. 46 and 47).

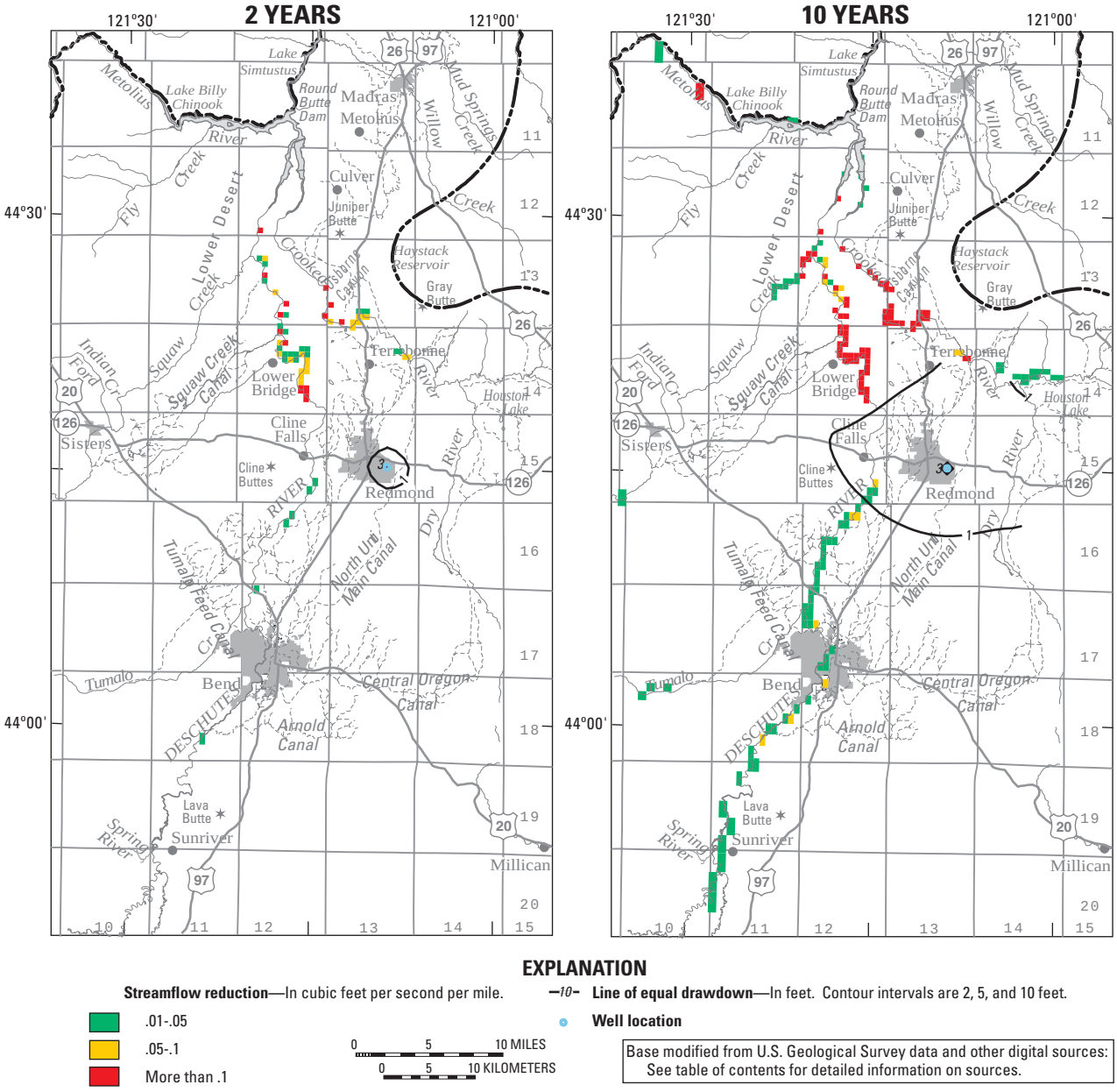

Figure 46. Simulated drawdown and net reduction in ground-water discharge to streams after 2 and 10 years of pumping 10 ft^3/s from model layer 2 in the Redmond area.

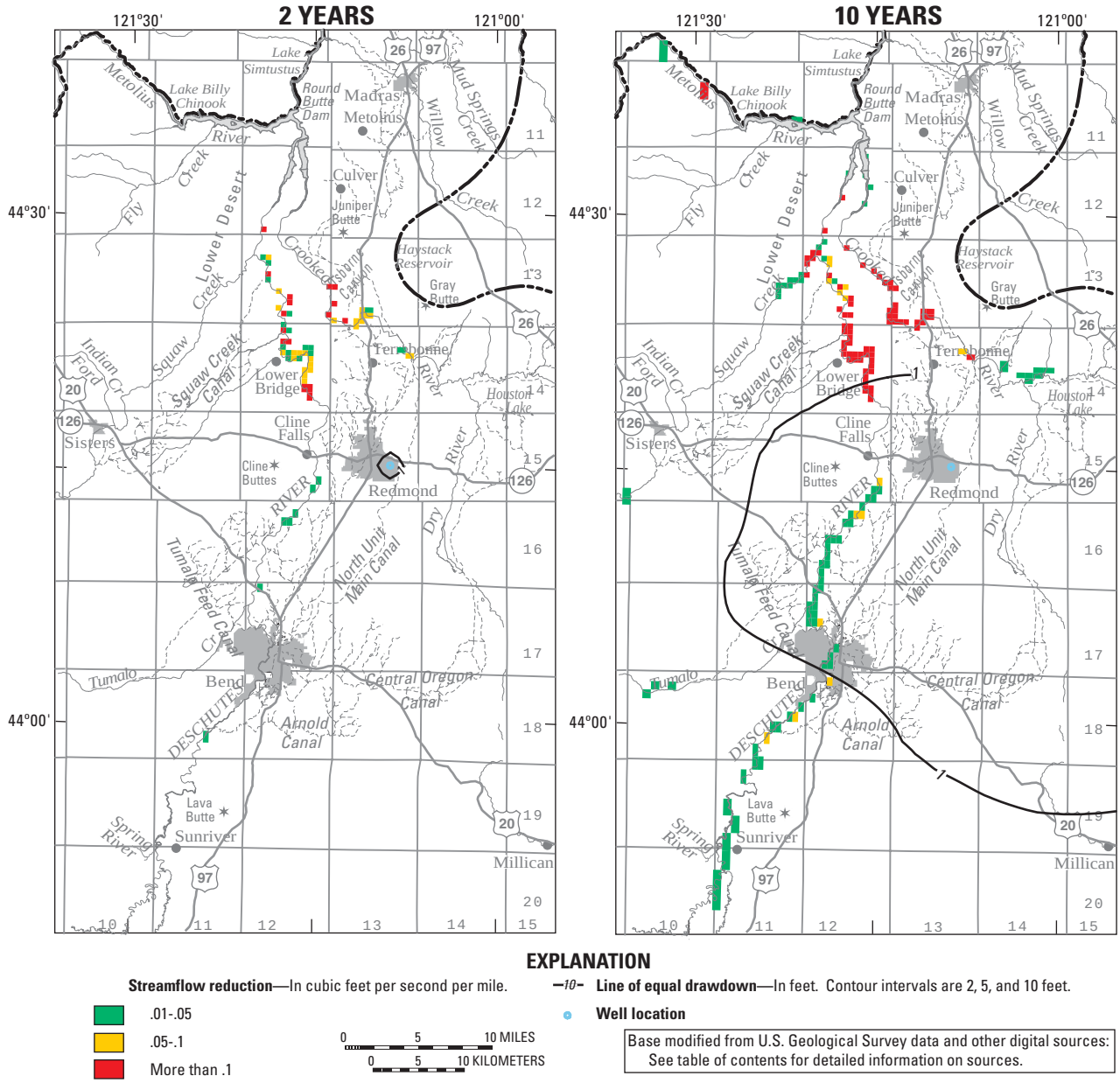

Figure 47. Simulated drawdown and net reduction in ground-water discharge to streams after 2 and 10 years of pumping 10 ft^3/s from model layer 7 in the Redmond area.

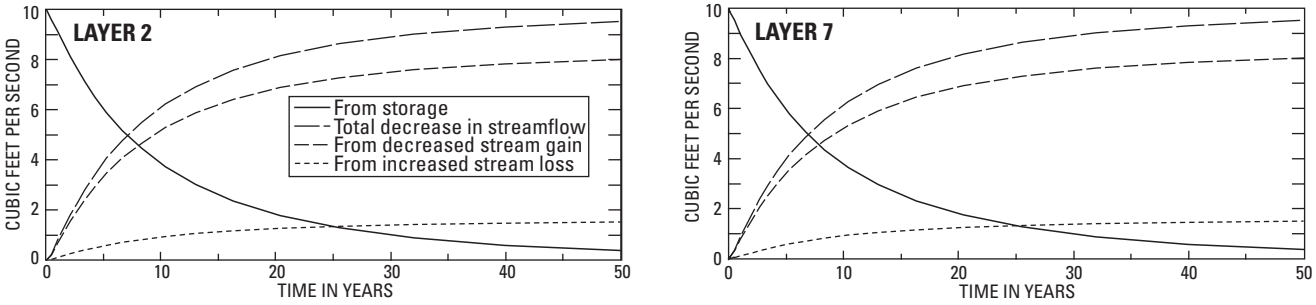

Figure 48. Variations with time in the amounts of ground water coming from storage and from diminished streamflow in response to pumping 10 ft^3/s from model layers 2 and 7 in the Redmond area.

Simulated Pumping between the Deschutes and Crooked Rivers near Osborne Canyon

The last well simulations are at an arbitrary location between the Deschutes and Crooked Rivers near their confluence (row 37, column 53) and are intended to demonstrate the effects of pumping in close proximity to a major ground-water discharge area. After 2 years of pumping from model layer 2, about 7.3 ft^3/s (73 percent of the pumping rate) of the pumping comes from streamflow (fig. 49). Effects after 2 years are limited to the lower Crooked and the Deschutes Rivers just above Lake Billy Chinook and to lower Squaw Creek. After 10 years of pumping from model layer 2, about 8.5 ft^3/s (85 percent of the pumping rate) comes from streamflow depletion, predominantly from the same stream reaches. Simulation of pumping from model layer 2 at this location indicates that the amounts of water coming from storage and from diminished streamflow are equal after only about 2 weeks and, that 90 percent of the pumping comes from streamflow depletion after about 12 years (fig. 50). Maximum drawdown in model layer 2 is about 10 feet after 2 years of pumping and does not significantly increase by 10 years (fig. 49). Maximum drawdown in model layer 1 is about 2 feet.

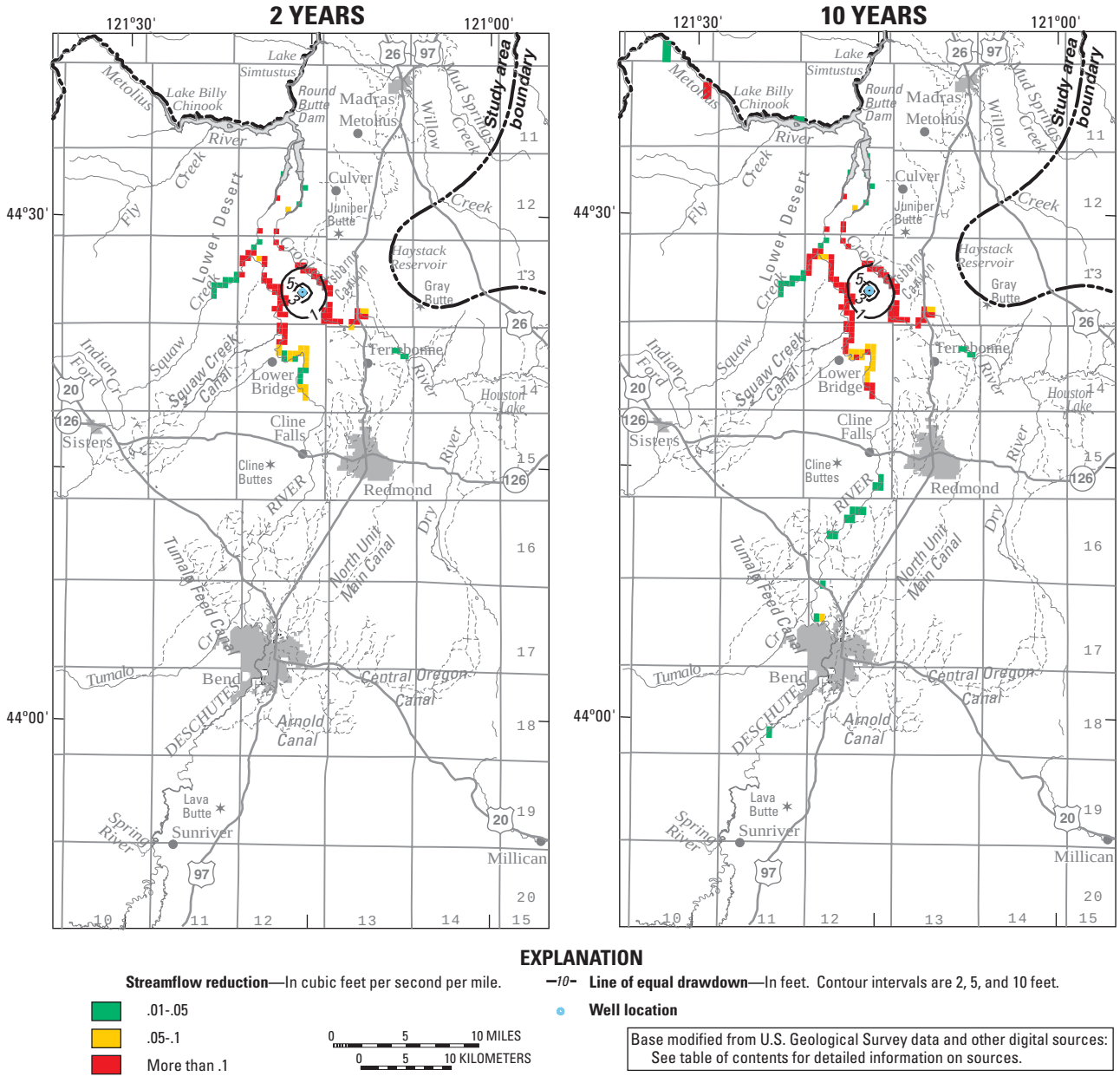

Figure 49. Simulated drawdown in model layer 2 and net reduction in ground-water discharge to streams after 2 and 10 years of pumping 10 ft^3/s from model layer 2 between the Deschutes and Crooked Rivers near Osborne Canyon.

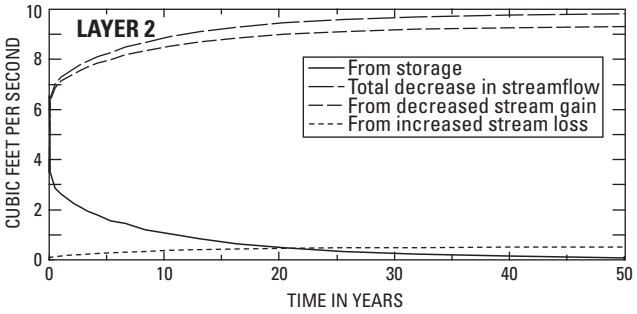

Figure 50. Variations with time in the amounts of ground water coming from storage and from diminished streamflow in response to pumping 10 ft^3/s from model layer 2 between the Deschutes and Crooked Rivers near Osborne Canyon.

The response of streamflow to simulated pumping from model layer 7 near the confluence is only slightly slower then the response to pumping from model layer 2. After 2 years of pumping from model layer 7, about 4.7 ft^3/s (47 percent of the pumping rate) comes from diminished streamflow (fig. 51). The affected stream reaches are virtually identical to those affected during the model layer 2 simulation, lower Squaw Creek and the lower Crooked River and Deschutes River just above Lake Billy Chinook (fig. 51). After 10 years of pumping, about 7.2 ft^3/s or 72 percent of the pumping rate is supplied by diminished streamflow.

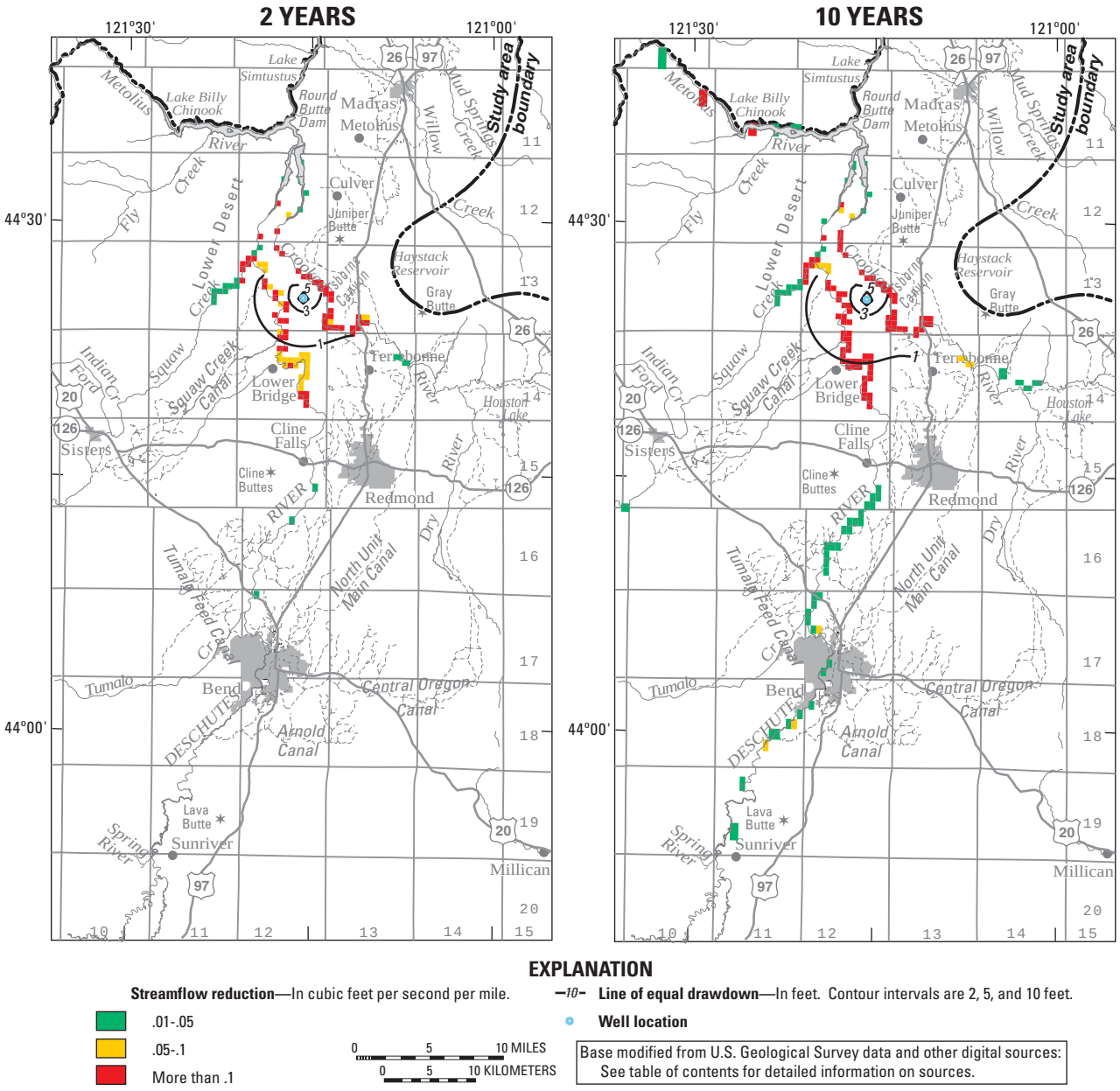

Figure 51. Simulated drawdown in model layer 7 and net reduction in ground-water discharge to streams after 2 and 10 years of pumping 10 ft^3/s from model layer 7 between the Deschutes and Crooked Rivers near Osborne Canyon.

By 10 years, simulated effects expand up the Deschutes River beyond Bend and to the lower Metolius River (fig. 51), but are still concentrated along the Deschutes and Crooked Rivers and lower Squaw Creek just above Lake Billy Chinook. The amounts of water from storage and streamflow depletion are equal after about 2 years, and 90 percent of the pumping rate is supplied from streamflow depletion after about 21 years (fig. 52). After 2 years, maximum drawdown is about 7 feet in model layer 7 and less than 1 foot in model layer 1.

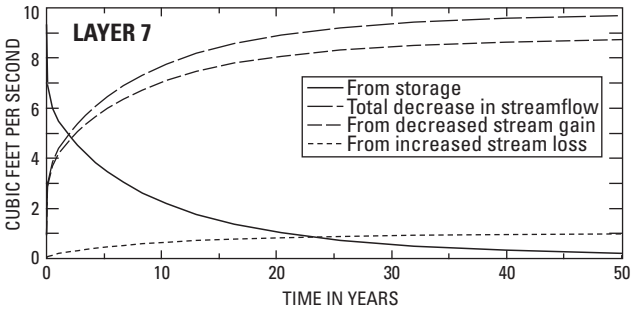

Figure 52. Variations with time in the amounts of ground water coming from storage and from diminished streamflow in response to pumping 10 ft^3/s from model layer 7 between the Deschutes and Crooked Rivers near Osborne Canyon.

Simulated Effects of Canal Lining

Lining canals to reduce leakage affects the ground-water system by locally reducing artificial recharge. As a result, the water-table elevation drops in the vicinity of the lined canal and, eventually, streamflow diminishes by the amount artificial recharge is reduced. As with pumping, streamflow does not respond immediately to canal lining. Streamflow responds gradually as the water table drops and approaches a new equilibrium. As the water table drops, a certain amount of the reduced recharge is accommodated for by changes in aquifer storage. Two canal-lining scenarios are presented in this section of the report.

In the first scenario, leakage in all main canals in the vicinity of Bend was reduced by 50 percent (fig. 53). This results in an average annual reduction in leakage of 69 ft^3/s (based on 1994 leakage estimates). After 2 years, net streamflow reduction is about 30 ft^3/s, mostly occurring in the vicinity of Bend. The changes in streamflow include both increased stream leakage and diminished stream gains. Gaging-station data discussed in preceding sections indicate that both gaining and losing stream reaches occur in the vicinity of Bend; this result is reasonable and expected. After 10 years, streamflow depletion is about 47 ft^3/s, and the effects expand to the major ground-water discharge area just above Lake Billy Chinook. After roughly 3 years, about one-half of the reduced canal leakage is reflected as diminished streamflow (fig. 54); the other one-half is accommodated by changes in aquifer storage. After 31 years, streamflow depletion reflects about 90 percent of the reduced canal-leakage rate. Maximum head changes due to the simulated canal lining are as much as 60 feet near the canal diversions north of Bend, but range between 5 and 30 feet over a larger area (fig. 53).

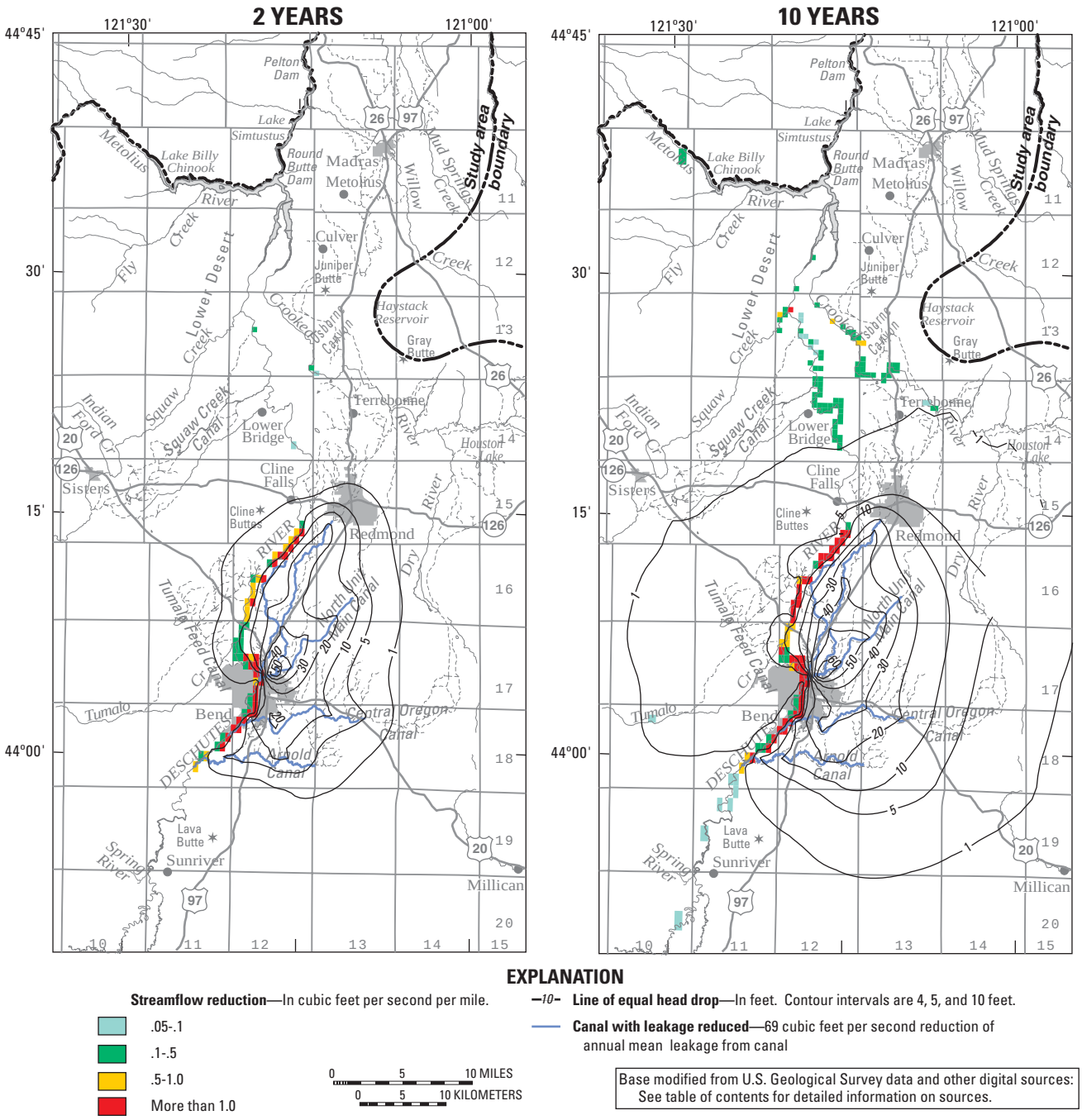

Figure 53. Simulated head decline in model layer 1 and diminished streamflow due to a 50 percent reduction in leakage of main irrigation canals in the vicinity of Bend after 2 and 10 years.

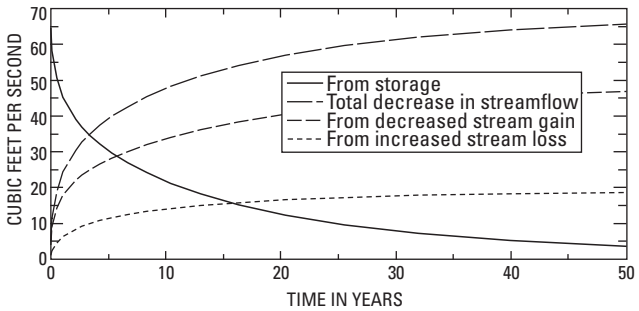

Figure 54. Variations with time in the amounts of ground water coming from storage and from diminished streamflow in response to a 50 percent reduction in leakage of main irrigation canals in the vicinity of Bend.

The second canal-lining scenario involved reducing the leakage in the northern sections of main canals (between Redmond and Madras) by 50 percent (fig. 55). This results in an average annual reduction in canal leakage of about 19 ft^3/s (based on 1994 leakage estimates). The response of streamflow to the reduction in recharge is slower than the previous canal-lining scenario. After 2 years, the net reduction in streamflow due to the reduced recharge is only about 2.1 ft^3/s, or about 11 percent of the reduced recharge. Ground-water discharge is affected along the lower Crooked River above Osborne Canyon, the Deschutes River between Lower Bridge and Squaw Creek, and at Mud Springs Creek (fig. 55). After 10 years, about 8.2 ft^3/s, or about 43 percent of the reduced recharge, is reflected as diminished streamflow. Similar stream reaches are affected, although the effects spread to include Willow Creek west of Madras (fig. 55).

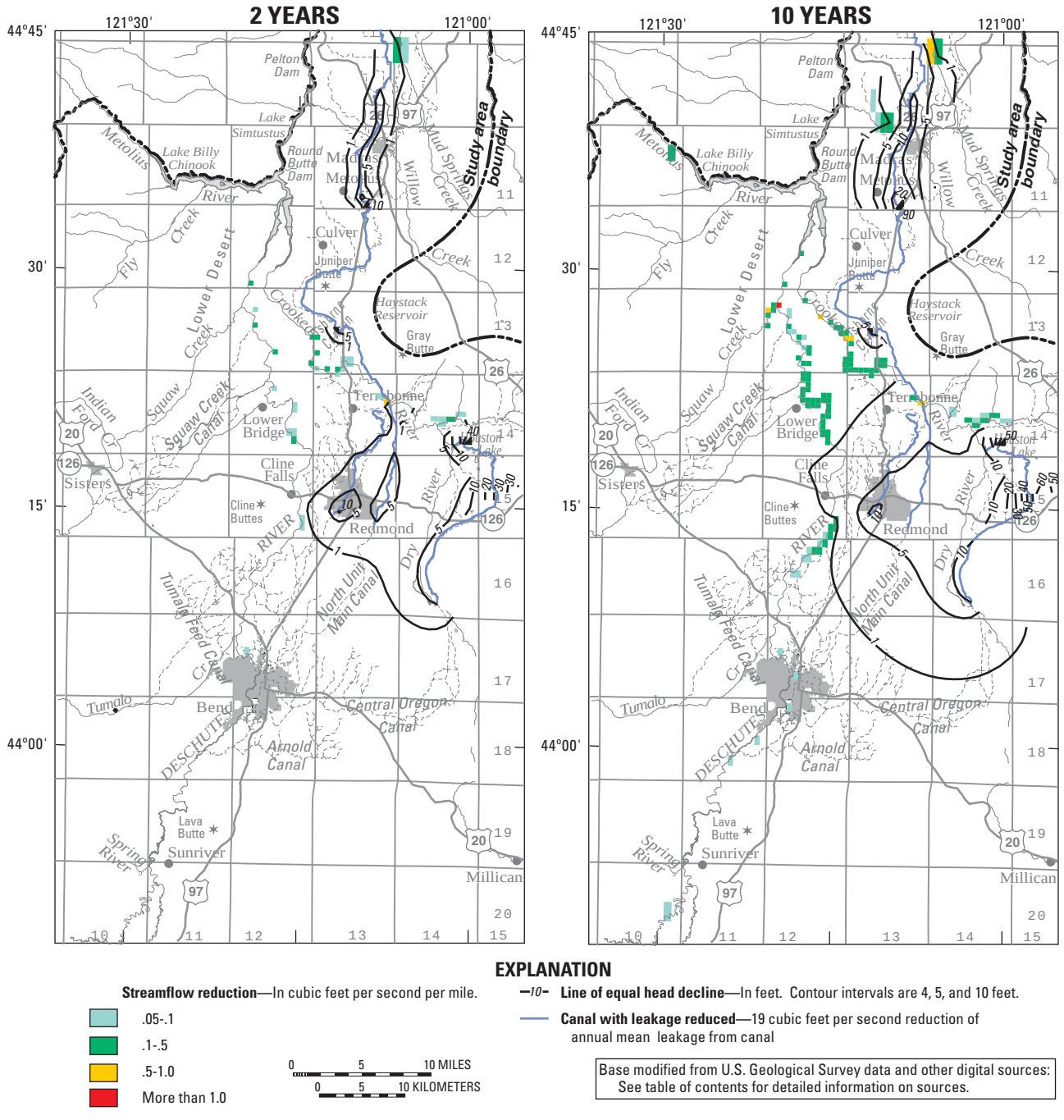

Figure 55. Simulated head decline in model layer 1 and diminished streamflow due to a 50 percent reduction in leakage of main irrigation canals north of Redmond after 2 and 10 years.

It takes 13 years until one-half of the reduction in canal loss is reflected as diminished streamflow (fig. 56). Only 80 percent of the loss rate reduction is reflected as diminished streamflow after 50 years, the end of the simulation. The increased time to equilibrium in this simulation compared to the canal-lining simulation near Bend is due to the larger storage coefficients in the northern part of the model area and the larger distance to the affected stream reaches. Maximum head changes are only about 5 to 10 feet and occur mostly along the canals (fig. 55). Head changes of up to 10 feet are localized along the North Unit canal in the Madras area. Head changes of 5 to 10 feet are widespread east of Redmond, between the North Unit and Central Oregon Canals.

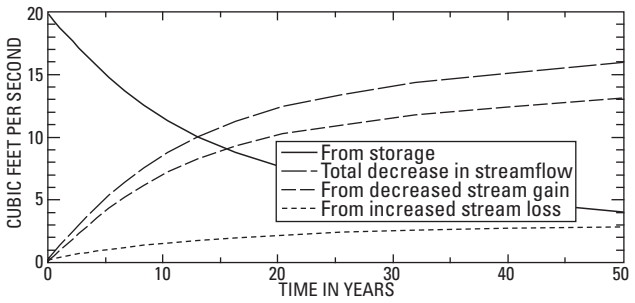

Figure 56. Variations with time in the amounts of ground water coming from storage and from diminished streamflow in response to a 50 percent reduction in leakage of main irrigation canals north of Redmond.

The simulations in this section show how the upper Deschutes Basin ground-water model can be used. The ground-water model could also be used to evaluate other types of pumping scenarios, such as with multiple wells or with intermittent or varying pumping schedules. Other possible canal scenarios could include different locations for lining or the use of canals for artificial ground-water recharge. Another potential use of the model would be to evaluate the effects of long-term climate change on the regional ground-water system.

SUMMARY AND CONCLUSIONS

Rapid population growth is increasing demand for water in the upper Deschutes Basin. Surface-water resources are fully allocated, so the increased demand is being supplied chiefly by ground water. Numerous hydrologic investigators over the past 100 years have recognized that ground water and surface water are intimately connected in the upper Deschutes Basin and that most of the flow of the Deschutes River is supplied by ground water (Russell, 1905; Stearns, 1931; Sceva, 1960, 1968; Gannett and others, 2001). Because of this connection, pumping and consumptively using ground water in the upper Deschutes Basin reduces the amount of ground water discharging to streams and, consequently, streamflow. Reducing artificial recharge by lining leaking irrigation canals will affect streams in a similar manner. Until now, regulatory agencies and the public have had no means to evaluate the effects of pumping, canal lining, or other activities on the ground-water and surface-water systems. The model described in this report provides a means for evaluating the possible effects of such activities, particularly with regard to water-level changes and the timing and distribution of the effects on streamflow.

The model covers most of the Deschutes Basin upstream of the mouth of Trout Creek north of Madras. Recharge is principally from precipitation in the Cascade Range, with a lesser amount of artificial recharge from leaking irrigation canals. Ground water moves from the Cascade Range east and north and ultimately discharges to streams in the basin. There are two principal settings where ground water discharges: to streams along the topographic margin of the Cascade Range, and to the Deschutes, Crooked, and Metolius Rivers near their confluence in the vicinity of Lake Billy Chinook. Approximately one-half of the ground-water discharge occurs at each of these settings. Geology is the principal factor controlling the discharge of ground water in the confluence area. It is not far north of the confluence area where the permeable Deschutes Formation strata pinch out against uplands of the low-permeability John Day Formation. The northward-flowing ground water hits this low permeability boundary and discharges to the deeply incised streams.

Ground-water flow is simulated by the finite-difference method using the programs MODFLOW (McDonald and Harbaugh, 1988) and MODFLOWP, a version of MODFLOW modified by Hill (1992) to estimate parameters by nonlinear regression. The finite-difference grid consists of 8 layers, 127 rows, and 87 columns. Geographic boundaries are simulated as no-flow except in two areas where there is inferred subsurface inflow across topographic divides. All major streams and most principal tributaries in the upper Deschutes Basin are included in the model as head-dependent flux boundaries. Ground-water

recharge from precipitation was estimated using the Deep Percolation Model of Bauer and Vaccaro (1987). Artificial recharge from leaking irrigation canals and on-farm losses was estimated from diversion and delivery records, seepage studies, and crop data. Details of recharge estimation can be found in Boyd (1996) and Gannett and others (2001). Evapotranspiration from the water table in areas of shallow depths to water is simulated as a head-dependent process. Ground-water pumpage for irrigation and public water supplies is included in the model. Irrigation pumpage was estimated using information on water rights and crop data. Public-supply pumpage was estimated from pumping records provided by water suppliers and from population data. Hydraulic conductivities were estimated from well-yield tests, aquifer tests, and literature values. Data are too sparse and the geology too heterogeneous to allow continuous cell-by-cell mapping of the hydraulic-conductivity distribution. The distribution of hydraulic conductivity is represented by a set of discrete zones within which conductivity values were uniform. The zonation scheme is based on hydrogeologic units defined by Lite and Gannett (2002), which were further subdivided during model calibration.

The model was calibrated to time-averaged steady-state conditions from 1993 to 1995 using parameter-estimation programs and techniques of Hill (1992, 1998). These methods involve determining the set of optimal parameter values that best fit the observed hydraulic heads and flows by using nonlinear regression to minimize a weighted sum-of-squares objective function. Fourteen hydraulic-conductivity parameters and two vertical conductance parameters were determined using nonlinear regression. Other parameter values mostly had sensitivities too low to allow optimization. Parameter values not determined by regression were set to reasonable and expected values and adjusted judiciously by trial and error during model calibration. Final parameter values are all within reasonable and expected ranges.

The steady-state model fit to measured heads and flows is good. Residuals are reasonably random and normally distributed. The general shape and slope of the simulated water-table surface and overall hydraulic-head distribution match the geometry determined from field measurements. The fitted standard deviation for hydraulic head is about 76 feet, which is considered good given that heads in the upper basin span a range of over 4,500 feet and field measurements range from 1,797 to 5,586 feet. The only area of significant systematic error in simulated heads is in the La Pine subbasin, where simulated heads are too high. The general magnitude and distribution of ground-water discharge to streams is also reasonably well simulated throughout the model. Ground-water discharge to streams in the area of the confluence of the Deschutes, Crooked, and Metolius Rivers is closely matched. Significant differences between simulated and measured ground-water discharge to streams, where they occur, are generally attributable to scale problems where highly heterogeneous hydrogeologic conditions occur in areas where subsurface data are sparse and the model grid is coarse. Systematic errors in ground-water discharge to streams occur in high-elevation tributary streams in the Cascade Range, where simulated discharge is less than observed. Overall, the steady-state model reasonably reproduces the behavior of the regional ground-water system.

The model was calibrated to transient conditions from 1978 to 1997 (using 40 semiannual stress periods) by traditional trial-and-error methods. Climatic cycles during this period provided an excellent regional hydrologic signal for calibration. Model parameterization is the same as used in the steady-state calibration, with the addition of storage coefficient parameters that were set up to follow the hydraulic-conductivity zonation scheme. Unlike hydraulic conductivity, storage coefficients were varied from model layer to model layer, usually decreasing with depth. Final storage coefficient values are all within reasonable and expected ranges, and are consistent with aquifer-test results. Other model parameters are the same as for the steady-state calibration.

Simulated variations in ground-water discharge to streams were evaluated by comparing simulated values and measured values in six areas. Overall, the transient model simulated the volumetric distribution and temporal variations in ground-water discharge reasonably well. The match between simulated and measured volume of and variations in ground-water discharge was, however, somewhat dependent on geographic scale. Simulated discharge fluxes and variations matched observed conditions best at regional scales. At smaller scales (as would be represented by first-order tributaries) geologic heterogeneities, topographic complexity, and model discretization combine to reduce the accuracy of matches between observed and simulated discharge fluxes and variations. Nevertheless, simulated fluxes

and variations are very close for certain small streams, such as Odell Creek. The overall magnitude and temporal variations of stream discharge in the confluence area are reproduced by the transient model with reasonable accuracy.

Simulated variations in hydraulic head were evaluated by comparing simulated and measured water-level fluctuations in 64 wells in 12 subareas. The transient model simulates fluctuations caused by climate cycles, annual recharge cycles, and canal leakage and irrigation. Water-level fluctuations caused by stream-stage variations are not simulated. Climate-driven water-level fluctuations are simulated with reasonable accuracy over most of the model area. The timing of the simulated water-level response to the change to wet conditions starting in 1996 matches the observed response within months in most cases and generally within a year. The timing and magnitude of simulated water-level fluctuations caused by annual pulses of recharge from precipitation match those observed reasonably well, given the limitations of the time discretization in the model. Water-level fluctuations caused by annual canal leakage are simulated very well over most of the area where this occurs.

Example simulations were run to demonstrate the model usefulness for predicting the effects of changes to the hydrologic stresses on the system. The examples involve increased ground-water pumping or canal lining. All example pumping simulations assumed continuous pumping, but this is not required. All pumping simulations show that pumped water comes largely from aquifer storage when pumping begins, but that as the water table stabilizes the pumping increasingly diminishes the discharge to streams and, hence, streamflow. The time it takes for pumping to affect streamflow varies geographically. Simulations involving continuous pumping of wells near Bend and Redmond show that, in general, about one-half of the pumping comes from diminished streamflow after 5 to 10 years and 90 percent of the pumping comes from diminished streamflow after 30 to 40 years. Pumping in the Bend and Redmond areas generally affects streamflow in the regional discharge area near the confluence of the Deschutes, Crooked, and Metolius Rivers. However, shallow wells in the Bend area tend to affect streamflow in and around Bend. Wells placed very close to streams have a more rapid effect because of the lack of intervening aquifer storage. Simulated pumping of a well between the Crooked and Deschutes Rivers at about the latitude of Osborne Canyon showed that 50 percent of the pumping rate was supplied by diminished streamflow after a few weeks.

Two example simulations were run to demonstrate the model's ability to estimate the effects of canal lining and consequent reduction in artificial recharge. The simulations show that canal lining has effects similar to pumping wells. The reduction in artificial recharge is at first offset by releases from aquifer storage as the water table drops. With time, however, ground-water discharge to streams diminishes in response to the reduced recharge and head changes. Simulated canal lining in the Bend area affected streamflow in much the same way as pumping shallow wells in the area, with the effects most prominent along the Deschutes River in the vicinity of Bend. Simulated ground-water levels dropped tens of feet in the Bend area in response to this canal-lining scenario. A second canal-lining simulation in the area from Redmond to Madras showed that one-half of the amount of reduced recharge is supplied by diminished streamflow after about 12 years, and that streamflow is diminished by about 80 percent of the amount after 50 years (the length of the simulation). In this simulation, the stream reaches most affected include the lower Crooked River, the Deschutes River between Lower Bridge and Squaw Creek, and Mud Springs Creek.

The model described in this report simulates the behavior of the regional ground-water flow system in the upper Deschutes Basin and its response to new conditions. Examples in this report show how simulations can be used to understand the effects of new pumping or reduced recharge due to canal lining. The model could also be used to evaluate the effects of extended drought or climate change.

The model is intended to simulate the regional ground-water flow system and is most useful at regional scales. The model accurately simulated hydrologic conditions in specific local areas (usually corresponding to areas where data were plentiful); however, there are also areas where the model does not accurately simulate local or small-scale conditions. Simulation results must be evaluated within the context of overall hydrologic knowledge of the area. All model predictions have inherent error and uncertainty that is difficult to quantify. Nonetheless, this model should be a useful tool for resource managers and others for evaluating the response of the regional ground-water flow system to a range of management strategies and conditions.

REFERENCES CITED

Anderson, M.P., and Woessner, W.W., 1992, Applied ground-water modeling: Academic Press Inc., San Diego, California, 381 p.

Bauer, H.H., and Vaccaro, J.J., 1987, Documentation of a deep percolation model for estimating ground-water recharge: U.S. Geological Survey Open-File Report 86–536, 180 p.

Blackwell, D.D., and Priest, G.R., 1996, Comment on "Rates and patterns of groundwater flow in the Cascade Range volcanic arc and the effect on subsurface temperatures" *by* S.E. Ingebritsen, D.R. Sherrod, and R.H. Mariner: Journal of Geophysical Research, v. 101, no. B8, p. 17561–17568.

Boyd, T.G., 1996, Groundwater recharge of the middle Deschutes Basin, Oregon: M.S. thesis, Portland State University, 86 p.

Caldwell, R.R., and Truini, Margot, 1997, Ground-water and water-chemistry data for the upper Deschutes Basin, Oregon: U.S. Geological Survey Open-File Report 97–197, 77 p.

Century West Engineering Corporation, 1982, La Pine aquifer management plan: Bend, Oregon, prepared for Deschutes County, Oregon, variously paginated, several appendices.

Cooley, R.L., and Naff, R.L., 1990, Regression modeling of ground-water flow: U.S. Geological Survey Techniques of Water-Resources Investigations, book 3, chap. B4, 232 p.

Draper, N.R., and Smith, Harry, 1998, Applied regression analysis (3d ed.): John Wiley and Sons, New York, New York, 706 p.

Freeze, R.A., and Cherry, J.A., 1979, Groundwater: Prentice-Hall, Englewood Cliffs, N.J., 604 p.

Gannett, M.W., Lite, K.E., Jr., Morgan, D.S., and Collins, C.A., 2001, Ground-water hydrology of the upper Deschutes Basin, Oregon: U.S. Geological Survey Water-Resources Investigations Report 00–4162, 77 p. [http://or.water.usgs.gov/pubs/WRIR00-4162/]

Gonthier, J.B., 1985, A description of aquifer units in eastern Oregon: U.S. Geological Survey Water-Resources Investigations Report 84–4095, 39 p.

Hansen, A.J., Vaccaro, J.J., and Bauer, H.H., 1994, Ground-water flow simulation of the Columbia Plateau regional aquifer system, Washington, Oregon, and Idaho: U.S. Geological Survey Water-Resources Investigations Report 91–4187, 81 p.

Harbaugh, A.W., 1990, A simple contouring program for gridded data: U.S. Geological Survey Open-File Report 90–144, 37 p.

Hill, M.C., 1990, Preconditioned conjugate-gradient 2 (PCG2), a computer program for solving ground-water flow equations: U.S. Geological Survey Water-Resources Investigations Report 90–4048, 43 p.

Hill, M.C., 1992, A computer program (MODFLOWP) for estimating parameters of a transient, three-dimensional, ground-water flow model using nonlinear regression: U.S. Geological Survey Open-File Report 91–484, 358 p.

Hill, M.C., 1994, Five computer programs for testing weighted residuals and calculating linear confidence and prediction intervals on results from the ground-water parameter-estimation program MODFLOWP: U.S. Geological Survey Open-File Report 93–481, 81 p.

Hill, M.C., 1998, Methods and guidelines for effective model calibration: U.S. Geological Survey Water-Resources Investigations Report 98–4005, 90 p.

Hill, M.C., Cooley, R.L., and Pollock, D.W., 1998, A controlled experiment in ground-water flow model calibration using nonlinear regression: Ground Water, v. 36, p. 520–535.

Ingebritsen, S.E., Sherrod, D.R., and Mariner, R.H., 1992, Rates and patterns of groundwater flow in the Cascade Range volcanic arc, and the effect on subsurface temperatures: Journal of Geophysical Research, v. 97, no. B4, p. 4599–4627.

Lite, K.E., Jr., and Gannett, M.W., 2002, Geologic framework of the regional ground-water flow system in the upper Deschutes Basin Oregon: U.S. Geological Survey Water-Resources Investigations Report 02–4015, 44 p. [http://or.water.usgs.gov/pubs/WRIR02-4015/]

Mac Nish, R.D., and Barker, R.A., 1976, Digital simulation of a basalt aquifer system, Walla Walla River Basin, Washington and Oregon: State of Washington Department of Ecology Water-Supply Bulletin 44, 51 p.

Manga, Michael, 1996, Hydrology of spring-dominated streams in the Oregon Cascades: Water Resources Research, v. 32, no. 8, p. 2435–2439.

Manga, Michael, 1997, A model for discharge in spring-dominated streams and implications for the transmissivity and recharge of Quaternary volcanics in the Oregon Cascades: Water Resources Research, v. 33, no. 8, p. 1813–1822.

Mantua N.J., Hare, S.J., Zhang, Yuan, Wallace, J.M., and Francis, R.C., 1997, A Pacific interdecadal climate oscillation with impacts on salmon production: Bulletin of the American Meteorology Society, v. 78, no. 6, p. 1069–1079.

McDonald, M.G., and Harbaugh, A.W., 1988, A modular three-dimensional finite-difference ground-water flow model: U.S. Geological Survey, Techniques of Water-Resources Investigations, book 6, chap. A1, 586 p.

McFarland, W.D., and Ryals, G.N., 1991, Adequacy of available hydrologic data for evaluation of declining ground-water levels in the Fort Rock Basin, south-central Oregon: U.S. Geological Survey Water-Resources Investigations Report 89–4057, 47 p.

Miller, D.W., 1986, Ground-water conditions in the Fort Rock Basin, northern Lake County, Oregon: State of Oregon, Water Resources Department, Ground-Water Report No. 31, 196 p.

Newcomb, R.C., 1953, Ground water available for irrigation in the Fort Rock Basin, northern Lake County, Oregon: U.S. Geological Unpublished Open-File Report, 5 p.

Oregon Water Resources Department, 1965, Compilation of surface water records of Oregon: 219 p.

Packard, F.A., Hansen, A.J., and Bauer, H.H., 1996, Hydrogeology and simulation of flow and the effects of development alternatives on the basalt aquifers of the Horse Heaven Hills, south-central Washington: U.S. Geological Survey Water-Resources Investigations Report 94–4068, 92 p.

Prudic, D.E., 1989, Documentation of a computer program to simulate stream-aquifer relations using a modular, finite-difference, ground-water flow model: U.S. Geological Survey Open-File Report 88–729, 113 p.

Redmond, K.T., and Koch, R.W., 1991, Surface climate and streamflow variability in the western United States and their relationship to large-scale circulation indices: Water Resources Research, v. 27, no. 9, p. 2381–2399.

Russell, I.C., 1905, Geology and water resources of central Oregon: U.S. Geological Survey Bulletin 252, 138 p.

Sceva, J.E., 1960, A brief description of the ground water resources of the Deschutes River Basin, Oregon: Oregon State Engineer (now Oregon Water Resources Department), Salem, Oregon, 55 p.

Sceva, J.E., 1968, Liquid waste disposal in the lava terrane of central Oregon: U.S. Department of the Interior, Federal Water Pollution Control Administration, Technical Projects Branch Report No. FR-4, 66 p., plus a 96 page appendix.

Smith, G.A., 1986, Stratigraphy, sedimentology, and petrology of the Neogene rocks in the Deschutes basin, central Oregon: A record of continental-margin volcanism and its influence on fluvial sedimentation in an arc-adjacent basin: Corvallis, Oregon, Oregon State University doctoral dissertation, 464 p. (also Richland, Washington, Rockwell Hanford Operations Report RHO-SA-555P, 260 p.)

Stearns, H.T., 1931, Geology and water resources of the middle Deschutes River Basin, Oregon: U.S. Geological Survey Water-Supply Paper 637–D, 220 p.

Tanaka, H.H., Hansen, A J., and Skrivan, J.A., 1974, Digital-model study of ground-water hydrology, Columbia Basin Irrigation Project area, Washington: State of Washington Department of Ecology Water-Supply Bulletin 40, 60 p.

Taylor, G.H., 1993, Normal annual precipitation, State of Oregon: Corvallis, Oregon State University, Oregon Climate Service, map.

1879–2004

Printed on recycled paper

USGS